ELECTRON PARAMAGNETIC RESONANCE OF Eu^{2+}, Mn^{2+} AND VO^{2+} IN SINGLE CRYSTALS

BY

SHANKAR DATT PANDEY

DEPARTMENT OF PHYSICS

INDIAN INSTITUTE OF TECHNOLOGY KANPUR

September,

1969

ELECTRON PARAMAGNETIC RESONANCE OF Eu^{2+}, Mn^{2+} AND VO^{2+} IN SINGLE CRYSTALS

A thesis submitted

in partial fulfilment of the requirements

for the degree of

DOCTOR OF PHILOSOPHY

SHANKAR DATT PANDEY

DEPARTMENT OF PHYSICS

INDIAN INSTITUTE OF TECHNOLOGY, KANPUR

1969.

ACKNOWLEDGEMENTS

I must express my sense of deepest gratitude to Professor Putcha Venkateswarlu under whose guidance and supervision this work has been carried on and due to whose suggestions and advice it has been possible to give this work its present shape. My thanks are due to Director P.K. Kelkar for providing a permanent job and thus relieving me from the financial worries and also to Professor J. Mahanty, the present Head of the Department, for his interest particularly during the graduate course work. Furthermore, I thank Dr. G.C. Upreti for his sincere help.

I am obliged to my friends around for the support, active or otherwise, given to me during my work. In particular I would like to acknowledge the help of Sharmajee(V.K.) , Shri S.D. Phatak, Shri K.N. Swamy Rao, Shri Sarin Saheb and Dr/s. M.D. Sastry, B.L. Jha, M.S. Tomar and K.V. Subbaram . My thanks are due to Shri Nathai Ram for his help in some of the X-ray work and further to the personnel of our different technical shops for their timely assistance.

Pursuance and patience are the twin companions on way to any goal. In respect to pursuance the inspiration of Prof.(now late) B.K. Mathur has always been with me while the importance of the latter was brought home to me by one of my acquaintances with exalted patienee and piocity, accordingly , they can not elude my appreciation.

Finally I thank Mr. A.A. Khan for typing the thesis according to my ease.

S. D. PANDEY

Certified that the work presented in this thesis has been done by Mr. S. D. Pandey under my supervision.

September 26, 1969

Putcha Venkateswarlu
Professor of Physics
Indian Institute of Technology
Kanpur

CONTENTS

PREFACE

The Chapter I of the thesis gives a general introduction to electron paramagnetic resonance and a mention is made of the some of the problems being studied by EPR.

Crystals doped with iron-group ions have been extensively studied by EPR. The study of crystals doped with rare-earth ions is also extensive, but the divalent europium ions associated with vacancies in crystals have not been studied much. At the time of the beginning of this work the only published paper seemed to be that of R. Rohrig (Phys. Letters 16, 20 (1965)). He has reported the crystal field parameters for Eu^{2+}- doped NaCl. The best way of getting the Eu^{2+} ions associated with a vacancy would be to get them doped in some alkali halide lattice. Therefore, an EPR study of Eu^{2+}- doped KCl and RbCl is made. Part of the thesis is devoted to this study. During the progress of the work two papers, one by Porret and Lambert (Helv. Phys. Acta 40, 264 (1966)) on Eu^{2+}-doped KI and the other by Nair et al (J.Phys.Chem. Solids 29, 2183 (1968)) on Eu^{2+}- doped KCl, have appeared. The present work on Eu^{2+}- doped KCl has also been published in J. Chem. Phys. 47, 3094 (1967) .

From the present study of Eu^{2+}- doped KCl and RbCl and the results of Rohrig it is found that the variation of b_2^0 for Eu^{2+} in changing the host from NaCl to RbCl is different from that found by Watkins (Phys. Rev. 113, 79 (1959)) for Mn^{2+} from LiCl to KCl hosts. An attempt was, therefore, made to investigate this variation, further, by extending the studies to Mn^{2+} in RbCl host.

Vanadium has a stable oxy-ion called a vanadyl ion. The vanadyl ion VO^{2+} is supposed to exist in a sort of octahedral coordination with its surroundings. The present literature on EPR study of VO^{2+}- doped single crystals is restricted to only a few lattices. Mainly reported are the EPR studies of randomly oriented VO^{2+} ions. The literature on preferentially oriented VO^{2+} ions is further restricted to those hosts which grow with the water of hydration or which possess regular octahedra of anions. The EPR study of VO^{2+} ions in some lattice gives an idea of the bonding of its vanadium with the surroundings and also the orientation of VO^{2+} (linear) ions in the lattice. It would be very interesting therefore, to find the orientation of VO^{2+} in a host which grows without the water of hydration and which does not possess any octahedron of anions. Ammonium sulphate could be such a lattice. Further, ammonium sulphate is paraelectric at room temperature and changes its phase to ferro-electric at $-50^{o}C$. Thus, a study of VO^{2+}- doped $(NH_4)_2SO_4$ lattice could be expected to give some information about the phase transition mainly as to how it affects the EPR spectrum of VO^{2+}. It is worthwhile to mention that the available data on $(NH_4)_2SO_4$ to this date includes the crystal structure as determined by X-ray, electron and neutron diffraction. Further, $(NH_4)_2SO_4$ host has widely been studied in our laboratory. The work of Chowdary on Mn^{2+}- doped $(NH_4)_2SO_4$ to understand the lattice defects and phase transitions is important in this regard.

Theoretical details regarding the EPR of rare earth ions in orthorhombic and cubic crystal fields are given in Chapter II. Eu^{2+} is taken as a special case. The formulae for the various fine structure and hyperfine structure transitions are given therein. Also given is

the matrix of the spin-Hamiltonian for a field of orthorhombic symmetry.

In Chapter III a brief description is given of the electronic structure of the complex VO $(H_2O)_5$ of VO^{2+}. The symmetry of the complex has a strong tetragonal distortion from octahedral one. The procedure due to Schonland for finding the principal values and the direction cosinesof the principal axes of g and A is also described, with a few simplifying additions, in this Chapter.

Chapter IV deals with the methods of growing single crystals: from the melt and also from the solution. It also deals with the method of mounting, in the microwave cavity, of the crystals particularly the $(NH_4)_2SO_4$ crystal so that it could be rotated about an axis perpendicular to one of its three basal planes ab, bc and ca. Some other details of the general experimental techniques are also given.

Chapter V describes the EPR spectra obtained in the case of Eu^{2+} doped in KCl. Different vacancy and defect models explaining the charge compensation for Eu^{2+}- doped KCl are discussed. The EPR spectra obtained are assigned due to Eu^{2+} associated with a vacancy at a first neighbour cation position. Also reported is the cubic spectrum corresponding to Eu^{2+} without any vacancy near it. The cubic spectrum shows itself up at 300°C. The crystal field parameters and the g-values for both the types of Eu^{2+} ions in KCl are determined and given in this Chapter.

In the study of Mn^{2+}- doped alkali chlorides Watkins (Phys. Rev. 113, 79 (1959)). has reported the crystal field parameters for Mn^{2+} associated with a first neighbour cation vacancy. The crystal field parameters for Eu^{2+}- doped NaCl and KCl wherein Eu^{2+} is associated

with a first neighbour cation vacancy are also now known. The absolute value of the parameter b_2^0 is determined by using the spectra at room and liquid helium temperatures for Eu^{2+}-doped KCl as published by Nair et al. Therefore, though the individual values of the crystal field parameters cannot be compared for the two cases (Mn^{2+} and Eu^{2+}) in the same lattice, a comparison could be made of the variation of the crystal field parameters for Eu^{2+}- doped alkali chlorides in going from NaCl to KCl with that obtained for Mn^{2+} associated with a first neighbour cation vacancy in going from LiCl to KCl. The main crystal field parameter is $D(\equiv b_2^0)$. The magnitude of D continuously increases from LiCl to KCl for Mn^{2+}- doped alkali chlorides whereas a decrease is found for Eu^{2+}- doped alkali chlorides from NaCl to KCl. This is shown in Chapter V.

To see as to whether D would further decrease if one moves up one step further i.e. upto RbCl in the series of alkali chlorides, a study was made of Eu^{2+}- doped RbCl. The results obtained are mentioned in Chapter VI. The hyperfine sets towards the end of the spectrum appeared as single broad bands. But all this can check one only from evaluating the value of A, the hyperfine interaction parameter; and the g-value and most of the crystal field parameters b_n^m can still be determined. The crystal field parameters obtained for Eu^{2+}- doped RbCl are given in this Chapter. The magnitude of D is, indeed, found to continuously decrease from NaCl to RbCl. The absolute value of D, however, increases in both the cases i.e. for Mn^{2+} from LiCl to KCl and for Eu^{2+} from KCl to RbCl. The difference in the variation of D for the two ions is understood by considering the simultaneous linear and quadratic dependence of D on $A_2^0 \langle r^2 \rangle$. The abnormal widths of the lines, as

one moves away from the centre of the spectrum to the two ends, are related to the probable off-centre positions of Eu^{2+} in RbCl lattice. A cubic spectrum also shoots up at about 200°C. A comparison is made of the crystal field parameter b_4^0, for Eu^{2+} at the cubic sites, in the three lattices viz. NaCl, KCl and RbCl.

Chapter VII deals with the EPR of Mn^{2+} - doped RbCl. Also reported are the results for the substance Rb_4MnCl_6, obtained by fusing RbCl and anthydrous $MnCl_2$ in the stoichiometric ratio under vacuum. An explanation is given as to why no axial spectrum appears for Mn^{2+} - doped RbCl. The observed narrow single line spectrum is related to the super-exchange from the Mn^{2+} to an another neighbouring one through a Cl^- or a pair of Cl^- ions. A model is proposed which explains as to why Mn^{2+} accumulate together even in such RbCl crystals which are doped with a mere $\sim$ .02% of $MnCl_2$.

Chapter VIII deals with the EPR of VO^{2+}-doped $(NH_4)_2SO_4$. VO^{2+} seems mainly to occupy two types of sites I and II in the lattice. It also occupies two more types of sites III & IV but with a lesser probability .The spectra due to VO^{2+} at site IV could not be followed for all orientations of H in the crystal basal planes. The principal values and the direction - cosines of the principal axes of the g and A tensors corresponding to the three types of sites I, II and III of VO^{2+} are determined. As V^{4+} of VO^{2+} usually seems surrounded by six oxygens; looking into the availability of oxygens in the present case, a classical model is proposed for explaining the position of V^{4+} in the lattice. The bonding scheme of this model also describes the orientation of VO^{2+} in the lattice, if account be made of the cation vacancy caused when VO^{2+}

with 2+ charge replaces a NH_4^+ ion. Also described in chapter VIII is the effect on the spectrum of the downward sweep of temperature through -50^0C.

The later part of the chapter VIII reports the optical absorption spectra as found for the present sample of VO^{2+} - doped $(NH_4)_2\ SO_4$. Three absorption maxima are observed. They are related to the two predominantly occupied sites I & II of VO^{2+}. As reported by Ballhausen (Inorg. Chem. 1, 111(1962)) one should get two absorption maxima for each of the predominantly occupied sites I & II of VO^{2+}. The occurrence of only three maxima indicates that ~~the~~ two maxima one for each type of the sites I & II coincide at least within their widths.

CHAPTER I

GENERAL INTRODUCTION

A system of charges associated with a resultant angular momentum $\sqrt{J(J+1)}\hbar$ and thus a magnetic moment (except in very rare cases) exhibits paramagnetism. The sufficient condition for a substance to be paramagnetic is that such constituent systems in the substance be either not coupled or only very weakly coupled by exchange forces. If the systems are strongly exchange coupled we have ferro - or antiferro-magnetism.

Paramagnetism is exhibited by a vast range of matter: atoms having an odd number of electrons like (H, N, Na...), molecules like (O_2, NO_2, ClO_2...), free radicals like (CH_3...), ions with partly filled electron shells (those in transition group, rare earth group...), impurities in semiconductors, colour - centres, substances irradiated by X-rays, metals and semiconductors having unfilled conduction bands and even some biological matter.

In the present discussion we shall be concerned only with the electronic paramagnetism of ions of iron and rare-earth groups.

Under the action of an external magnetic field H the resultant magnetic moment associated with angular momentum $\sqrt{J(J+1)}\,\hbar$ of the paramagnetic centre has (2J+1) Zeeman sublevels as shown for J = 7/2 in figure 1.1, and resonant absorption can be observed between the resulting set of levels. The sublevels are associated with energies $E = g\beta HM$, where g is the spectroscopic splitting factor, β is the Bohr magneton and M is the projection of J on H and takes on the values + J to -J.

If an alternating microwave field of frequency ν is applied at right angles (for maximum absorption) to H, magnetic dipole transitions are produced according to the selection rule $\Delta M = \pm 1$. Thus $h\nu = g\beta H$

gives the necessary H for a resonant absorption at a given ν. For a free ion the spectroscopic splitting factor g is given by the following expression

$$g = 3/2 + \frac{S(S+1) - L(L+1)}{2J(J+1)} \quad \text{where } \vec{L}+\vec{S}=\vec{J}.$$

But in actual practice the whole thing is not so simple. The ions are subjected to crystalline electric field and spin-orbit coupling which causes the individual $\vec{L}$ and $\vec{S}$ and their coupling scheme to change tremendously.

Fine structure and its origin

For ions with d electrons the effect of the crystalline field is more than the effect of spin-orbit coupling. The cubic part of the crystalline field produces a splitting ($\sim 10^4 cm^{-1}$) in the free ion terms. The spin-orbit coupling and any noncubic part of the crystal field produces further splittings of these levels. These splittings are usually of the order of $100cm^{-1}$ to $1000cm^{-1}$, if the ground level obtained after cubic field splitting has orbital degeneracy; and only $\sim 1cm^{-1}$, if it has only spin degeneracy. Certain restrictions exist, however. If the system's total spin quantum number S is a half integer, there always exists a two-fold Krammer's degeneracy[1]. Paramagnetic resonance is usually observed between those lower levels which lie within a range of few cm^{-1} of the resulting ground level. This range, of course, depends on the frequency of the microwave radiation used. On the application of the magnetic field even the Krammer's degeneracy is removed and magnetic dipole transi - tions are observed between the resulting levels. The splitting of the order of $1cm^{-1}$ caused in the lowest orbital singlet, (which is not always the case) because of crystalline field and spin-orbit coupling, is called

zero field splitting. This splitting is the origin of fine structure in electron paramagnetic resonance (EPR) (figure 1.2).

In some of the paramagnetic systems there exists an additional effect which removes the orbital degeneracy of the ground state even in the absence of any crystalline electric field. This is called Jahn Teller Effect.[2,3] Because of it a system which has degeneracy in its lowest state spontaneously distorts itself in such a way as to remove the maximum possible degeneracy.

In the case of d-electrons, because of the effect of the crystal field (mainly cubic), the ground orbital quantum number is changed appreciably. It takes up some effective value L'. Some times ground orbital quantum number is zero but then there comes some contribution from higher lying orbitally degenerate levels through spin-orbit coupling, (and L' slightly differs from zero).

For rare earth ions the spin-orbit coupling is stronger than the effect of the crystalline field[4]. Thus for example in the case of $Ce^{3+}(4f^1)$ out of the two ground state terms $^2F_{7/2}$ and $^2F_{5/2}$, obtained because of spin-orbit splitting, $^2F_{5/2}$ lies lower. The crystal field splits the six M(5/2 to -5/2) levels of $^2F_{5/2}$ in such a way that the Krammer's doublet---- approximately characterised by $M = \pm \frac{1}{2}$ --- lies more than $10cm^{-1}$ below all other levels. Only this doublet is appreciably populated at 4^oK(a temperature suitable for the paramagnetic study of Ce^{3+}) and the resonance spectrum consists of a single fine structure line.

The ions with seven f electrons (Eu^{2+} and Gd^{3+}) are an exception to above. In these ions the crystal field splitting between the eight levels belonging to $^8S_{7/2}$ ground state is extremely small

($\lesssim 0.1 cm^{-1}$), the splitting entering into the EPR spectrum as zero field splitting. This is shown in figure 1.2 . Because of Krammer's theorem even the least symmetrical crystal field can cause the $^8S_{7/2}$ level to split only into four spin doublets.

For both d and f electron ions the number of levels (obtained after the application of the magnetic field) among which electron paramagnetic resonant absorption takes place is equated to 2S +1 and the S thus obtained gives an effective or fictitious spin value.

Hyperfine structure

If the nucleus of the paramagnetic ion has a nonzero spin I and thus a magnetic moment, different orientations of I with respect to the orientation of electronic magnet will have different energies . So each electronic level is split into 2I+1 sublevels and because of the selection rule $\Delta m=0$ (m is the projection of I in the electronic-magnetic field of the ion) each fine structure transition is split into (2I+1) hyperfine transitions (figure 1.2). The hyperfine splitting is isotropic for S- state ions and anisotropic for others.

Quadrupole interaction

For nuclei having $I > \frac{1}{2}$ there exists an electrostatic interaction (energy $\sim 10^{-3} cm^{-1}$) between the quadrupole moment of the nucleus and the gradient of the crystalline electric field at the nucleus of the ion. The result of this quadrupole interaction is to shift the energy of hyperfine levels by an amount proportional to m^2 (m taking values from +I to -I).

Then comes in decreasing order of energy the effect of the applied external magnetic field on the magnetic moment of the nucleus.

This is very small ($\sim 10^{-4} cm^{-1}$).

Finally we have the interaction of the spin of the paramagnetic centre with the surroundings consisting of the diamagnetic lattice and other paramagnetic spins. The effect of these is felt in the shape and the width of the absorption lines. These do not change the position of the absorption lines in first order. Among these phenomena we have 1) Spin - lattice relaxation, 2) Spin - spin interaction , and 3) exchange interaction.

Spin - Lattice relaxation

The mechanism of spin- lattice relaxation considered by Van Vleck[5] is that the thermal vibrations of the lattice give a random crystalline field at the ion. This random electric field affects the orbital motion and thus the magnetism of the ion; but if the magnetism of the ion comes solely from the spin the effect is via the spin-orbit coupling. Thus the spin (ion - magnet for $L \neq 0$) feels the temperature of the lattice and the spins (ion-magnets) try to acquire the temperature of the lattice. By absorption of electromagnetic energy, the spin temperature increases but the spin-lattice relaxation brings the temperature down and makes the system ready for fresh absorption.

The reverse of the spin-lattice relaxation time (T_1) is a measure of the rate at which spin (ion - magnet) reverses its direction and either takes from or gives to the lattice a quantum of energy. T_1 is temperature dependent ($\sim T^{-4}$). Relaxation process gives a half width at half intensity of the order of $1/2\pi T_1$ sec^{-1}. Thus for line width of the absorption line to be small T_1 should be large. For some of the ions e.g. Eu^{2+}, Mn^{2+}..., T_1 is sufficiently large at room temperature.

while for others we may have to cool the sample in order to reduce the line width. But T_1 can not be increased infinitely because that would cause the microwave excited levels to saturate.

If N_k and N_{k+1} be the populations at thermal equilibrium of two consecutive levels among the set of levels between which electron paramagnetic resonance absorption is taking place, then

$$N_{k+1}/N_k = \exp(-g\beta H/kT)$$

N_{k+1} being the population of the higher of the two levels. Thus $N_k > N_{k+1}$; the number of absorptions, therefore, exceeds the number of emissions at thermal equilibrium and thus the net result is the absorption of energy from the microwave source.

Now even though the absorption of energy would try to equalize N_k and N_{k+1}, the net absorption continues because of the spin-lattice relaxation process which acts in the reverse direction, takes up energy from the spin (ion - magnet) and gives the same to the lattice, which is at a lower temperature, in the form of heat and makes the spins (ion magnets) ready for fresh absorption. For this reverse process to act effectively T_1 should be small and so a upper limit on the value of T_1. T_1 is usually kept at about 10^{-5} sec.

Spin - spin interaction:

The theory of spin - spin interaction has been given by Van Vleck[6] and Pryce and Stevens[7]. A spin under consideration is influenced by the varying fields of the neighbouring spins. These varying fields are not negligible; for example in the tutton salt $CuK_2(SO_4)_2 6H_2O$ the paramagnetic Cu^{2+} ions separated by $6A^0$ are exposed to a resultant magnetic field of $\sim$100 gauss due to neighbouring ion - magnets. Therefore, for resonant absorption of

microwave power of some fixed frequency, there is a distribution of the magnetic fields. This distribution causes the line width. In order to reduce this broadening the paramagnetic substance is usually diluted by some suitable diamagnetic substance. The spin - spin interaction is direction dependent according to $(1 - 3\cos^2\theta)$, θ being the angle between the steady magnetic field H and the line joining the magnetic dipoles.

Exchange interaction

(6-8)

Exchange interaction occurs when electrons are exchanged between the orbitals of different paramagnetic centres. The effect of the exchange interaction is to reduce* the dipolar broadening by modulating the spin orientation of the unpaired electrons. This form of interaction changes a line from Gaussian to Lorentzian shape, and is often met whenever the concentration of paramagnetic centres in the substance is high.

By the knowledge of perturbations which determine the EPR spectra of ions in crystals one can enumerate the applications of EPR study of ions in crystals as follows:

(1) It gives a direct and accurate description of the crystalline environment on the low lying energy levels of the paramagnetic ion. Careful measurements of EPR spectra enables us to determine the zero - field splittings which decide the use of paramagnetic ion - doped crystals for solid state masers and for producing very low temperature by using the techniques of adiabatic demagnetisation.

---

* if the paramagnetic centres have different Larmour frequencies the effect may be reversed.

(2) As the spectra are extremely sensitive to the strength and symmetry of the crystalline field the ion experiences, the EPR technique helps one to determine the crystal field parameters, nature of vacancy (or vacancies) associated with the ion, positions of the ions in the host lattice etc.

(3) It gives information about the nuclear properties like nuclear spin and nuclear quadrupole moment.

(4) Electron spin resonance seems to be ideal for determining the physical changes that take place in materials when pressure is applied. Some work has been done on paramagnetic ions subject to stresses which might be expected to induce changes in their electronic structure in the pressure range of about 10 Kilobarns.[9-11]

(5) We can also study the phase transformations in solids and some times we can get such information which is difficult to be obtained through x-ray studies.

(6) It can also be used to study as to how oxy-ions for example VO^{2+}, NpO_2^{2+} enter the host lattice, and to get information about the covalent bonding of such ions with the surrounding ligands.

REFERENCES

(1) W. Low, Paramagnetic Resonance in Solids, Page 34, (Academic Press, New York and London, 1960).

(2) H.A. Jahn & E. Teller, Proc. Roy. Soc. A161, 220 (1937).

(3) H.A. Jahn, Proc. Roy. Soc. A164, 117 (1938).

(4) R. J. Elliott & K.W.H. Stevens, Proc. Roy. Soc. A219, 387 (1953).

(5) J.H. Van Vleck, Phys. Rev. 57, 426 (1940).

(6) J.H. Van Vleck, Phys. Rev. 74, 1168 (1948).

(7) M.H.L. Pryce and K.W.H. Stevens, Proc. Phys. Soc. 63A, 36 (1950).

(8) P.W. Anderson and P.R. Weiss, Revs. Modern Phys. 25, 269 (1953).

(9) T. Kushida, G.B. Benedek and N. Bloembergen, Phys. Rev. 104, 1364 (1956).

(10) G.B. Benedek, E.M. Purcell, J. Chem. Phys. 22, 2003 (1954).

(11) W.M. Walsh, Phys. Rev. 114, 1473 (1959); 114, 1485 (1959).

FURTHER READINGS

(1) B. Bleaney and K.W.H. Stevens, Repts. Progr. Phys. 16, 108 (1953).

(2) K.D. Bowers and J. Owen, Ibid 18, 304(1955).

(3) J. Orton, Ibid 22, 204 (1959).

(4) G.E. Pake, Paramagnetic Resonance, (W.A.Benjamin Inc., New York, 1962).

(5) C.P. Slitcher, Principles of Magnetic Resonance, (Harper and Row Publishers, New York, London, 1963).

(6) S.A. Al'tshuler and B.M. Kozyrev, Electron Paramagnetic Resonance, (Academic Press, New York and London, 1964).

(7) H. M. Assenheim, Introduction of Electron Spin - Resonance, (Hilger and Watts Ltd., London, 1966).

(8) Roy S. Anderson, Electron Spin Resonance, Methods of Experimental Physics-Molecular Physics (Academic Press, New York and London, 1962).

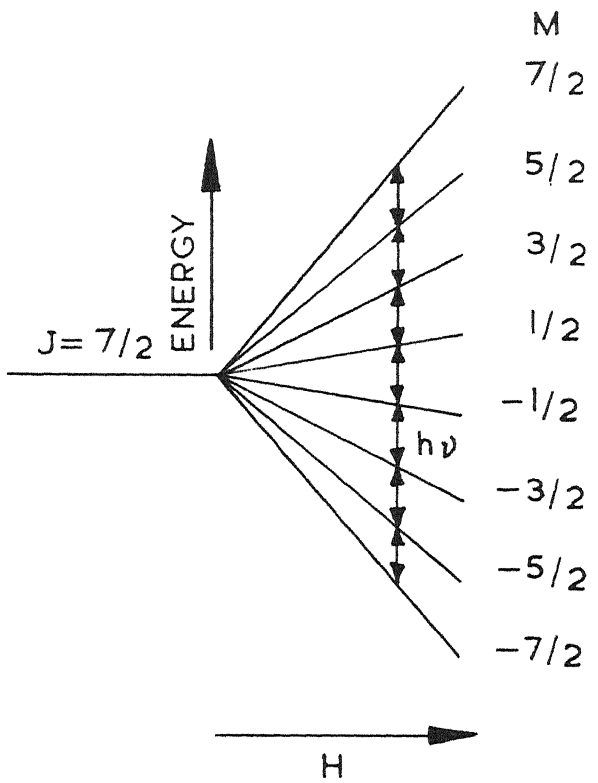

FIG.1.1 ENERGY LEVEL DIAGRAM AND THE ALLOWED TRANSITIONS OF A FREE ION WITH $J=7/2$.

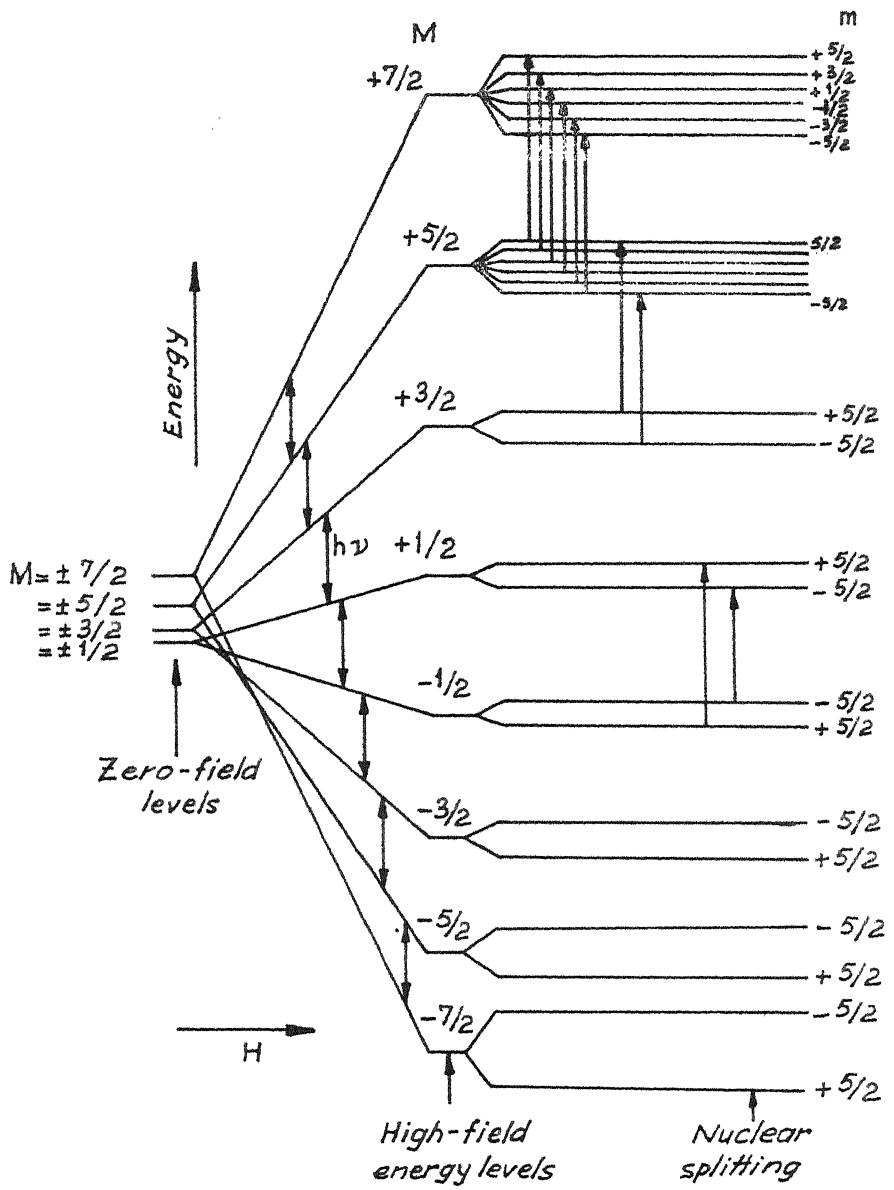

Allowed Transitions $\Delta M = \pm 1$ $\Delta m = 0$

1.2 – Energy level diagram showing zero field splitting & nuclear splitting of an ion with $J = 7/2$, $I = 5/2$. Permissible fine structure transitions are indicated by arrows. Nuclear splitting is shown only for top two

CHAPTER II

THEORY RELATED TO ELECTRON PARAMAGNETIC RESONANCE OF Eu^{2+} ION

In electron paramagnetic resonance absorption only those levels are involved which lie within a range of a few cm^{-1} from the lowest level. In zero magnetic field the energy separation between these levels depends upon the crystalline electric field, hyperfine interactions etc. On the application of a magnetic field H these levels, if degenerate, get further split and diverge as H is increased. Resonant absorption takes place whenever two of the resulting levels are separated by an energy quantum $h\nu$, ν being the klystron - frequency. The major term which decides the energies of the levels is the zeeman term, then comes in decreasing order of energy —— the effect of crystal field, hyperfine interaction etc.

So the effective Hamiltonian to decide the energies of the levels is

$$\mathcal{H} = \mathcal{H}_{\text{zeeman}} + \mathcal{H}_{\text{cryst.}} + \mathcal{H}_{\text{hyperfine}}$$

where, $\mathcal{H}_{\text{zeeman}} = (\vec{L} + 2\vec{S}).\vec{H}$

$= g\beta \vec{S}.\vec{H}$, $\vec{S}$ being the effective spin

and g (the spectroscopic splitting factor) a scalar.

If g be a tensor $(\underset{\sim}{g})$

$$\mathcal{H}_{\text{zeeman}} = \beta \vec{H}.\underset{\sim}{g}.\vec{S}$$

$$\mathcal{H}_{\text{cryst.}} = -\sum_i e V_{cr}(x_i, y_i, z_i)$$

where V_{cr} is the potential of the crystalline field, and x_i, y_i, z_i are

the coordinates of the i-th electron of the unfilled shell of the ion. In crystal field approximation i.e. by assuming that the surroun - ding ligands do not overlap the electron cloud of the paramagnetic ion, V_{cr} can be expanded in a series of spherical harmonics

$$V_{cr} = \sum_{n,m} A_n^m r^n Y_n^m (\theta, \phi)$$

This expression gets considerably simplified by taking into consideration the fact that for the ions having d -electrons, the spherical harmonics for $n > 4$ give zero - matrix elements between the states $|L, S, L_z, S_z\rangle$ [1] . Analogously, in the case of f- electrons the terms in the series with $n > 6$ can be discarded [1]. We also omit the terms of the series with odd n because the matrix elements of odd order spherical harmonics equal zero. The term with $n = 0$ gives an additive constant, which may be set equal to zero. Further, since V_{cr} is real $A_n^m = (A_n^{-m})^*$. The number of relevant terms in the expression for V_{cr} can further be reduced if one takes into account the symmetry of the crystalline field. If we denote $A_n^o r^n Y_n^o(\theta, \phi)$ by U_n^o and $A_n^m r^n Y_n^m (\theta, \phi) + A_n^{-m} r^n Y_n^{-m} (\theta, \phi)$ by $U_n^{|m|}$, the potential V_{cr}, depending on the symmetry of the field, can be written as series sum of $U_n^{|m|}$'s e.g. for orthorhombic symmetry we have

$$V_{cr} = U_2^o + U_2^2 + U_4^o + U_4^2 + U_4^4 + U_6^o + U_6^2 + U_6^4 + U_6^6$$

It is easy to note that one can write $U_n^m = C_n^m V_n^m$, wherein C_n^m's differ from A_n^m's only through some numerical factor and V_n^m's do not involve θ and ϕ explicitly and are homogeneous polynomials of degree n of coordinates x, y, and z e.g. $V_2^o = (3z^2 - r^2)$.

The most convenient method for evaluating the matrix elements of the V_{cr} is the use of operator - equivalents[2,3,4,5] method. In order to find the operator - equivalent of V_n^m one replaces, x,y and z by J_x, J_y and J_z respectively, always allowing for the non-commutation of J_x, J_y and J_z.

The matrix elements of the functions V_n^m's and the corresponding equivalent operators O_n^m's coincide except for a certain common factor, which is identical for all functions with a given n.

$$V_2^m \equiv \alpha \langle r^2 \rangle O_2^m$$

$$V_4^m = \beta \langle r^4 \rangle O_4^m$$

$$V_6^m = \gamma \langle r^6 \rangle O_6^m$$

$$V_{cr} = \sum_{n,m} C_n^m \cdot \Theta_n \cdot \langle r^n \rangle \cdot O_n^m$$

$\Theta_n = \alpha, \beta$ or γ for n = 2, 4 or 6 respectively.

Therefore, $\mathcal{H}_{cryst.} = - \sum_{n,m} e\, C_n^m \cdot \Theta_n \cdot \langle r^n \rangle\, O_n^m$

$$= \sum_{n,m} B_n^m \; O_n^m \;, \quad \text{if } B_n^m = -e\, C_n^m \cdot \Theta_n \cdot \langle r^n \rangle \;.$$

here B_n^m's are the coefficients dependent upon the crystalline electric field.

Matrix elements between the states $|\, L, S, J, J_z \rangle$ of various O_n^m's are tabulated by a number of authors[6,7,8,9]. Those necessary for a crystalline field of orthorhombic symmetry and J = 7/2(Eu^{2+}, Gd^{3+}) are given on next page.

	F	$\pm 1/2$	$\pm 3/2$	$\pm 5/2$	$\pm 7/2$ $\leftarrow J_z$
O_2^0	3	-5	- 3	+ 1	+ 7
O_4^0	60	+9	- 3	- 13	+ 7
O_6^0	120	-5	+ 9	- 5	+ 1

	F	$\langle \pm 5/2 \| \mp 3/2 \rangle$	$\langle \pm 7/2 \| \mp 1/2 \rangle$
O_4^4	12	$5\sqrt{3}$	$\sqrt{35}$
O_6^4	60	$-7\sqrt{3}$	$3\sqrt{35}$

	F	$\langle \pm 3/2 \| \mp 1/2 \rangle$	$\langle \pm 5/2 \| \pm 1/2 \rangle$	$\langle \pm 7/2 \| \pm 3/2 \rangle$
O_2^2	1	$2\sqrt{15}$	$3\sqrt{5}$	$\sqrt{21}$
O_4^2	6	$-4\sqrt{15}$	$\sqrt{5}$	$5\sqrt{21}$
O_6^2	24	$7\sqrt{15}$	$-21\sqrt{5}$	$5\sqrt{21}$

	F	$\langle \pm 7/2 \| \mp 5/2 \rangle$
O_6^6	360	$\sqrt{7}$

The numbers in column F are multiplying factors common to all elements in the row.

For tetragonal fields

$$\mathcal{H}_{cryst.} = B_2^0 O_2^0 + B_4^0 O_4^0 + B_4^4 O_4^4 + B_6^0 O_6^0 + B_6^4 O_6^4$$

In cubic fields the symmetry is such that $B_2^0 = 0$, $B_4^4 = 5B_4^0$ and $B_6^4 = -21 B_6^0$. Thus the operator equivalent form of $\mathcal{H}_{cryst.}$ for cubic fields is

$$\mathcal{H}_{cryst.} = B_4^0 (O_4^0 + 5O_4^4) + B_6^0 (O_6^0 - 21O_6^4)$$

Hyperfine interaction: The interaction of the magnetic moment of the electron with the magnetic moment of the nucleus V_N is given by

$$V_N = gg_N \beta \beta_N \left[\sum_k \left\{ (\vec{l}_k - \vec{s}_k).\vec{I}/r_k^3 + 3(\vec{r}_k . \vec{s}_k)(\vec{r}_k . \vec{I})/r_k^5 \right\} + (8\pi/3)\, \delta(r_k)\, (\vec{s}_k . \vec{I}) \right]$$

wherein s_k and l_k are the spin and orbital angular momenta, I is the nuclear spin, g and g_N are the electronic and nuclear g-values, β and β_N are the Bohr and nuclear magnetons, r is the distance between electron and nucleus and $\delta(r)$ is the Dirac - delta function.

In the above expression for V_N the first two terms are anisotropic and represent dipole - dipole interaction between the nuclear moment and the magnetic moment of the electron. To first order they contribute to the Hamiltonian of the system a term $\mathcal{H}_{anisotropic}$ given by

$$\mathcal{H}_{anisotropic} = gg_N\beta\beta_N((3\cos^2\Theta - 1)/r^3) I_z S_z$$

The third term in the expression for V_N is the Fermi-contact term and is isotropic. Combining the isotropic and anisotropic terms, we have

$$\mathcal{H}_{hyperfine} = \vec{I}_\alpha \underset{\sim}{A}_{\alpha\beta} \vec{S}_\beta \quad \text{where } \underset{\sim}{A}_{\alpha\beta} \text{ is the hyperfine tensor.}$$

If A is isotropic the hyperfine contribution to the effective Hamiltonian equals $A\ \vec{I}.\ \vec{S}$.

In case $I > 1/2$, the hyperfine interaction also includes the electrostatic interaction of the quadrupole moment of the nucleus with the electric field gradient (at the nucleus). In the effective Hamiltonian this is reflected as

$$\mathcal{H}_{quadrupole} = Q' \left[I_z^2 - (1/3)I(I+1) \right] + Q'' (I_x^2 - I_y^2)$$

Q' and Q'' being the quadrupole interaction constants.

The role of spin - orbit coupling in the spin-Hamiltonian has not been mentioned in the discussion as yet. The spin - orbit

coupling does not seem to enter into the effective Hamiltonian explicitly, though it plays a great role in deciding the effectiveness of various effective spin - Hamiltonian parameters. The spin- orbit coupling splits the free ion terms and also the ground orbital singlet levels (through some complicated mechanism involving the higher lying orbitally degenerate states) and causes the zero - field splitting. The crystal field parameters such as b_2^0 thus depend on λ, the spin - orbit coupling constant. This spin - orbit coupling also affects the g-value which decreases if there be an orbitally degenerate level in the vicinity of the ground state e.g. in the case of Eu^{2+} and Gd^{3+}, because of the spin - orbit coupling, the g-value $g(^8S_{7/2})$ changes to a new value 'g' given by

$$g = (1 - \alpha^2)\, g(^8S_{7/2}) + \alpha^2\, g(^8P_{7/2})$$

where α is the amount of admixture of $^8P_{7/2}$ into the ground level $^8S_{7/2}$, and is given by

$$\alpha = \sqrt{14}\,\lambda / \left[E(^8P_{7/2}) - E(^8S_{7/2})\right]$$

Here E(x) stands for the energy of the state x.

Coming back to the hyperfine interaction one can, for axial fields, if the principal axes are taken to be the cartesian axes, write the hyperfine contribution to the spin - Hamiltonian $\mathcal{H}_{hyperfine}$ in the form

$$\mathcal{H}_{hyperfine} = A_z S_z I_z + B(S_x I_x + S_y I_y) + Q' \left[I_z^2 - (1/3)I(I+1)\right]$$

Here A and B determine the axial hyperfine tensor and the second order terms in quadrupole interaction are not taken into consideration.

Considering the case of Eu^{2+} ion, we find that its ground state is $(4f^7)\ ^8S_{7/2}$. In a crystalline field this eight - fold

degeneracy is removed due to admixture with higher states[10,11]. In axial and lower symmetry, the J = 7/2 level splits into four Krammer's doublets. In a cubic field also, because of spin - orbit coupling, the J = 7/2 state gives four spin doublets. The external magnetic field removes even the Krammer's degeneracy and paramagnetic resonance absorption can be observed between the resulting levels. The expressions for the energies E_M of the levels M = + 7/2, + 5/2 ,....., -7/2 when H // z axis of the crystalline field are given below. In these expressions the crystalline field is taken to be orthorhombic and g is assumed to be isotropic.

$$E_{7/2} = 7/2\ g\beta H + 2a + P^2/\left[2H + 2(a - c)\right]$$

$$E_{5/2} = 5/2\ g\beta H + 2b + Q^2/\left[2H + 2(b - d)\right]$$

$$E_{3/2} = 3/2\ g\beta H + 2c - P^2/\left[2H+2(a - c)\right]+R^2/\left[2H + 2(c - d)\right]$$

$$E_{1/2} = 1/2\ g\beta H + 2d - Q^2/\left[2H +2(b - d)\right]+R^2/\left[2H +2\ (d - c)\right]$$

$$E_{-1/2} = -1/2g\beta H + 2d + P^2/\left[2H -2(b -d)\right]-R^2/\left[2H -2\ (d - c)\right]$$

$$E_{-3/2} = -3/2g\beta H + 2c + P^2/\left[2H-2(a -c)\right]-R^2/\left[2H -2\ (c - d)\right]$$

$$E_{-5/2} = -5/2g\beta H + 2b - Q^2/\left[2H-2(b -d)\right]$$

$$E_{-7/2} = -7/2g\beta H + 2a - P^2/\left[2H - 2(a - c)\right]$$

where,

$$2a = 7b_2^0 + 7b_4^0 + b_6^0\ ,$$

$$2b = b_2^0 - 13b_4^0 - 5b_6^0\ ,$$

$$2c = -3b_2^0 - 3b_4^0 + 9b_6^0\ ,$$

$$2d = -5b_2^0 + 9b_4^0 - 5b_6^0\ ,$$

$$P = \sqrt{21}\ (b_2^2/3 + b_4^2/2),$$

$$Q = \sqrt{5}\ (b_2^2 + b_4^2/10\ ),$$

$$R = \sqrt{15}\ (2b_2^2/3 - 2b_4^2/5),$$

and $b_2^m = 3\ B_2^m,\ b_4^m = 60\ B_4^m,\ b_6^m = 1260\ B_6^m$

The sixth order terms are small hence they have not been included in the expressions for P, Q abd R which contribute to the energy of the levels in second order.

The expressions for the various fine structure transitions are thus

$$H_{\substack{+7/2\\-5/2}} = Ho \mp 2(a-b) - P^2/\left[2H_{\substack{+7/2\\-5/2}} \pm 2(a-c)\right] + Q^2/\left[2H_{\substack{+7/2\\-5/2}} \pm 2(b-d)\right]$$

$$H_{\substack{+5/2\\-3/2}} = Ho \mp 2(b-c) - Q^2/\left[2H_{\substack{+5/2\\-3/2}} \pm 2(b-d)\right] - P^2/\left[2H_{\substack{+5/2\\-3/2}} \pm 2(a-c)\right]$$
$$+ R^2/\left[2H_{\substack{+5/2\\-3/2}} \pm 2(c-d)\right]$$

$$H_{\substack{+3/2\\-1/2}} = Ho \mp 2(c-d) + P^2/\left[2H_{\substack{+3/2\\-1/2}} \pm 2(a-c)\right] - R^2/\left[2H_{\substack{+3/2\\-1/2}} \pm 2(c-d)\right]$$
$$- Q^2/\left[2H_{\substack{+3/2\\-1/2}} \pm 2(b-d)\right] + R^2/\left[2H_{\substack{+3/2\\-1/2}} \pm 2\ (d-c)\right]$$

$$H_{+1/2} = Ho + Q^2/\left[2H_{+1/2} + 2(b-d)\right] - R^2/\left[2H_{+1/2} + 2(d-c)\right] +$$
$$+ Q^2/\left[2H_{+1/2} - 2(b-d)\right] - R^2/\left[2H_{+1/2} - 2(d-c)\right]$$

here H_M stands for $M \leftrightarrow M-1$ transition and $Ho = h\nu/g\beta$

Expressions for H_M's when H is parallel to x or y principal axis can be obtained from those for H parallel to z by making the transformations as given in table II.1.

Table II.1

Transformation of $b_n^{m's}$

H//z	H//x	H//y
b_2^0	$(-b_2^0 + b_2^2)/2$	$(-b_2^0-b_2^2)/2$
b_4^0	$(3b_4^0 - b_4^2 + b_4^4)/8$	$(3b_4^0 + b_4^2+b_4^4)/8$
b_6^0	$(-5b_6^0+b_6^2 - b_6^4+ b_6^6)/16$	$(-5b_6^0-b_6^2-b_6^4 -b_6^6)/16$
b_2^2	$(-b_2^0-b_2^2/3)/2$	$(-b_2^0+b_2^2/3)/2$
b_4^2	$(5b_4^0 - b_4^2- b_4^4)/2$	$(5b_4^0+b_4^2-b_4^4)/2$

The H_M's corresponding to the cubic crystalline field can be obtained from the equations for the orthorhombic field by putting $b_2^0 = b_2^2 = b_4^2 = b_6^2 = b_6^6 = 0$, $b_4^4 = 5b_4^0$ and $b_6^4 = -21b_6^0$.

Europium has two stable isotopes of nearly equal natural abundance. Both the isotopes have $I = 5/2$. Therefore, each of the seven allowed fine structure transitions ($\Delta M = \pm 1$) between the set of levels $M = +7/2, +5/2, \ldots, -7/2$ splits into twelve hyperfine components ($\Delta m=0$). The hyperfine correction to the fine structure transitions $M \leftrightarrow M-1$ in axial crystalline field, after neglecting the quadrupole correction, is given[12] as

$$h.f.c. = Km + (B^2/2H_0)\,((A^2+K^2)/K^2)\left[I(I+1)-m^2\right] + (B^2/2H_0)(A/K)m(2M-1)$$

wherein $K^2=A^2g_{\parallel}^2\cos^2\theta + B^2 g_{\perp}^2 \sin^2\theta$, $g_{\parallel}$ being the value of g along z-axis, $g_{\perp}$ its value in x-y plane and θ is the angle measured

from z-axis.

If A is assumed to be isotropic, as is approximately the case for S-state ions

$$h.f.c. = Am + (A^2/2H_0)\left[I(I+1)-m^2\right] + m(2M-1)(A^2/2H_0).$$

At ordinary temperatures, the relative intensities I_Ms of the fine structure transitions $M \leftrightarrow M-1$ are

$I_{+7/2}$	$I_{+5/2}$	$I_{+3/2}$	$I_{+1/2}$	$I_{-1/2}$	$I_{-3/2}$	$I_{-5/2}$
7	12	15	16	15	12	7

But at low temperatures the relative intensities are much different from those mentioned above for ordinary temperatures, and actually depend upon the sign of b_2^o. The sign of b_2^o [13] can thus be determined by observing the relative intensities of the fine structure lines (or hyperfine groups) at liquid Helium temperature. The relative signs of b_2^o and A, and the value of A are determined by the measurement of the hyperfine separations of different hyperfine groups. The knowledge of the value of A , coupled with the experimental hyperfine line positions, then gives H_M's , the field values at which absorption would have taken place, had there been no hyperfine interaction. By knowing H_M's along the three principal axes one can calculate H_o and the various b_n^m parameters. The value of g can be calculated from that of H_o by using the relation

$$g = h\nu/\beta H_o$$

In order to calculate the zero-field splitting it would not be correct to calculate the values of E_M's from the expressions

already given for these, by putting H = 0 , because the second order contribution of perturbation terms, involving b_2^2 and b_4^2, in the spin - Hamiltonian (of the ion) will be comparable to the zero order energies. Therefore, we substitute the values of various parameters in the elements of the matrix given in Table II.2 and diagonalise it. This matrix includes the contribution of b_2^2 and b_4^2 in off-diagonal terms. The two fold degenerate eigenvalues obtained, after diagonalisation of the matrix represent the zero field splittings. There is also a hyperfine splitting of these zero-field levels.

Table II.2

The matrix representing the contribution of various terms in orthorhombic symmetry for the ion with J = 7/2. The parameters 2a, 2b, 2c, 2d, P, Q, and R are already explained in the text. The matrix is symmetric about the main diagonal.

M	7/2	5/2	3/2	1/2	-1/2	-3/2	-5/2	-7/2
7/2	7H/2+2a	0	P	0	0	0	0	0
5/2		5H/2+2b	0	Q	0	0	0	0
3/2			3H/2+2c	0	R	0	0	0
1/2				H/2 +2d	0	R	0	0
-1/2					-H/2+2d	0	Q	0
-3/2						-3H/2+2c	0	P
-5/2							-5H/2+2b	0
-7/2								-7H/2+2a

REFERENCES

(1) L. D. Landau, E. M. Lifshitz, Quantum Mechanics, (English translation) (Pergamon Press Ltd., London-Paris, 1958).

(2) B. Bleaney and K.W.H. Stevens, Rept. Progr. Phys. 16, 108(1953).

(3) K.W.H. Stevens, Proc. Phys. Soc. A 65, 209 (1952).

(4) R. J. Elliott and K.W.H. Stevens, Proc. Roy. Soc. A 218, 553(1953).

(5) B.R. Judd, Proc. Roy. Soc. A 227, 552 (1955).

(6) M.T. Hutchings, Solid State Physics (Advances in Research and Applications) Vol. 16, 227 (Academic Press, New York, 1964).

(7) K.W.H. Stevens, Proc. Phys. Soc. A65, 209 (1952).

(8) R. J. Elliott and K.W.H. Stevens, Proc. Roy. Soc. A 219, 387 (1953).

(9) D.A. Jones, J.M. Baker and D.F.D. Pope , Proc. Phys. Soc. (London) 74, 249 (1959).

(10) J.H. Van Vleck and W.G. Penney, Phil. Mag. 17, 961 (1934).

(11) R. Lacroix, Helv. Phys. Acta 30, 374 (1957).

(12) W. Low, Paramagnetic Resonance in Solids, (Academic Press, New York, 1960).

(13) B. Bleaney, H.E.D. Scovil and R.S. Trenam, Proc. Roy. Soc. (London) A 223, 15 (1954).

CHAPTER III

THEORY RELATED TO ELECTRON PARAMAGNETIC RESONANCE OF VANADYL COMPLEXES

VO^{2+} usually occurs in octahedral coordination with its surrounding atoms or ligands. In VO^{2+}- doped $(NH_4)_2SO_4$ single crystals, studied presently, a similar type of bonding is expected. V^{4+} of VO^{2+} is expected to be bonded to six oxygen atoms. One of these six oxygen atoms is that of vanadyl ion itself while the rest five belong to the surroundings.

Ballhausen and Gray[1] have given the molecular orbital picture of VO^{2+} bonded with five other oxygens belonging to water molecule ligands. This is shown in figure 3.1. The 3d, 4s and 4p metal orbitals along with the 2s, $2p_\sigma$ and $2p_\pi$ ($2p_x$, $2p_y$) orbitals of oxide (vanadyl) oxygen and the sp_σ hybrid orbitals for the water oxygens are used for bonding. In view of the sufficiently long V to O bond - length ($\sim 2.3\text{Å}$), and further because the combining orbitals are so aligned as to have little overlap the π-bonding involving the vanadium orbitals and water oxygens seems unlikely and thus will be ignored. V^{4+} having the surroundings as shown in figure 3.1 has C_{4v} site symmetry. The transformation scheme for the metal and ligand orbitals in C_{4v} symmetry is given in table III.1

The bonding in $VO(H_2O)_5^{2+}$ is pictured as follows: a strong σ bond of symmetry a_1 between the sp_σ oxygen hybrid orbital (σ_5) and the (4s + $3d_{z^2}$) vanadium hybrid orbital; two π-bonds of symmetry e between the vanadyl oxygen $2p_x$ and $2p_y$ orbitals (π_5) and the vanadium $3d_{xz}$ and $3d_{yz}$ orbitals, make a total of three vanadium

Table III.1

Transformation scheme for metal and ligand orbitals in C_{4v} symmetry.*

Representation	Vanadium orbitals	Ligand orbitals
a_1	$3d_z2 + 4s$	σ_5
	$4s - 3d_z^2$	$(\sigma_1+\sigma_2+\sigma_3+\sigma_4)/2$
	$4p_z$	σ_6
e	$3d_{xz}$, $3d_{yz}$	$\pi_5(2p_x, 2p_y)$
	$4p_x$, $4p_y$	$(\sigma_1-\sigma_3)/\sqrt{2}$, $(\sigma_2-\sigma_4)/\sqrt{2}$
b_1	$3d_x^2-y^2$	$(\sigma_1-\sigma_2+\sigma_3-\sigma_4)/2$
b_2	$3d_{xy}$	---

* Reference (1).

to oxygen bonds in VO^{2+} and , accordingly , explain why vanadyl VO is the strongest link in $VO(H_2O)_5^{2+}$. The four waters in the square plane (figure 3.1) are equivalent and the sp_σ hybrid orbitals of these equivalent water oxygens ($\sigma_1, \sigma_2, \sigma_3$ and σ_4) with the vanadium ($4s - 3d_z^2$) (a_1) , $4p_x$ and $4p_y$ (e), and $3d_x^2-y^2$ (b_1) orbitals make the next four bonds. The sixth ligand, the axial water oxygen (σ_6) is bonded to the remaining vanadium 4_{p_z} (a_1)

orbital. The $3d_{xy}$ vanadium orbital, of symmetry b_2, is non-bonding.

The L.C.A.O. - M.O. description of the complex is shown in figure 3.2. There are a total of seventeen electrons to be filled. Thus the unpaired electron lies in the nonbonding b_2 vanadium orbital ($3d_{xy}$). Because of the proximity of the e_{π}^{*} and b_1^{*} level to the b_2 level, g is anisotropic and

$$g_{//} = 2.0023\left[1 - 4\lambda\alpha^2/\Delta E(b_2 \rightarrow b_1^{*})\right] \qquad \ldots(3.1)$$

$$g_{\perp} = 2.0023\left[1 - \lambda\gamma^2/\Delta E(b_2 \rightarrow e_{\pi}^{*})\right] \qquad \ldots(3.2)$$

Here λ is the spin - orbit coupling constant, α and γ indicate the covalent character and ΔE is the energy separation. Two constants are needed for the covalent character, because the symmetry of the complex is C_{4v}. For zero covalent character $\alpha = \gamma = 1$.

If, because of some constraints, V-O bond of VO^{2+} is not perpendicular to the square plane of oxygens O_1, O_2, O_3 and O_4, or if the square plane becomes a rectangle, the site symmetry of V^{4+} is less than C_{4v}. Now if, further, the V-O bond is not parallel to the line joining the vanadium and oxygen O_6, there is no symmetry in the complex. But even in such cases, because of the fact that most of the bonding is in the vanadyl ion itself, the local symmetry can be taken to be almost a tetragonal one, the low-symmetry components acting simply as a perturbation. The perturbation of no symmetry will cause the degenerate e_{π}^{*} level of C_{4v} symmetry to split into two orbital singlet levels, say a_x and a_y, and thus electronic transitions $b_2 \rightarrow e_{\pi}^{*}$ will split into two transitions $b_2 \rightarrow a_x$ and $b_2 \rightarrow a_y$.

In such complexes V-O will exhibit anisotropic g-value and the principal values of the g-tensor will be given by

$$g = (\cong g_z) = 2.0023 \left[1 - 4\lambda \alpha^2 / \Delta E(b_2 \rightarrow b_1^*)\right] \quad \ldots(3.3)$$

$$g_x = 2.0023 \left[1 - \lambda \gamma_x^2 / \Delta E(b_2 \rightarrow a_x)\right] \quad \ldots(3.4)$$

$$g_y = 2.0023 \left[1 - \lambda \gamma_y^2 / \Delta E(b_2 \rightarrow a_y)\right] \quad \ldots(3.5)$$

wherein γ_x and γ_y are the new constants needed for the covalent character which ceases to be axial.

Covalent bonding reduces[2] the hyperfine splitting due to the nuclei of the paramagnetic centre itself, because this splitting depends on $\langle 1/r^3 \rangle$. Analogously, it increases the superhyperfine splitting due to the nuclei of the ligands surrounding the ion in question. Covalent bonding is established to occur in all the vanadyl complexes for example in $VOSO_4$[3] this has been done by comparing the paramagnetic resonance data with the results of optical absorption spectra and x-ray analysis.

In vanadyl ion complexes the unpaired electron is in the orbital singlet state b_2. On the application of a magnetic field this spin - doublet splits into two and paramagnetic resonance absorption can be observed between the two levels. So we have a case of effective spin $S = 1/2$.

As $S = 1/2$, the crystal field terms do not enter into the spin - Hamiltonian and thus the resonance data are described by a spin - Hamiltonian of the form

$$\mathcal{H} = \vec{H}.\underset{\sim}{g}.\vec{S} + \vec{S}.\underset{\sim}{A}.\vec{I} \quad \ldots(3.6)$$

where β is the Bohr magneton , H the applied magnetic field, $\vec{S}$ (S = 1/2) and $\vec{I}$ the electron and nuclear spin vectors and $\underset{\sim}{g}$ and $\underset{\sim}{A}$ are symmetric second rank tensors describing the interaction of the electron spin with the applied field and the nuclear spin respectively.

The energy eigen values for this spin - Hamiltonian in the general case, where $\underset{\sim}{g}$ and $\underset{\sim}{A}$ are not required to be axially symmetric and their principal axes are not required to be parallel, are

$$E = g\beta HM + mM(\hat{H}.\underset{\sim}{g}.\underset{\sim}{A}.\underset{\sim}{A}.\underset{\sim}{g}.\hat{H})^{1/2}/g + \text{second order terms} \quad ...(3.7)$$

where g, the spectroscopic splitting factor is given by

$$g = (\hat{H}.\underset{\sim}{g}.\underset{\sim}{g}.\hat{H})^{1/2} \quad ...(3.8)$$

$\hat{H}$ being a unit vector parallel to the applied magnetic field H , and M and m are quantum numbers associated respectively with the electron and nuclear spin.

Thus the observed transitions, which obey the selection rules $\Delta M = \pm 1$ and $\Delta m = 0$, are given by

$$h\nu = g\beta H + m(\hat{H}.\underset{\sim}{g}.\underset{\sim}{A}.\underset{\sim}{A}.\underset{\sim}{g}.\hat{H})^{1/2}/g + \text{second order terms} \quad ...(3.9)$$

ν being the klystron frequency.

If the tensor $\underset{\sim}{g}$ is isotropic and $\underset{\sim}{A}$ is axial, equation (3.9) reduces to

$$H(m) = H_0 - Km/g\beta - (B^2/4H_0g^2\beta^2K^2)(A^2 + K^2)\left[I(I+1) - m^2\right] - \left[(A^2-B^2)^2/2H_0g^2\beta^2K^2\right]\sin^2\theta\cos^2\theta\, m^2 \quad ...(3.10)$$

with $H_0 = h\nu/g\beta$ & $K^2 = A^2\cos^2\theta + B^2\sin^2\theta$, θ being the angle between the (axial) symmetry axis of $\underset{\sim}{A}$ and the direction of magnetic field H.

In the case of VO^{2+} as I = 7/2(V^{51} being the almost cent percent abundant isotope), m may have the values + 7/2, 5/2 ..., - 7/2 and thus there are eight hyperfine transitions. The transitions are equally spaced in first order theory. The second order contribution makes the separation between the adjacent hyperfine lines unequal. From the above expression (3.9) for H (m) we find that

$$\left[H(m=-I) + H(m=+I) + \text{second order terms}\right] = 2h\nu / g\beta$$

or,
$$g = (2h\nu/\beta)\left[H(m=-I) + H(m=+I) + \text{second order terms}\right]^{-1}$$
$$= g_{DPPH}\ 2H_{DPPH} \Big/ \left[H(m=-I) + H(m=+I) + \text{second order terms}\right] \qquad \ldots(3.11)$$

The second order terms may be evaluated with enough accuracy from equation (3.10) by assuming that $\underset{\sim}{g}$ is scalar and $\underset{\sim}{A}$ is axial.

Further in first order (identical to second order in axial case, as we have approximately the case for VO^{2+})

$$\left[H(m=-I) \sim H(m=+I)\right]/2I = (\hat{H}.\underset{\sim}{g}.\underset{\sim}{A}.\underset{\sim}{A}.\underset{\sim}{g}.\hat{H})^{1/2} \Big/ g^2\beta \qquad \ldots(3.12)$$

In order to find the principal values and corresponding direction cosines of g and A tensors a general method indicated by Schonland[4] is usually adopted.

Angular variation of g-values is plotted in three mutually perpendicular planes. In the case of an orthorhombic lattice such three planes could be the three basal planes ab, bc and ca. Maximum and minimum values of g are found in each of the three basal planes. Also found is the value of Θ (= Θ_+) at which g equals g_+, the maximum value of g in any plane, Θ being measured in conformity with right handed system of axes a, b and c. Then one evaluates the values of the components X_{ij} of the $\underset{\sim}{g}^2$ ($\equiv \underset{\sim}{g}.\underset{\sim}{g}$) tensor.

If $2\alpha = g_+^2 + g_-^2$, $2\beta = (g_+^2 - g_-^2)\cos^2\theta_+$, $2\gamma = (g_+^2 - g_-^2)\sin 2\theta_+$ the expressions for X_{ij} in terms of α, β, and γ are as follows

$$\begin{array}{lll} X_{11} = \alpha_3 + \beta_3 & X_{22} = \alpha_1 + \beta_1 & X_{33} = \alpha_2 + \beta_2 \\ X_{22} = \alpha_3 - \beta_3 & X_{33} = \alpha_1 - \beta_1 & X_{11} = \alpha_2 - \beta_2 \\ X_{12} = \gamma_3 & X_{23} = \gamma_1 & X_{31} = \gamma_2 \end{array} \quad \ldots(3.13)$$

In α_i, β_i and γ_i the suffix i = 3 stands for values in ab plane, i = 2 in c a plane and i = 1 in b c plane. The knowledge of nine X_{ij} ($X_{ji} = X_{ij}$) gives the matrix for the $\underset{\sim}{g}^2$ tensor. The g^2 - matrix so obtained is diagonalized and its eigenvalues and eigen vectors determined . The square roots of the three eigen values so determined gives the principal values of the $\underset{\sim}{g}$ - tensor, and the eigen vectors determine the direction cosines of the principal axes with respect to the a, b, c system of axes.

Since the sign of γ depends on the sign of θ_+, there exists an ambiguity about its sign. One can choose two of the γ's γ_1, γ_2 and γ_3 to be positive. In order to decide the sign of third γ, according to Schonland[4], one takes both positive and negative values for this third γ . One thus gets two sets of three γ's each. For both of these sets of γ's , the eigenvalues and eigen-vectors of the matrix are determined, and then the measurements are made in some fourth plane and out of two sets of γ's one which fits the data in the fourth plane more closely, is sorted out. But for paramagnetic centres having axial g-tensor as is approximately the case of VO - complexes all this can be eliminated because in this particular case $\tan\theta_{+1} \tan\theta_{+2} \tan\theta_{+3} = 1$ ... (3.14)

wherein θ_{+1} , θ_{+2} and θ_{+3} are the angles measured from b, c and a axes respectively, in bc, ca and ab planes taken in that order. The angles specify the position of maximum g in the different planes.

Next, one plots the angular variation of the value of the expression $\left[H(m=7/2) \sim H\ (m=-7/2)\right]\ /7$ in the three basal planes; and, by using the equation (3.12) and a procedure similar to that for $\underset{\sim}{g}.\underset{\sim}{g}$, the elements of the tensor $\underset{\sim}{g}.\underset{\sim}{A}.\underset{\sim}{A}.\underset{\sim}{g}$ are determined. Using the matrices for $\underset{\sim}{g}.\underset{\sim}{A}.\underset{\sim}{A}.\underset{\sim}{g}$ and $\underset{\sim}{g}.\underset{\sim}{g}$ the matrix for $\underset{\sim}{A}.\underset{\sim}{A}$ is then calculated. The matrix for $\underset{\sim}{A}.\underset{\sim}{A}$ on diagonalization gives the principal values and the direction cosines of the tensor $\underset{\sim}{A}$.

REFERENCES

(1) C. J. Ballhausen and H.B. Gray, Inorg. Chem. 1,111 (1962).

(2) B. Bleaney, K.D. Bowers and M.H.L. Pryce, Proc. Roy. Soc. A 228, 166 (1955).

(3) M.B. Palma - Vittorelli, M. U. Palma, D. Palumbo & F.Sgarlata, Nuovo Cemento 3, 718 (1956).

(4) D.S. Schonland, Proc. Phys. Soc. 73, 788 (1959).

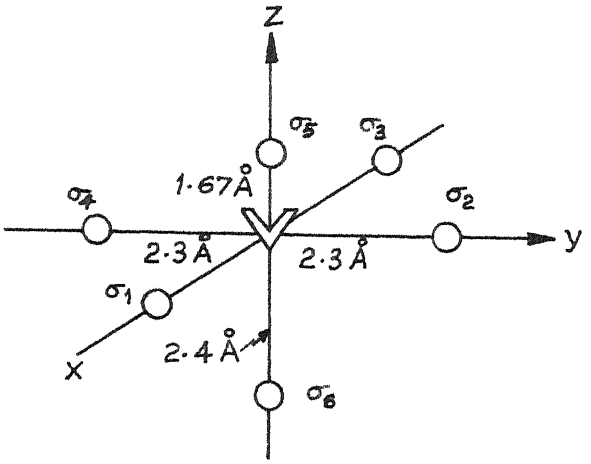

Fig. 3·1 - Structure of the $VO(H_2O)_5^{2+}$ molecular ion.

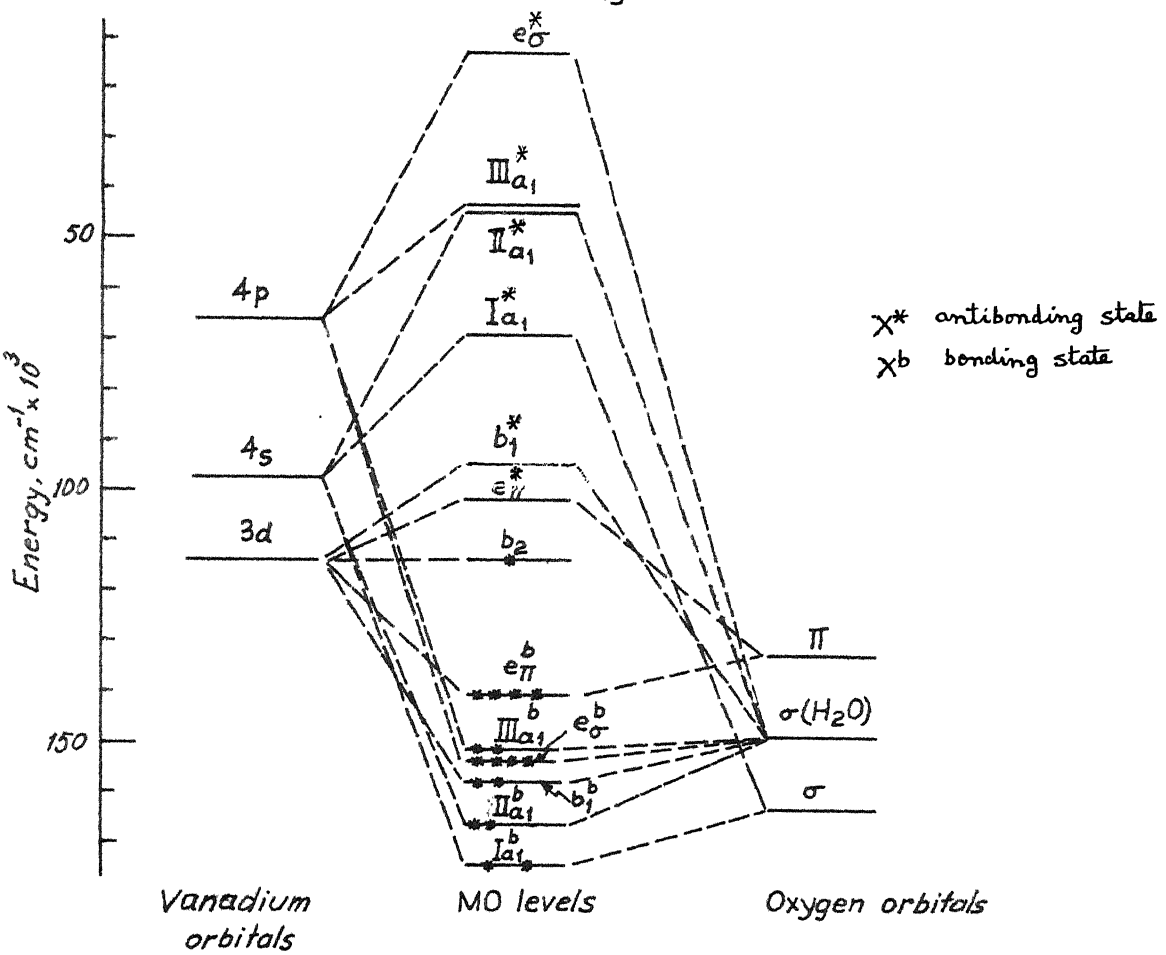

Fig. 3·2 - Bonding diagram for VO^{2+} in $VO(H_2O)_5^{2+}$, the site symmetry being C_{4v}. (Ligand Field Theory: Ballhausen, page 230)

CHAPTER IV

EXPERIMENTAL DETAILS

GENERAL

A Varian V-4502-12 EPR spectrometer with a 9 inch magnet and 100 Kc/sec field modulation was used to study the paramagnetic resonance absorption. The spectra were recorded by a G-14 strip chart recorder. Varian V-4540 variable temperature controller was used to obtain the regulated temperatures from 300°C to liquid nitrogen temperature for the sample under study. Angular variation was studied by using a Varian V-4533 rotating cavity. This cavity, with suitable mounting of the crystals, permitted the recording of spectra while H was rotated in crystal (001) and (110) planes for Eu^{2+} - doped alkali chloride crystals, and in basal planes ab, bc and ca in the case of VO^{2+} -doped ammonium sulphate single crystals. (The ammonium sulphate crystals have an orthorhombic unit cell). DPPH resonance served as a field marker. Its field was calculated by measuring the frequency of proton resonance with a Hewlett Packard frequency counter HP524C. The optical absorption spectra were taken with the help of a Cary - 14 spectrophotometer.

CRYSTAL GROWING

Europium doped alkali chloride single crystals were grown from the melt. Alkali chloride powder (Analar grade) was mixed with approximately 0.02% by weight of $EuCl_2$ and then the mixture was evenly grinded. The resulting powder was transferred to a quartz crystal growing crucible of usual shape and heated under vacuum for about 8-10 hours to remove air and any trace of water present. The

tube was then sealed under vacuum and lowered through a temperature gradient in a furnace employing the Stockberger* technique. The lowering rate was kept at about 2-3 mm/hour. The temperature was controlled within $\pm 5^{o}C$ by using a Hornwell Variable Temperature Controller.

VO^{2+}-doped ammonium sulphate crystals were grown by slow evaporation of a saturated solution of ammonium sulphate containing a known quantity of vanadyl sulphate. Ammonium sulphate used was of B.D.H. Analar grade. In one of the typical successful crystal growing attempts 50c.c. of the saturated solution of ammonium sulphate containing about 17.5 milligrams of $VOSO_4.5H_2O$ were kept for evaporation. Nice crystals with shining faces appeared after fifteen days. Some of the crystals thus obtained had hexagonal plate-like look, whereas the majority of them possessed long prismatic shape. Some of such prisms were as long as 25mm. Further, a lower temperature of the surroundings improved the growth rate and the size of the crystals.

MOUNTING OF CRYSTALS

In order to study the angular variation of the electron paramagnetic resonance spectra it is necessary to rotate the crystal about suitable crystal axes with respect to the direction of the external magnetic field H. The suitable axes are $\langle 001 \rangle$ and $\langle 110 \rangle$ for alkali chlorides and a,b, and c for ammonium sulphate. In the present experiments, this was accomplished by mounting properly cut crystal pieces on teflon rods with suitable wedges. The alkali chloride crystals easily cleave to the shape of a cuboid. The

---

* D.C. Stockberger, Rev. Sci. Instru. 7, 133 (1956).

(alkali chloride) crystals cut to this shape were, therefore, used for mounting purposes. In the case of VO^{2+} doped ammonium sulphate crystals the help was taken of its growth habit* and the fact that these crystals cleave in their (001) planes.

---

* The direction of the longest dimension in the prismatic crystals of ammonium sulphate is crystal a-axis. This was confirmed by the study of their x-ray patterns.

CHAPTER V

ELECTRON PARAMAGNETIC RESONANCE OF Eu^{2+}-DOPED KCl

Abstract

EPR of Eu^{2+} has been observed in doped single crystals of KCl at X-band from liquid Nitrogen temperature to 300°C. The room temperature spectrum is attributed to Eu^{2+} substituting for K^{+} and associated with a vacancy in a first neighbour cation position. The corresponding crystal field parameters b_n^m and g and A are determined. The signs of the parameters are also found by using the spectra reported by Nair, Lingam and Venkataraman (J. Phys. Chem. Solids 29, 2183 (1968)). The variation of b_2^0 with temperature is studied. At approximately 300°C a cubic spectrum appears. Its parameters b_4^0 and b_6^0 are estimated.

In going from NaCl to KCl host the magnitude of b_2^0 is found to decrease. This is contrary to what is observed for Mn^{2+}-doped alkali chlorides.

INTRODUCTION

Enough experimental work has accumulated during the past few years on electron paramagnetic resonance (EPR) spectra of S-state ions, in alkali halides. Watkins[1], Morigaki, Fujimoto and Itoh,[2] Yokozama and Kazumata[3], and Shrivastava and Venkateswarlu[4] have dealt with EPR spectra of Mn^{2+} in alkali chlorides. Rohrig[5] has reported the crystalline field parameters for Eu^{2+}-doped NaCl. Proceeding on the similar lines an investigation of the EPR spectra of Eu^{2+}-doped KCl has been attempted and the results obtained are published[6]. During the progress of this work, the EPR of Eu^{2+}-doped KI by Porret and Lambert[7] has appeared in the literature. Recently, Nair, Lingam and Venkataraman[8] have also reported the crystal field parameters for Eu^{2+} in KCl by extending the studies to liquid Helium temperature.

ORTHORHOMBIC SPECTRUM AND ITS ORIGIN

EPR of Eu^{2+} has been observed in doped single crystals of KCl at X-band from liquid Nitrogen temperature to 300°C. Angular variation of the line positions suggests that from 250°C to as low as liquid Nitrogen temperature, the Eu^{2+} ion in KCl lattice is associated with a crystalline field of orthorhombic symmetry. The probable origin of such a crystalline field could be in

1) Eu^{2+} substituting for K^{+} and a Cl_2^{2-} molecular ion substituting for Cl^{-} nearest to Eu^{2+}, the resulting site symmetry axis being along $\langle 001 \rangle$.

2) Eu^{2+} substituting for K^+ and causing a first neighbour cation vacancy, the resulting site symmetry axis being along ⟨110⟩ or,

3) Eu^{2+} occupying some interstitial position and thus causing two K^+ vacancies at nearest cation positions whereby the site symmetry axis will be along ⟨001⟩ .

The possibility of Eu^{2+} occupying an interstitial posi - tion in KCl lattice is a remote one because the largest spherical space available at an interstitial position has a radius of .91 Å, whereas Eu^{2+} has a radius of 1.14 Å (9)

If Cl_2^{2-} is responsible for the crystalline field at the Eu^{2+} site, it could go into the lattice in such a way as to align its internuclear axis parallel to a ⟨001⟩ direction, prependicular to the line joining Eu^{2+} and Cl_2^{2-} itself, but in that case the spectra would be represented by model IV in the notations of Watkins (1) and Shrivastava and Venkateswarlu (4), and one would expect two 90^0 parts IV′ and IV″ along with IV when H is parallel to ⟨001⟩ . (Experimentally we do not get two 90^0 parts).

The other equilibrium position of Cl_2^{2-} which can cause orthorhombic symmetry would be with its axis parallel to ⟨110⟩ . But this equilibrium position of Cl_2^{2-} is an unstable* one and, therefore, the possibility of a Cl_2^{2-} defect also appears to be remote. Thus a vacancy at a first neighbour cation position seems to be responsible for the crystalline field at the Eu^{2+} site and the model seems to be the same as III_1 in the notations of Watkins (1), Shrivastava and Venkateswarlu (4) and Morigaki et al (2). Further support in favour of this model comes from the intensity and

* At this equilibrium position Cl_2^{2-} has maximum potential energy

polarization measurements of emission in sm^{2+}- doped KCl by Bron and Heller[10] and EPR studies of Eu^{2+}-doped NaCl by Rohrig.[5] Bron and Heller[10] have reached a conclusion that the local crystalline field at Sm^{2+} site in Sm^{2+}- doped KCl is orthorohombic with z-axis parallel to the crystal ⟨110⟩ direction. We can thus expect the charge compensation mechanism for Eu^{2+}-doped KCl to be the same as that in Sm^{2+} doped KCl, because Sm^{2+} and Eu^{2+} have similar charges, radii and electron configurations. Rohrig[5] also assumed the first neighbour cation vacancy as responsible for charge compensation in Eu^{2+} - doped NaCl lattice.

Spin-Hamiltonian parameters for the orthorhombic spectrum.

Using this above model and taking the local site symmetry axis as z-axis the spectra obtained with H parallel to ⟨001⟩ and ⟨110⟩were analysed. These spectra are shown in figures 5.1 and 5.2 respectively. A spin - Hamiltonian suitable for orthorhombic symmetry

$$\mathcal{H} = g\beta \vec{H}.\vec{S} + (1/3) \sum_{k=0}^{1} b_2^{2k} O_2^{2k} + (1/60) \sum_{k=0}^{2} b_4^{2k} O_4^{2k}$$
$$+ (1/1260) \sum_{k=0}^{3} b_6^{2k} O_6^{2k} + A\vec{I}.\vec{S}$$

was used . Here the various terms have their usual meaning. The expression for the spin-Hamiltonian is the same as that given in chapter II, but for the transformations $b_2^m = 3B_2^m$, $b_4^m = 60B_4^m$ and $b_6^m = 1260B_6^m$. The spin - Hamiltonian parameters obtained are given in table V.1. Results obtained for Eu^{2+} in NaCl by Rohrig[5], for Eu^{2+} in KI by Porret and Lambert[7] , and for Eu^{2+} doped KCl by Nair et al[8] are also included in the same table for the sake

of comparison. Due to the lack of liquid Helium temperature facilities the author did not determine the sign of b_2^0 earlier[6]. But now the spectra for Eu^{2+} - doped KCl at liquid Helium temperature have been published by Nair et al[8]. Using their spectra, under the present choice of crystal principal - axes which differs from that of theirs, but coincides with those of Rohrig[5], Porret and Lambert[7], the sign of b_2^0 is found to be negative. The signs of the parameters for Eu^{2+}-doped KCl in table V.1, therefore, differ from those reported by the author[6] earlier. The results of the author very nearly coincide with those of Nair et al[8] if the necessary transformations of principal axes are brought in. There is a good correspondence between the various spin-Hamiltonian parameters for Eu^{2+} in the three lattices, viz. KCl, NaCl and KI .

There is no marked change in the spectra of Eu^{2+}-doped KCl in the temperature range from 250^0C to liquid nitrogen temperature. The magnitude of b_2^0 is found to increase with the decrease of temperature. The temperature variation is linear as shown in figure 5.3.

For a Eu^{2+} substituting at a cation position there are twelve positions for the first neighbour cation vacancy and, therefore , there are an equal number of possible orientations of the principal axes of the fine structure tensor. For any orientation of H, the directions of the principal axes of the fine structure tensor could be specified by two angles θ and ϕ ,θ being the angle between the direction of H and the z-principal

axis of the crystalline field and ϕ the angle made by the projection of H in xy principal plane from the z-axis. Out of the twelve possible sets of (θ, ϕ) many become interrelated when H is// $\langle 001 \rangle$ or $\langle 110 \rangle$. The possible independent sets of values of (θ, ϕ) for the two orientations of H are given in table V.2. A symbol A,B,C or D is assigned to each such set (θ, ϕ) , excepting the one with $\theta = 60^{\circ}$, $\phi = (1/2) \cos^{-1} (-1/3)$.

CUBIC SPECTRUM

Spectra obtained at 300°C indicate the appearance of a cubic spectrum. In the cubic spectrum the resonance lines overlap each other and it almost looks like a distorted hyperfine set. Assignment of invidual lines is difficult, but still the constants b_4^0 , b_6^0 and g have been estimated by using the fact that the whole spectrum may consist of seven closely spaced lines, each line being split into twelve by hyperfine interaction.

The cubic field spin-Hamiltonian parameters obtained at 300°C are

$$g = 1.995 \pm .002$$

$$b_4^0 = (2.68 \pm .05) \times 10^{-4} \text{ cm}^{-1}$$

$$b_6^0 = (-0.82 \pm .05) \times 10^{-4} \text{ cm}^{-1}$$

VARIATION OF b_2^0 ON CHANGING THE HOST CATION IN Mn^{2+} AND Eu^{2+}- DOPED ALKALI CHLORIDES

From the results of Watkins[1] for Mn^{2+}-doped alkali chlorides we find that $b_2^0 (\equiv D)$ continuously increases as we go from LiCl to KCl. But from Rohrig's[5] results and those mentioned in the present chapter we find that the magnitude of b_2^0 decreases for Eu^{2+}-doped alkali chlorides from NaCl to KCl. In fact the sign of b_2^0 would be the same for Eu^{2+} in both NaCl and KCl. This choice would make the signs of A identical in the two hosts. (Rohrig did not determine the absolute sign of b_2^0). Further support regarding the identity of signs in the two cases comes from a study of the EPR of Eu^{2+} in RbCl as reported in the next chapter. Watkins[1] explained the increase in b_2^0 for Mn^{2+} - doped in LiCl through KCl by taking into consideration the change in the ratio of anion to cation radii in the above hosts. This ratio determines the overlap of Mn^{2+} (divalent impurity) with the first neighbour cation and hence the effect of a first neighbour cation vacancy on Mn^{2+}. The larger the ratio of anion to cation radii, more is the effect of the first neighbour vacancy on Mn^{2+}. (This could be visualised from figure 7.2 of chapter VII). In this way one can understand the observed change in b_2^0 for Mn^{2+} from LiCl through KCl hosts. The above explanation for the variation of b_2^0 is important for Eu^{2+}-doped alkali chlorides as well, but the distance of the vacancy from the substituting divalent impurity also affects the value of b_2^0. In a classical picture b_2^0 should vary as r^{-3}, r being the distance of the vacancy from the divalent impurity ion. Perhaps, this second effect of variation of b_2^0 as r^{-3} is more

important for Eu^{2+}- doped alkali chlorides and thus we expect a decrease in b_2^o as we move from NaCl to KCl. The explanations suggested for the variation of b_2^o from one alkali chloride to another do not involve the absolute value of b_2^o. An explanation involving the absolute value of b_2^o will be given in chapter VI.

ADMIXTURE OF ^6P STATE INTO THE GROUND ^8S STATE

Assuming that it is mainly the $^6P_{7/2}$ state which has an admixture with the $^8S_{7/2}$ ground state, we can estimate the fraction of admixture α by using the formula

$$g = (1-\alpha^2)\, g\,(^8S_{7/2}) + \alpha^2\, g(^6P_{7/2}).$$

where $g\,(^8S_{7/2}) = 2.0023$ and $g(^6P_{7/2}) = 1.716$. The experimental value of g is 1.994, hence we get $\alpha^2 = .029$ or $\alpha \cong .17$. This value of α seems to be of the right order of magnitude as α is given by the following expression

$$\alpha = \lambda \langle {}^8S_{7/2} | \vec{L}.\vec{S} | {}^6P_{7/2} \rangle / \left[E_p - E_s\right]$$

$$= \sqrt{14}\,\lambda / \left[E_p - E_s\right] \sim 1320 \times \sqrt{14} / 29150 \sim .169$$

wherein λ, the spin-orbit coupling constant is taken to be $1320 cm^{-1}$. This value of λ for Eu^{2+} has been estimated by linear interpolation of the values of λ calculated for Eu^{3+} and Eu by Judd and Lindgren[11] They calculated $\lambda = 1361 cm^{-1}$ for Eu^{3+}, and $\lambda = 1228\ cm^{-1}$ for Eu. $(E_p - E_s)$ is taken to be $29,150 cm^{-1}$, the value found by Reisfeld and Glasner[12] for the centre of gravity of the first main absorption band in Eu^{2+}-doped KCl.

ZERO - FIELD SPLITTING

If we neglect the hyperfine interaction, the ground state $^8S_{7/2}$ would split into four Krammers doublets in the absence of the magnetic field. The effect of the hyperfine interaction is to give a set of twelve doublets from each of the four Krammers doublets. At zero magnetic field, therefore, we have forty eight doublets. In order to find their relative positions the only necessary thing to be done is to find the relative positions of the four parent doublets; the twelve doublets obtained from each of the parent doublet being arranged almost in the same fashion as the absorption lines in a hyperfine group of Eu^{2+} EPR spectrum. The relative positions of the four parent doublets are obtained by diagonalization of the matrix of the spin-Hamiltonian (given on page 23 of chapter II) after putting $H = 0$, and using the experimental values of various b_n^m parameters . The four doublets are found to be separated by 0.082 , 0.125 and 0.184cm^{-1}.

Table V.1

Spin-Hamiltonian parameters for Eu^{2+} in KCl, NaCl and KI at 25°C. Here $b_2^m = 3B_2^m$, $b_4^m = 60B_4^m$ and $b_6^m = 1260B_6^m$.

Parameter	Eu^{2+} in NaCl[a] $\times 10^{-4} cm^{-1}$	Eu^{2+} in KCl (present work) $\times 10^{-4} cm^{-1}$	Eu^{2+} in KI[b] $\times 10^{-4} cm^{-1}$	Eu^{2+} in KCl[c] in gauss
g	1.994±.002	1.994±.002	∥2.009±.01 ⊥1.995±.002	1.9922±.0006
b_2^0	265± 3	-218.3±3.2	235±3	342.5±1
b_2^2	646± 3	-462.9±6.5	-486±9	
b_4^0	-2.4±1.0	1.70±.25	-3.0±1.2	-4.9±0.2
b_4^2	50±10	-25.2±1.8	-72 ± 12	
b_4^4	26±8	-20.2±2.5	60±15	
b_6^0		.50±.15		0.3±0.2
$b_6^2 + b_6^6$*		-5.9±1.5		
b_6^4		4.6±2.5		
A^{151}	31.1± .3	-30.5±.3		
A^{153}	13.8±.2	-13.5±.2		

* b_6^2 and b_6^6 could not be separated because spectra were analysed only along the principal axes.

a From reference (5).

b From reference (7).

c From reference (8).

Table V.2

Classification of the orientation of fine structure axes with respect to H. Also given are the symbols by which the corresponding spectra are marked in figures 5.1 and 5.2

H. parallel to	θ	ϕ	Abundance*	Symbol
$\langle 001 \rangle$	90^0	90^0	4	A
	45^0	0^0	8	B
$\langle 110 \rangle$	0^0	-	2	C
	90^0	0^0	2	D
	60^0	$\frac{1}{2}\cos^{-1}(-1/3)$	8	Not marked in figure

* Abundance indicates the number of different orientations of the fine structure tensor which could be represented by the set of θ and ϕ given in the corresponding row.

REFERENCES

(1) G. D. Watkins, Phys. Rev. 113, 79 (1959).

(2) K.Morigaki, M. Fujimoto and J. Itoh, J. Phys. Soc.(Japan) 13, 1174 (1958).

(3) Y. Yokozama and Y. Kazumata, J. Phys. Soc. (Japan) 16, 694 (1961).

(4) K. N. Shrivastava and P. Venkateswarlu, Proc. Indian Acad. Sci. LXIII, 284 (1966).

(5) R. Rohrig, Phys. Letters 16, 20 (1965).

(6) S. D. Pandey, J. Chem. Phys. 47, 3094 (1967).

(7) F. Porret and E. Lambert, Helv. Phys. Acta 40, 264 (1967).

(8) P. G. Nair, K. V. Lingam and B. Venkataraman, J. Phys. Chem. Solids. 29, 2183 (1968).

(9) Q.H.F. Urehen and J. Volger, Physica 31, 854 (1965).

(10) W. E. Bron and W. R. Heller , Phys. Rev. 136, A1433 (1964).

(11) B. R. Judd and I. Lindgren, Phys. Rev. 122, 1802 (1962).

(12) R. Reisfeld and A. Glasner, J. Opt. Soc. (America) 54, 331 (1964).

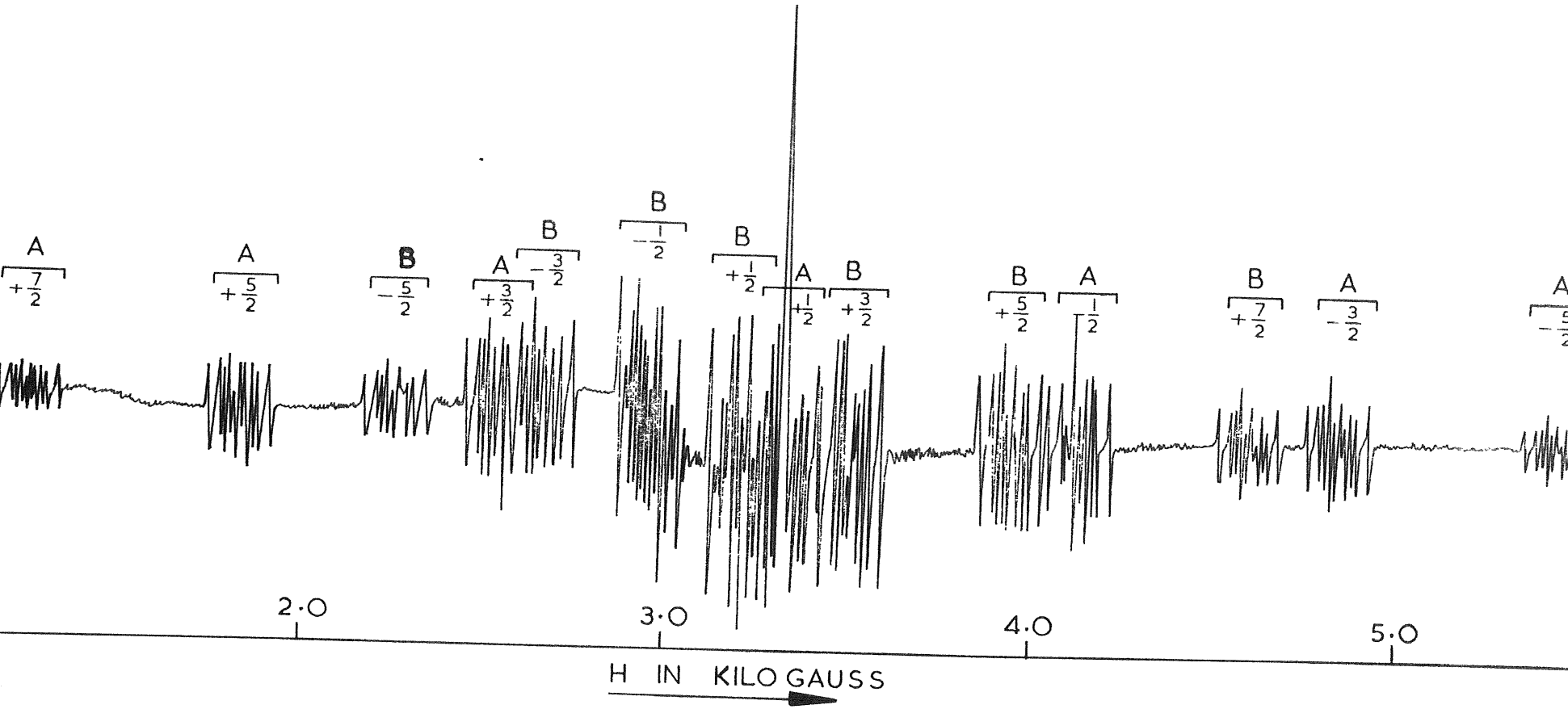

5.1 EPR SPECTRUM OF Eu^{2+} IN KCl AT 25 °C WITH H//<001>. M STANDS FOR THE TRANSITION -1. THE SYMBOLS A AND B ARE AS EXPLAINED IN TABLE V.2.

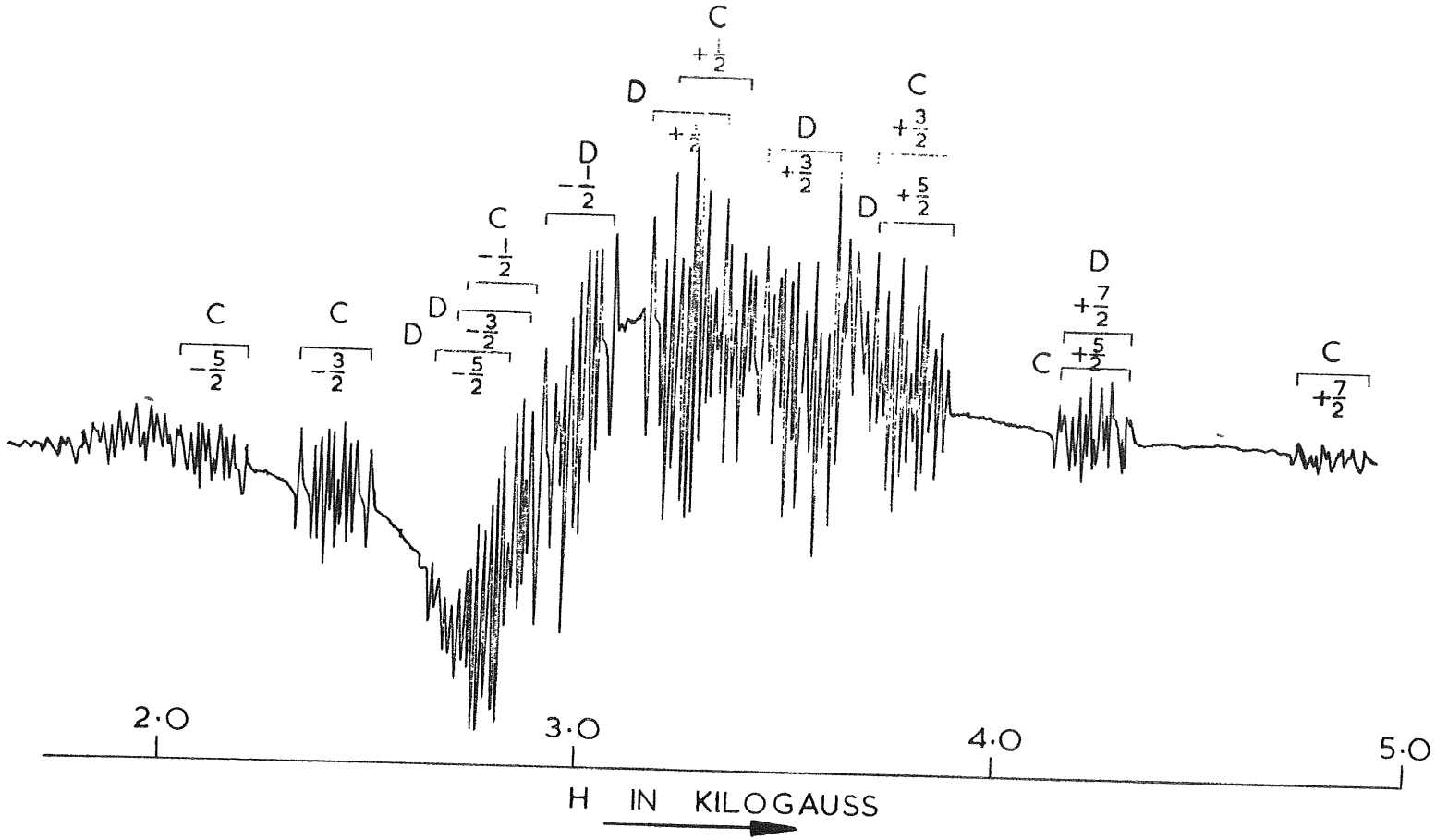

FIG.5.2 EPR SPECTRUM OF Eu^{2+} IN KCl AT 25 °C WITH H//<110>. M STANDS FOR THE TRANSITION M⟷M−1. THE SYMBOLS C AND D ARE AS EXPLAINED IN TABLE V.2

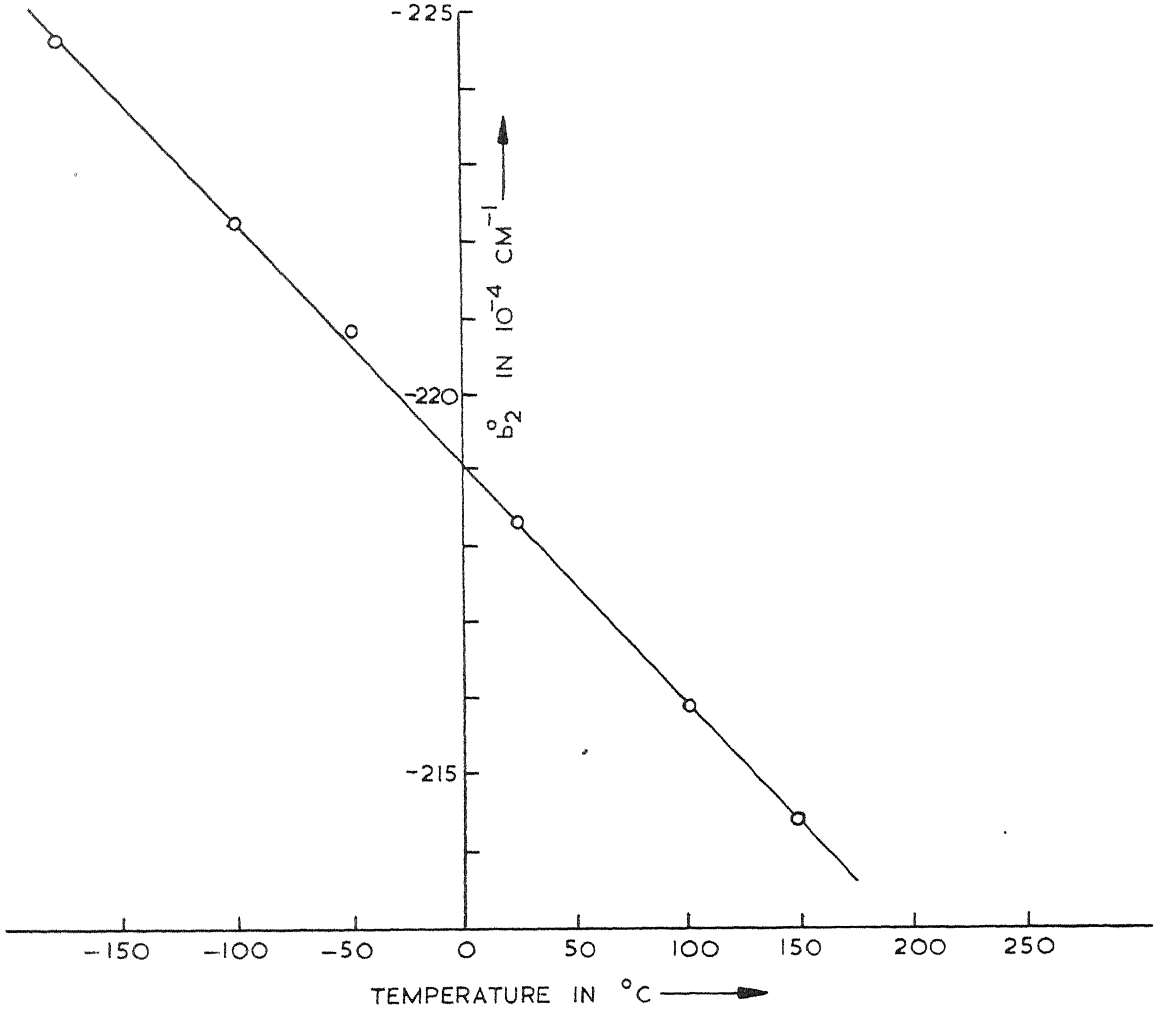

5.5.3 VARIATION OF b_2^o WITH TEMPERATURE FOR Eu^{2+} DOPED KCl.

CHAPTER VI *

ELECTRON PARAMAGNETIC RESONANCE OF Eu^{2+}-DOPED RbCl

Abstract

Two types of spectra, one orthorhombic and the other cubic have been observed for Eu^{2+} in RbCl single crystal host. The orthorhombic spectrum is similar to that observed in other alkali halides. The corresponding crystal field parameters are determined. From the results of chapter V it is known that the crystal field parameter b_2^0 is negative for Eu^{2+}-doped alkali chlorides. But it is positive for Mn^{2+} associated with a first neighbour cation vacancy in alkali chlorides. The absolute value of b_2^0, however, increases for both Mn^{2+} and Eu^{2+}-doped alkali chlorides if the alkali ion is replaced by the one (another alkali ion) following it in the periodic table. A qualitative explanation is suggested by considering the simultaneous linear and quadratic dependence of b_2^0 on $A_2^0 \langle r^2 \rangle$, the radial factor in the second order term of the crystalline field potential, A_2^0 being a lattice sum. The abnormal widths of the lines are related to probable off-centre positions of Eu^{2+} in the RbCl host. The spectrum which builds up in intensity at $\sim 200^0$C is confirmed to be cubic. The upper limits of its b_4^0 and b_6^0 parameters are estimated.

---

* A paper based on a part of the work presented in this chapter is to appear in Chem. Phys. Letters vol 3, No. 6 or 7 (1969).

INTRODUCTION

As reported in chapter V , the magnitude of the parameter b_2^0 for Eu^{2+} decreases as we move from NaCl to KCl host. This is contrary to what has been observed in the case of Mn^{2+} - doped alkali chlorides. In order to find out whether the magnitude of b_2^0 further decreases if we move to RbCl, a study of the electron paramagnetic resonance (EPR) spectrum of Eu^{2+}-doped RbCl is undertaken. Further such a study is expected to give information about the manner Eu^{2+} gets into the RbCl host crystal and also about the lattice defects, if any. It may be noted here that no EPR studies on Eu^{2+} in RbCl have been reported as yet in the literature.

Rohrig[1] and Porret and Lambert[2] have reported the EPR of Eu^{2+}doped in NaCl and KI respectively, whereas Eu^{2+}-doped KCl has been studied by the author[3] and Nair, Lingam and Venkataraman[4]. All of them report a prominent orthorhombic spectrum for the ion with line widths as are normally encountered in diamagnetic hosts. In this chapter a study of Eu^{2+}-doped RbCl is reported and the observed line widths, which are abnormally large, are attributed to the probable off-centre positions of Eu^{2+} ion in RbCl.

Two types of spectra have been obtained. The first one exhibits an orthorhombic site symmetry for the magnetic ion and will be called an orthorhombic spectrum. The second one indicates a cubic site symmetry for the magnetic ion and will be called a cubic spectrum. The orthorhombic spectrum is shown in figures 6.1, 6.2 and 6.6 for different orientations and temperatures of the crystal while figures 6.8 and 6.9 show the cubic spectrum. The orthorhombic spectrum shows

the expected fine structure involving the seven transitions $M \leftrightarrow M-1$ and a partly resolved hyperfine structure. The hyperfine structure is better resolved in the cubic spectrum at high temperatures (figures 6.8 & 6.9). As indicated in chapter II Eu has two isotopes Eu^{151} and Eu^{153} with almost equal natural percentage abundances (47.82 and 52.18% respectively). The spin of both nuclei is 5/2 and one expects a total of 12 hyperfine structure lines if the spectrum is well resolved.

ORTHORHOMBIC SPECTRUM

As far as the total spread and its angular variation is concerned, the orthorhombic spectrum obtained for Eu^{2+}-doped RbCl is found to have the same nature as reported in chapter V for Eu^{2+}-doped KCl. (The x,y, and z-axes of the crystalline field acting on the Eu^{2+} ion lie respectively along $\langle \bar{1}10 \rangle$, $\langle 001 \rangle$ and $\langle 110 \rangle$, and other symmetry related directions). The same convention as in chapter V of designating the spectra by the pair of angles (θ, ϕ) is, therefore, followed. Here θ is the angle between the direction of the magnetic field H and the z magnetic axis and ϕ represents the angle which the projection of H in xy plane of magnetic axes makes from the x-axis. As shown in figure 6.1 $(90^0, 90^0)$ and $(45^0, 0^0)$ spectra are obtained for $H // \langle 001 \rangle$, and as in figure 6.2 $(0^0, -)$ and $(90^0, 0^0)$ spectra are observed when $H // \langle 110 \rangle$. The $(60^0, \frac{1}{2}\cos^{-1}(-1/3))$ spectrum which should appear when $H // \langle 110 \rangle$ is completely masked by the lines of the other spectra due to increased line widths.

Because of the above mentioned similarities in the spectra of Eu^{2+} in KCl and RbCl hosts, the same model as in

Eu^{2+}- doped KCl of a defect in ⟨110⟩ direction is assumed to hold true for Eu^{2+}- doped RbCl too. The spectra for Eu^{2+}-doped RbCl have some peculiarities mainly with regard to the widths of the lines. As seen in figure 6.1, out of the two sets of spectra $A \equiv (90^0, 90^0)$ and $B \equiv (45^0, 0^0)$ observed for H// ⟨001⟩ , the hyperfine groups corresponding only to the set A which has more separation as compared to the other (B) are unmasked from the neighbouring groups. The hyperfine groups of the set B have much of overlap. In the case of KCl host all the lines of the set $(90^0, 90^0)$ had a width of~ 6gauss, but in RbCl host the corresponding widths show much of variation. As most of the hyperfine groups were unresolved, because of abnormal widths, which were present even at liquid Nitrogen temperature, the centres of the hyperfine groups were taken as the approximate positions of the fine structure transitions.

The following spin - Hamiltonian suitable for orthorhombic symmetry (see chapter II) is used:

$$\mathcal{H} = g\beta \vec{H}.\vec{S} + \sum_{k=0}^{1} (1/3)\, b_2^{2k}\, O_2^{2k} + \sum_{k=0}^{2} (1/60)\, b_4^{2k}\, O_4^{2k} \quad \ldots(6.1)$$

wherein g, β , b_n^m and O_n^m have the usual meanings as defined in chapter II. In this expression the higher order terms are neglected taking into consideration the limited accuracy of the line positions. Now as the hyperfine lines are not resolved in all the hyperfine groups and, moreover, the separation of the spectrum is less as compared to that in the case of Eu^{2+}- doped KCl, it was not possible to sort out all the hyperfine groups for $(90^0, 0^0)$ and $(0^0, -)$ spectra (see figure 6.2) . In fact, for the $(90^0, 0^0)$ set only the extreme hyperfine group on the high field side, D(+7/2), was free of overlap.

Therefore, the method of second order perturbation calculation as described in chapter II and actually adopted for the case of Eu^{2+}-doped KCl could not be used to find all the relevant b_n^m parameters. The following least square fitting procedure was, therefore, used to find the parameters.

An 8 x 8 matrix was formed for each of the four sets $(0^\circ,-)$, $(90^\circ,0^\circ)$, $(90^\circ,90^\circ)$ and $(45^\circ, 0^\circ)$ of (θ,ϕ). The matrix elements for the set $(0^\circ,-)$ are obtained with the help of the expression (6.1) for the Hamiltonian. To adopt for the general (θ,ϕ) case we transform the operators O_n^m to a new system of coordinates whose z-axis makes the polar angles (θ,ϕ) with the principal axes of the crystalline field, whence the following expression is obtained for the spin Hamiltonian

$$\mathcal{H} = g\beta \vec{H}.\vec{S} + \sum_{m=0}^{2} (1/3)\, a_2^m\, O_2^m + \sum_{m=0}^{4} (1/60)\, a_4^m\, O_4^m \quad \ldots(6.2)$$

Here a_n^m are functions of b_n^m and of angles (θ,ϕ) as given in the explicit form by Vinokurov et al[5] and Holuj[6]. The sign of b_2^0 in the expression for a_2^1 as given by Vinokurov et al[5] and Holuj[6] is wrong and is corrected, accordingly. Using the four 8 x 8 matrices thus obtained, the field positions of the various transitions ($\Delta M = \pm 1$) can be found. The $H_o \equiv 2.0036 \times H_{DPPH}/g$ and the b_n^m parameters are, accordingly, varied in an iterative way so that the calculated field positions for the different selected hyperfine groups have minimum r.m.s. deviation from the observed positions. It should be mentioned here that the positions of the five of the seven hyperfine groups for the $(45^\circ, 0^\circ)$ set are easily obtained and, hence, are included while finding the best fit parameters. The

starting values of some of the parameters are obtained from a second order perturbation calculation (mentioned in chapter II), while those of the rest are taken to be zero. For computation an IBM - 7044 computer was used. Various parameters thus obtained are given in table VI.1. b_2^0 is assumed to have the same sign (negative) as actually found in the case of Eu^{2+}-doped KCl, because the magnitude of all the b_n^m parameters in the KCl and RbCl hosts are comparable. The minimum r.m.s. deviation* was found to be 10 gauss. For the sake of convenience in comparison the corresponding parameters for Eu^{2+} in NaCl and KCl are also quoted in table VI.1. The parameters for NaCl are quoted by making a change in their signs. with this choice of the signs all the b_n^m parameters in the three hosts NaCl, KCl and RbCl have comparable values.

In table VI.2 the b_2^0 parameter for all the Mn^{2+} and Eu^{2+}-doped alkali chlorides studied to this date are quoted. While quoting these values the local two fold site symmetry axis is chosen to be the z-axis. We find that the magnitude of b_2^0 for Eu^{2+} continuously decreases in the series of three hosts namely NaCl, KCl and RbCl. The absolute value of b_2^0, however, increases from NaCl to RbCl. This change is similar to that observed in Mn^{2+}- doped alkali chlorides.

Qualitative explanation for the observed variation in b_2^0 for Mn^{2+}- and Eu^{2+} - doped alkali chlorides.

Watanabe[7] and Hutchinson, Judd and Pope[8] have suggested respectively for Mn^{2+} and rare earth S-state ions that the b_2^0 consists of two terms, one depending linearly on $A_2^0\langle r^2\rangle$ and the

* between the calculated and the experimental positions of the hyperfine groups.

other having a quadratic dependence on $A_2^o\langle r^2\rangle$. $A_2^o\langle r^2\rangle$ is the radial factor in the second order term of the crystalline field potential and has the dependence of $1/R^3$, R being the average separation of the charge on impurity ion from that on the neighbouring anions. A_2^o is a lattice sum. In the event of a vacancy being associated with the divalent impurity as is the case for Eu^{2+} and Mn^{2+}-doped alkali chlorides the effect of the vacancy would be the major one in determining the value of b_2^o. In such a case b_2^o could be represented by an expression of the type

$$b_2^o = a/R^3 - b/R^6 \qquad \ldots (6.3)$$

R being the distance of the vacancy from the impurity ion.

If we plot the value of b_2^o as given by equation (6.3) as a function of R, we get a curve as shown in figure 6.3. The curve crosses the axis of x at a value of $R = (b/a)^{1/3}$ and has a maximum at $R = (2b/a)^{1/3}$.

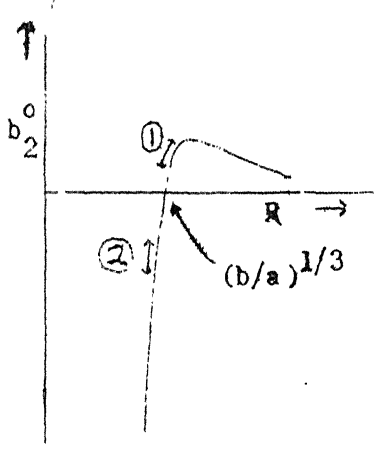

Figure 6.3

It is evident from table VI.2 that for Mn^{2+}-doped alkali chlorides in changing the host from LiCl to KCl we vary the parameter R from 3.67 to 4.48Å, whereas for Eu^{2+}-doped alkali chlorides R changes from 4.02 to 4.68 Å in going from NaCl to RbCl . It seems that for Mn^{2+} b and a are of such values so that we have $(b/a)^{1/3} \ll 3.67$ and for Eu^{2+} they are of such values so as to make $(b/a)^{1/3} \gg 4.68$. Such a large difference

in the values of $(b/a)^{1/3}$ for Mn^{2+} and Eu^{2+}-doped alkali chlorides is not ruled out as the Eu^{2+} ion is shielded by $5s^2 5p^6$ electrons and in Mn^{2+} the $3d^5$ electrons are the outermost ones. With such widely different values of $(b/a)^{1/3}$ for the ions we would be somewhere in the range indicated by (1) for Mn^{2+} and the range indicated by (2) for Eu^{2+} (Fig. 6.3).

Line widths, their estimation and probable explanation of their origin.

Because of overlap the line widths of the individual hyperfine lines could not be determined directly; An indirect method of comparing the contour obtained by considering the overlap of twelve lines of gaussian shape at relative distances appropriate to the Eu^{2+} ion with the observed line shapes of the hyperfine group was, therefore, adopted. The algebraic addition of the line shapes was done with the help of an IBM 7044 computer. Figure 6.4 shows the observed and computed first derivative contours of $5/2 \leftrightarrow 3/2$ and $-1/2 \leftrightarrow -3/2$ transitions for $H // \langle 001 \rangle$. The peak to peak (pp) derivative line widths, $(\Delta H)_M$ for the hyperfine lines of the various fine structure transitions (hyperfine groups) $M \leftrightarrow M-1$, as determined by the method described above are given below:

$$(\Delta H)_{3/2} \simeq (\Delta H)_{-1/2} = 20 \pm 4 \text{ gauss}$$

$$(\Delta H)_{5/2} \simeq (\Delta H)_{-3/2} = 42 \pm 6 \text{ gauss}$$

& $$(\Delta H)_{-5/2} = 65 \pm 11 \text{ gauss}$$

But $(\Delta H)_M = 65$ gauss, did not give a good fit for the contour of $M = +7/2$ hyperfine group, $(\Delta H)_M$, as found above, are found to vary very nearly as $|(2M-1)|$ and the mean value of $(\Delta H)_M / |(2M-1)|$

into a nice cuboid.

This abnormality in the linewidths can not be attributed to superhyperfine interaction (with Rb^+ ions) as it would not lead to observed M-dependence.

In recent years it has been reported that when the radius of the impurity ion is much less than that of the host cation, the impurity could have stable off-centre positions[9-11]. The stable off-centre positions have been experimentally concluded to exist from the quadrupole resonance study of Li^+ and Cu^+ doped KCl[12]. Das and Quigley[13] have calculated off-centre potential minima for Li^+-doped KCl and KBr and for Na^+-doped CsF. The minima are explored along ⟨111⟩ , ⟨110⟩, and ⟨001⟩ crystal axes. The potential energy is found to be minimum for off-centre positions along ⟨111⟩ , whereas the minima along ⟨110⟩ and ⟨001⟩ have increasingly more energy, e.g. , for a typical case of Li^+-doped KCl the theoretically calculated minima along ⟨001⟩ , ⟨110⟩ and ⟨111⟩ by Das and Quigley[13] are -0.762, -0.772 and -0.780 ev respectively. They have also mentioned a possibility of detecting stable off-centre minimum energy configurations through a variation of b_2^0 ($\equiv$ D) parameter, when a suitable paramagnetic ion is doped in a host whose cation radius is much larger than that of the impurity ion. The ionic radius of Rb^+ is 1.47 Å and that of Eu^{2+} is 1.14 Å[14]. The difference in the radii of these ions is quite appreciable. On this basis one might expect stable off-centre positions for Eu^{2+} in RbCl similar to that found in the case of Li^+ in KCl. Since for Eu^{2+} the $5s^2 5p^6$ shell shields the $4f^7$ electrons and bestows on the ion a semblance of an inert structure , at least as much as it remains

relatively isolated from the surroundings, one may extend the results of Li^+- doped KCl to Eu^{2+}-doped RbCl with due caution . It may be mentioned here that an extension of the results of Li^+-doped KCl to Mn^{2+}-doped KCl or RbCl can not be justified, since in this case the 3d electrons are the outermost and participate directly in interactions with their surroundings whereas the $4f^7$ electrons interact through the intermediary of the $5s^2 5p^6$ shell.

One may assume in the case of Eu^{2+}-doped RbCl that the potential minima along ⟨111⟩ , ⟨110⟩ and ⟨001⟩ shall be in increasing order of energy. In actual case, however, there might be a 3-dimensional shell of potential minima with extreme (minimummost) values along ⟨111⟩ axes. At room temperature the thermal energy (~.025 ev.) is of the order of the variation in energy on the minimum potential shell. Most probable positions of Eu^{2+} shall be 1 through 8, as shown in Fig. 6.5. These are along ⟨111⟩ . There will be a wide scatter about these positions as the thermal energy at room temperature is appreciable. In the absence of an off-centre displacement the vacancy is at a distance of $a\sqrt{2}$ along ⟨110⟩ from the Eu^{2+} position, 'a' being the nearest neighbour distance in the lattice. If off-centre displacement of magnitude x along ⟨111⟩ axes is taken into consideration, the distance between the vacancy and the Eu^{2+} ion position can have three distinct values d_{min}, d_{max} and d for eight possible positions of Eu^{2+} viz. d_{min} for the positions 7 and 8, d_{max} for the positions 5 and 6, and d for the positions 1, 2, 3 and 4 . These d's are given by the formulae (6.6) given on next page:

$$d_{max} = \left[(a+x/\sqrt{3})^2 + (a+x/\sqrt{3})^2 + (x/\sqrt{3})^2\right]^{1/2} \simeq a\sqrt{2} + x\sqrt{2/3}$$

$$d_{min} = \left[(a-x/\sqrt{3})^2 + (a-x/\sqrt{3})^2 + (x/\sqrt{3})^2\right]^{1/2} \simeq a\sqrt{2} - x\sqrt{2/3}$$

$$d = \left[(a-x/\sqrt{3})^2 + (a+x/\sqrt{3})^2 + (x/\sqrt{3})^2\right]^{1/2} \simeq a\sqrt{2} \qquad \ldots (6.6)$$

The line joining the Eu^{2+} ion positions and the vacancy however would not be parallel to $\langle 111 \rangle$, but it would be nearly so within 4° if $x \lesssim a/10$, as is expected.

In a point charge approximation, assuming no distortion of the lattice, the b_2^0 ($\equiv D$) and b_2^2 ($\equiv E$) vary nearly as d^{-3}. Assuming $x \lesssim a$, the effective parameter $b_2^{0\prime}$ for $H \parallel \langle 001 \rangle$ would also vary as inverse cube of d. Therefore, with these approximations we will have three distinct values of $b_2^{0\prime}(\equiv D')$ viz. D'_{min}, D'_{max} and D' corresponding to the three values of d. (In actual case, however, there would be a spread of D' about these three values). So each hyperfine line may be consisting of three lines, one corresponding to each of the three values D'_{min}, D'_{max} and D' of $b_2^{0\prime}$. At room temperature and for $H \parallel \langle 001 \rangle$ of the crystal a faint hump shows itself up in the extreme hyperfine lines of $M = +3/2$ and $M = -1/2$ transitions (Fig.6.7). This building up of the structure is, perhaps, indicative of the composite nature of the hyperfine lines. We assume that these lines are on the verge of splitting and that each of the three constituent lines are gaussian of same peak to peak derivative width, but with intensity ratios 1:2:1 as expected. By considering the overlap of such lines we are led to the conclusion that $(D'_{max} - D'_{min}) \lesssim$ p-p derivative width of the three component lines and

also of the width of the composite line. (In the transition $M = +7/2$ for $H // \langle 001 \rangle$ we find some structure which is not explained by considering the simple overlap of twelve gaussian lines. This, perhaps, too, is because of the composite nature of the hyperfine lines.)

While finding the $(\Delta H)_M$ for the hyperfine lines corresponding to a fine structure transition $M \leftrightarrow M-1$, we had assumed a gaussian shape for the individual hyperfine lines. But this may not be rigorously true (consider the building up of hump at low temperatures in figure 6.7). Now as the extreme hyperfine lines of the fine structure transition $3/2 \leftrightarrow 1/2$ are seen unmasked from the rest, the calculations for the determination of $(\Delta H)_M$ were repeated and instead of taking a gaussian shape for the individual hyperfine lines, we took the shape to be the same as that of the extreme hyperfine line of the group $M = 3/2 \leftrightarrow 1/2$. The $(\Delta H)_M$, thus found, almost equal those determined earlier. The mean value of $(\Delta H)_M / |(2M-1)|$ is, therefore, 10.5 gauss. Equation (6.5) then gives

$$\Delta D' \equiv \Delta b_2^{o\prime} = 10.5 \text{ gauss}$$

Now

$$D'_{max}/D'_{min} = d^3_{min}/d^3_{max}$$

Subtracting 1 from both sides

$$\Delta D'/D' = \left[(a\sqrt{2} + x\sqrt{2/3})^3 - (a\sqrt{2} - x\sqrt{2/3})^3\right]/(a\sqrt{2})^3$$

$$= 2x/a\sqrt{3}$$

therefore, $x = 3\,a.\,\Delta D'/2D' \cong .025a$ ...(6.7)

This value of x is of the same order as that calculated theoretically by Das and Quigley[13] for off-centre minima positions along ⟨111⟩ .

If the temperature of the crystal is raised, (for a particular position of the vacancy) the scatter of Eu^{2+} ion positions about the minimum energy position along ⟨111⟩ would increase. This would cause an increase in the width of the constituent lines. This, in fact, is evident from the experimental results. The hyperfine groups corresponding to M = 3/2 and M = -1/2, which were partially resolved at room temperature cease to be so at 300°C, as is clear from figure 6.6.

At liquid Nitrogen temperature the humps on M = 3/2 and M = -1/2 hyperfine groups become more pronounced as shown in figure 6.7, indicating a decrease in the width of the three constituents of the hyperfine lines. It would be interesting to make a study at liquid Helium temperatures, where the distance of the line corresponding to the hump from the main line could directly give the value of D′ and thence of x.

The non-observance of such abnormal linewidth in KCl, NaCl and KI hosts is consistent with the above explanation, as the difference in the radii of Eu^{2+} and the cation of these hosts is not large enough. As for other S-state ions e.g. Mn^{2+}, no abnormal widths are found in alkali halide hosts, since stable off-centre positions are probably not expected for the reason mentioned earlier.

CUBIC SPECTRUM

The temperature variation of the central part of the spectrum is shown in figures 6.8 and 6.9 from 80^{0}C to 280^{0}C in steps of 40^{0}C. As is evident from the figures a spectrum henceforth called C continuously builds up in intensity as the sample is heated. At about 200^{0}C the intensity of the spectrum C is at least twenty times to that of the orthorhombic spectrum.

The vacancies become more and more mobile on heating the crystal. The spectrum C, therefore, seems to be due to such Eu^{2+} ions which have no vacancy or defect in the nearby positions and is thus called the cubic spectrum. It has the looks of a usual twelve lines hyperfine group of the Eu^{2+} ion, for all orientations of H. Each line of the hyperfine group is, infact, a superposition of seven fine structure transitions represented by M=7/2 to M=-5/2. In the present case the magnitude of the cubic field splitting parameter $|b_4^0| << |A^{151}|$, therefore, the splitting due to the cubic field reflects itself in the width of the individual lines of the twelve lines' hyperfine group. The cubic field parameter b_4^0 has an angular dependence. The effective b_4^0 for any orientation (l,m,n) of H with respect to the cubic axes of the crystal is[15]

$$(b_4^0)_{eff.} = b_4^0 \left[1-5(l^2m^2+ m^2n^2+ n^2l^2)\right] \qquad ...(6.8)$$

l,m,n being the direction cosines of H with respect to the cubic axes. If $(b_4^0)_{eff}$ is large, the cubic field splitting would be large and the peak to peak derivative height of the composite line ~~would~~ would be small. Opposite would be the case if $(b_4^0)_{eff}$ is small. In

this way the value of $(b_4^0)_{eff}$ is reflected in the pp derivative height. From equation (6.8) we find that $(b_4^0)_{eff}$ would be the least and thus the pp derivative height would be the largest if θ, the angle between H and ⟨001⟩ direction in (100) plane is given by

$$\sin 2\theta = \sqrt{4/5} \quad \text{or, if } \theta = 31^0 42'$$

Indeed, as is clear from figure 6.10 the pp derivative height is found to be maximum for $\theta = 32.5^0$. This value of θ very nearly equals the one expected theoretically and thus it is confirmed that the twelve lines hyperfine group arises because of Eu^{2+} ions at the cubic sites.

The cubic spectrum has almost the same separation for both H//⟨001⟩ and ⟨110⟩ axes of the crystal and hence if it is fitted to the usual spin Hamiltonian for the cubic symmetry (see chapter II)

$$\mathcal{H} = g\beta \vec{H}.\vec{S} + b_4^0/60 \; O_4^0 + b_6^0/1260 \; O_6^0 + A \vec{I}.\vec{S} \qquad \ldots(6.9)$$

the magnitudes of the parameters b_4^0 and b_6^0 come out to be nearly equal to zero and at least less than $0.1 \times 10^{-4} cm^{-1}$. (The upper limit for the parameter b_4^0 is determined by studying the angular variation of the apparent peak to peak derivative widths of the extreme lines in the cubic spectrum observed). This may not be an inconceivable situation as the more significant of the two parameters, the b_4^0 is found to decrease monotonously from NaCl to RbCl, as is evident from the work of Rohrig[1], the author[3] and the present results. At 200°C, the g value of the spectrum is found to be $1.994 \pm .002$. The average widths of the lines are about 6 to 7 gauss. The hyperfine structure parameter A^{151} is determined to be $(-29.7 \pm 0.2) \times 10^{-4} cm^{-1}$.

Table VI.1

Spin - Hamiltonian parameters for Eu^{2+} in NaCl , KCl and RbCl at 25°C. Here $b_2^m = 3B_2^m$, $b_4^m = 60B_4^m$, $b_6^m = 1260B_6^m$ and all energy values are in units of $10^{-4}cm^{-1}$.

Parameter	Eu^{2+} in NaCl[a]	Eu^{2+}in KCl[b]	Eu^{2+}in RbCl*,[c]
g	1.994 ± .002	1.994 ± .002	1.993 ± .002
b_2^o	-265 ± 3	-218.3± 3.2	-213.6
b_2^2	-646 ± 3	-462.9± 6.5	-372.0
b_1^o	+2.4 ± 1.0	+1.7± .25	+1.3
b_1^2	-50 ± 10	-25.2± 1.8	-21.3
b_1^1	-26 ± 8	-20.2± 2.3	-14.6

* The r.m.s. deviation between the experimental & calculated fine structure line positions was ~10 Gauss.

a From reference (1)
b From reference (3), (see chapter V).
c Present work

Table VI.2

D ($\equiv b_2^0$) parameter for Mn^{2+} and Eu^{2+} , associated with a first neighbour cation vacancy in alkali chlorides. Two-fold local site symmetry axis has been chosen to be the z-axis. R represents the nearest neighbour cation separation.

ost system	D $\times 10^{-4}$ cm^{-1}	Lattice constant Å	R Å
LiCl: Mn^{2+}	109.5	5.14	3.67
NaCl: Mn^{2+}	128.9	5.63	4.02
KCl: Mn^{2+}	160.5	6.28	4.48
NaCl:Eu^{2+}	-265.0	5.63	4.02
KCl:Eu^{2+}	-218.3	6.28	4.48
RbCl:Eu^{2+}	-213.6	6.58	4.68

The corresponding D parameter is obtained by using Watkins' (Phys. Rev. 113, 79(1959)) results and accounting for the change in the z-axis .

The sign of D should be negative for Eu^{2+}-doped NaCl and RbCl, because with this choice of the sign the value of all the b_n^m parameters for Eu^{2+} in the three alkali chlorides NaCl, KCl and RbCl are comparable.

REFERENCES

(1) R. Rohrig , Physics Letters 16, 20 (1965).

(2) F. Porret and E. Lambert, Helv. Phys. Acta 40, 264 (1967).

(3) S. D. Pandey, J. Chem. Phys. 47, 3094 (1967).

(4) P.G. Nair, K. V. Lingem and B. Venkataraman, J. Phys. Chem. Solids 29, 2183 (1968).

(5) V.M. Vinokurov , M.M. Zaripov and V.G. Stepanov, Soviet Phys. Solid State (English Translation) 6, 870 (1964).

(6) F. Holuj, Can. J. Phys. 46, 287 (1966).

(7) H. Watanabe, Progr. Theoret. Phys. Japan 18, 405 (1957).

(8) C.A. Hutchinson, B.R. Judd and D.F.D. Pope , Proc. Phys. Soc. (London) B70 , 514 (1957).

(9) G. Lambardo and R.O. Pohl, Phys. Rev. Lett. 15, 291 (1965).

(10) H.S. Sack and M.C. Moriarity, Solid State Commun. 3, 93(1965).

(11) N.E. Byer and H.S. Sack, Phys. Rev. Lett. 17, 72 (1966).

(12) W.D. Wilson and M. Blume, J. Phys. Chem. Solids 29, 1169 (1968).

(13) T.P. Das and R.J. Quigley, Phys. Rev. 164, 1185 (1967).

(14) Q.H.F. Urehen and J. Volger, Physica 31, 845 (1965).

(15) H. Unoki and T. Sakudo, J. Phys. Soc. Japan 21, 1730 (1966).

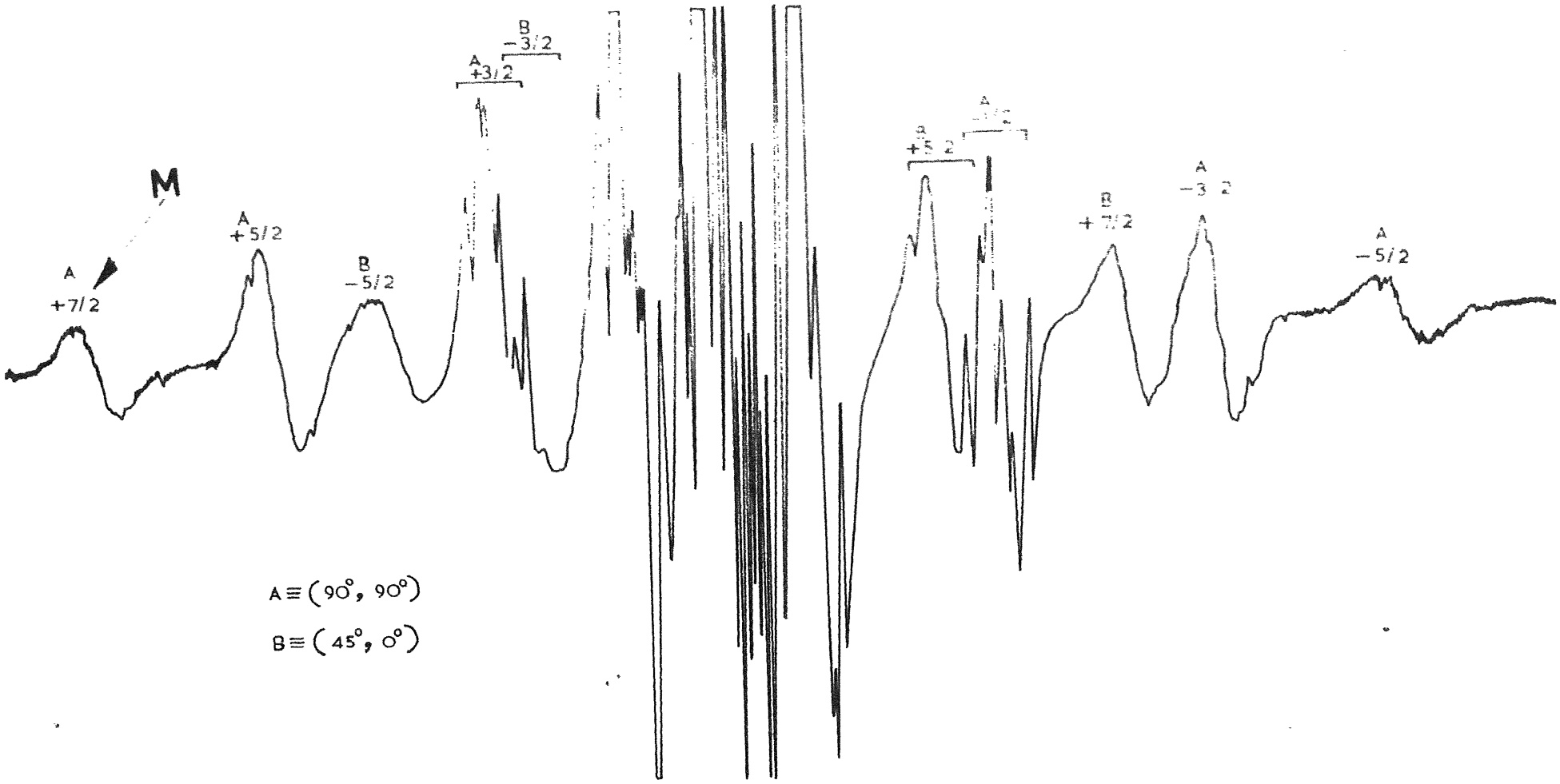

6·1 EPR SPECTRUM OF Eu^{2+} IN RbCl AT 25 °C WITH H // <001>. M STANDS FOR THE TRANSITION M ⟷ M−1.

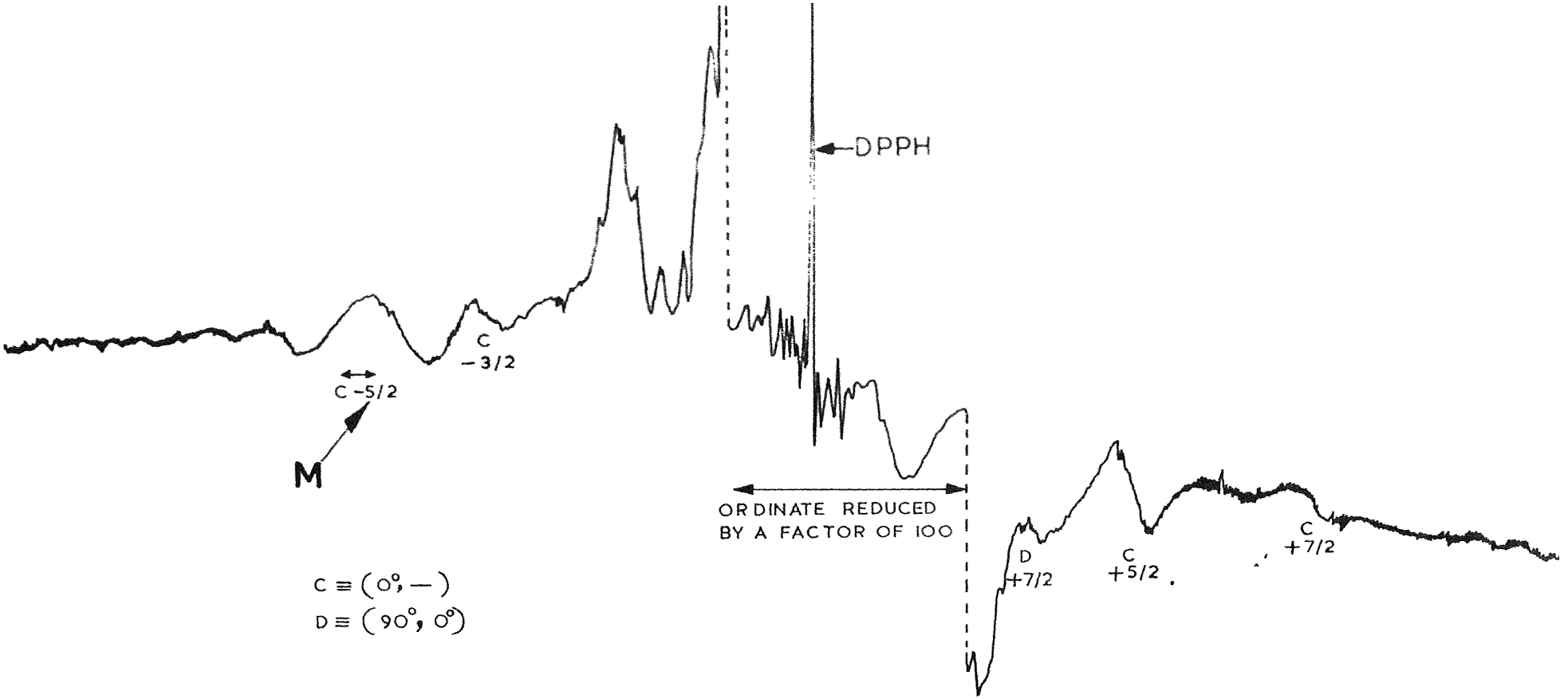

2 EPR SPECTRUM OF Eu^{2+} IN RbCl AT 25 °C WITH H //<110>. M STANDS FOR THE TRANSITION M ⟷ M−1. THE POSITION OF HYPERFINE GROUP CORRESPONDING TO C(−5/2) IS DETERMINED BY THE STUDY OF ANGULAR VARIATION.

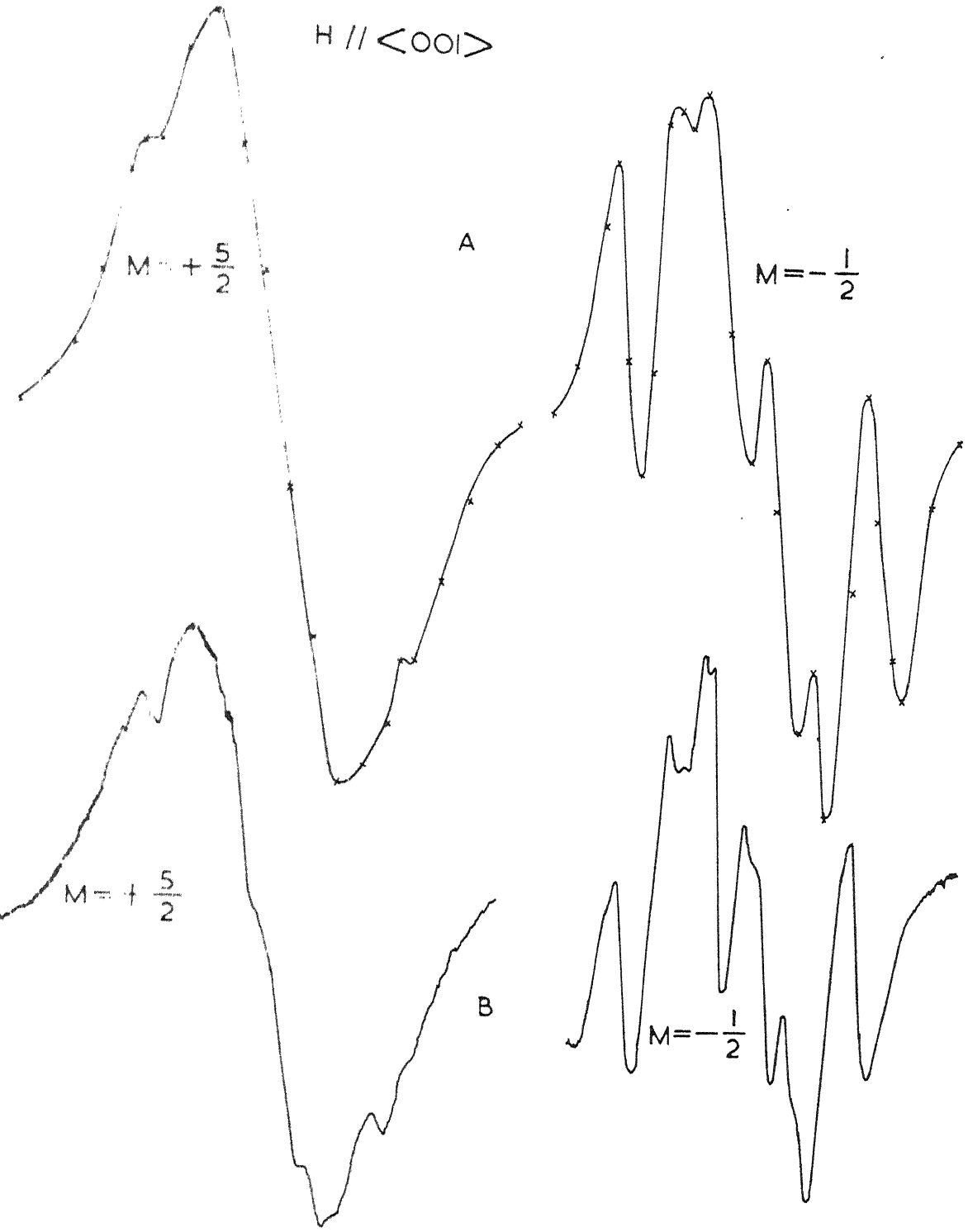

·4 FIRST DERIVATIVE CONTOURS FOR 5/2 ↔ 3/2 AND −1/2 ↔ −3/2 TRANSITIONS (NOT TO SCALE)

A = COMPUTED, B = EXPERIMENTAL

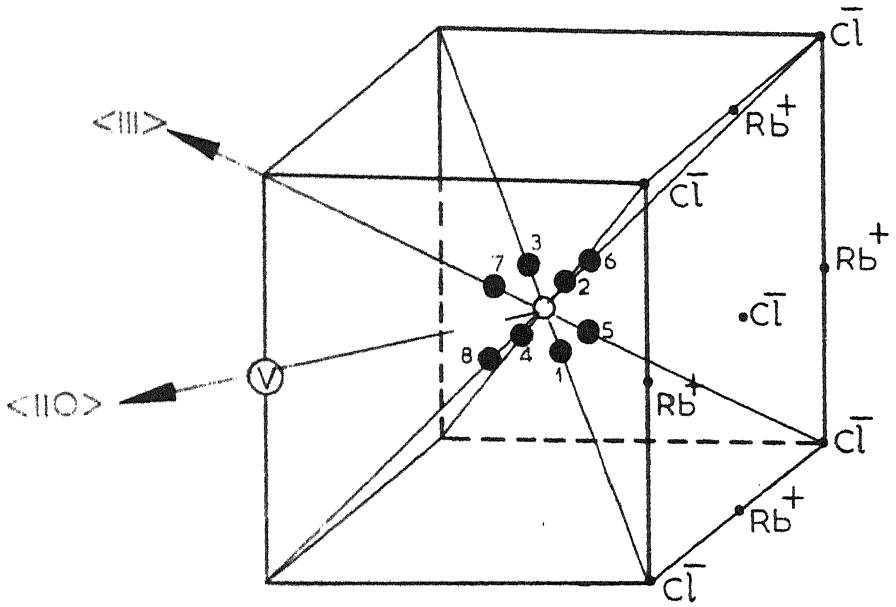

Ⓥ = Rb^+ VACANCY

O = USUAL Eu^{2+} POSITION

● = OFF-CENTRE Eu^{2+} POSITION

FIG.6·5 PROBABLE POSITIONS OF Eu^{2+} WITH RESPECT TO A VACANCY IN FIRST NEIGHBOUR Rb^+ POSITION, Rb^+ AND Cl^- IONS ARE SHOWN ON ONLY ONE FACE OF THE CELL.

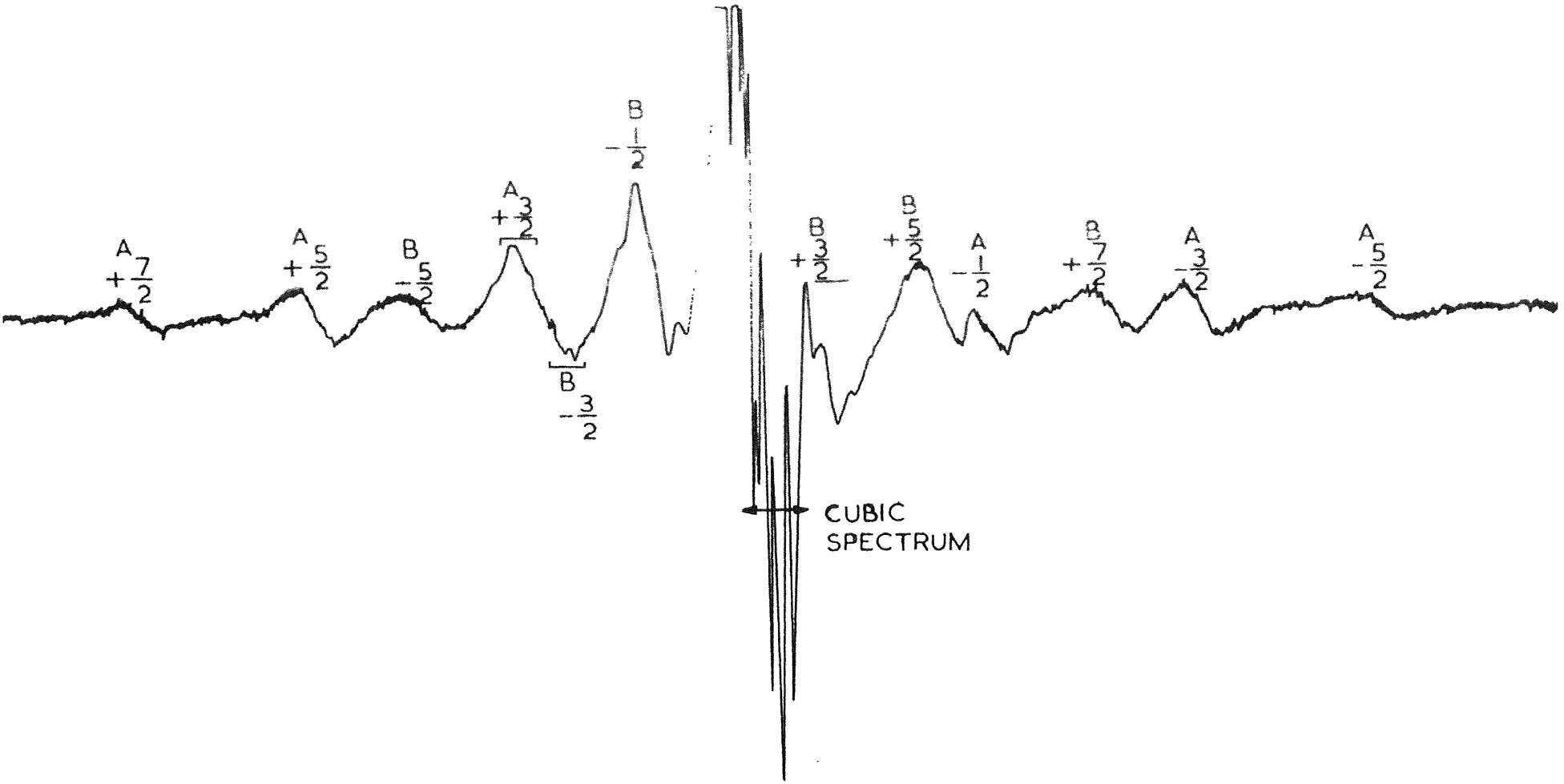

FIG. 6.6 EPR SPECTRUM OF Eu^{2+} DOPED RbCl AT 300°C.

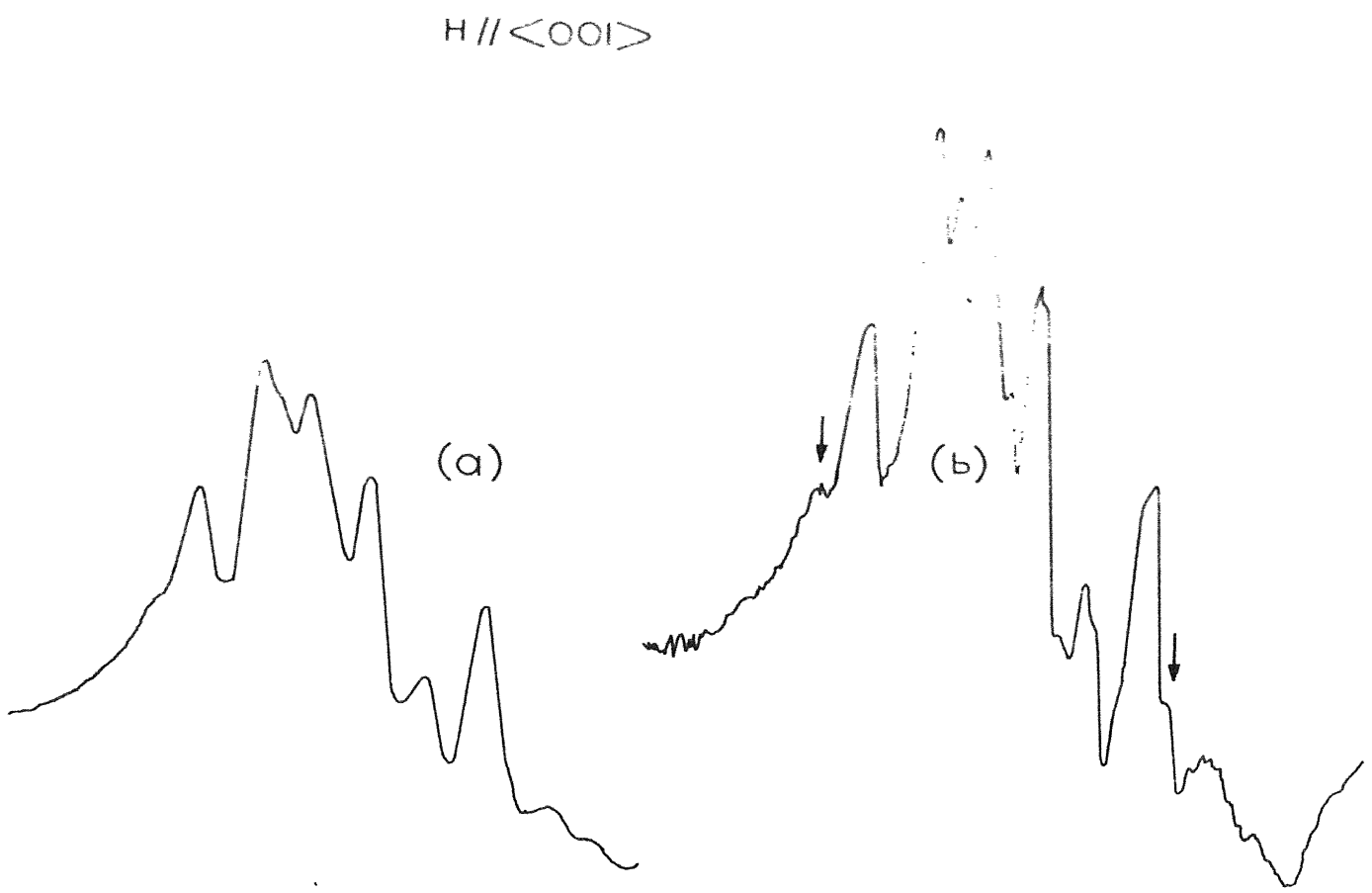

FIG. 6·7 EPR SPECTRA FOR 3/2↔1/2 TRANSITION AT (a) 25°C, (b) LIQUID-N_2 TEMPERATURE.

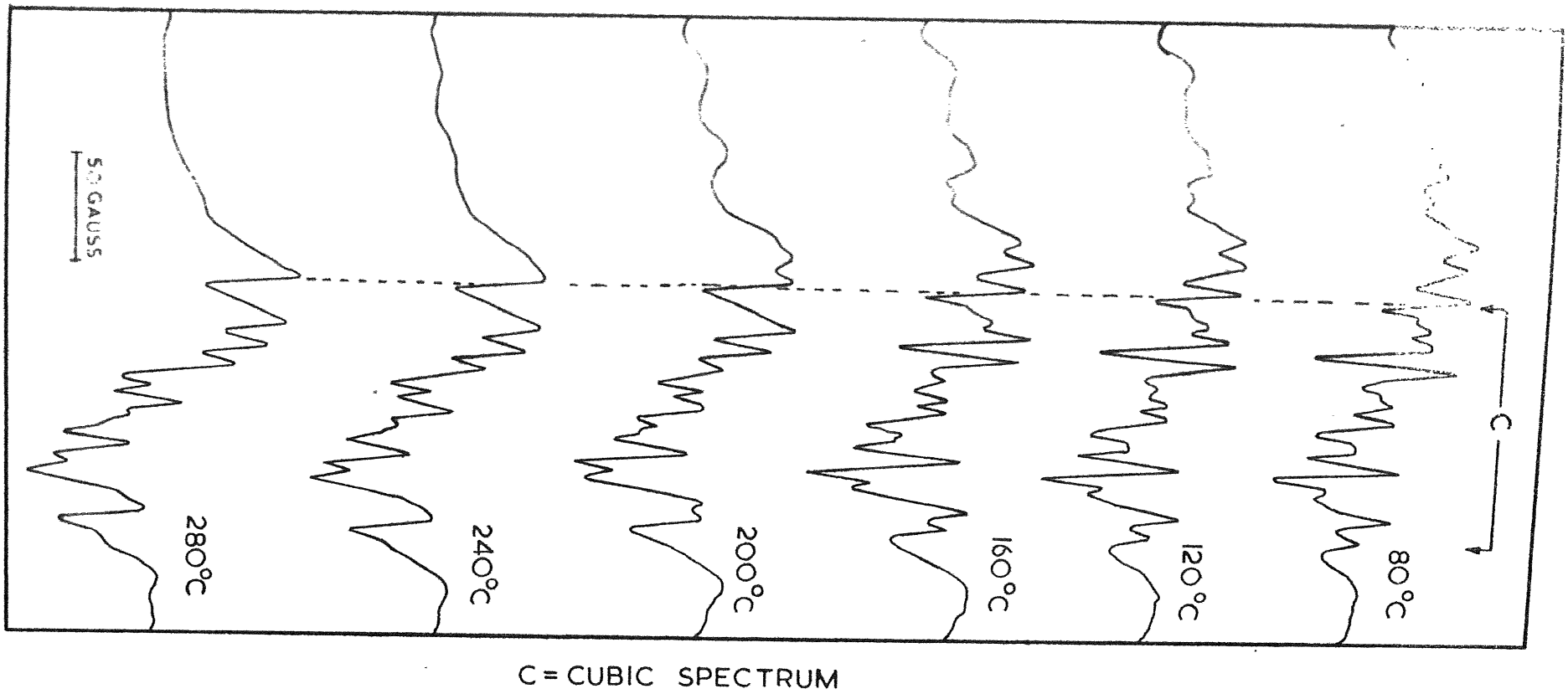

FIG. 6·8 TEMPERATURE VARIATION OF THE INTENSITY OF THE CUBIC SPECTRUM FOR H // <001>.

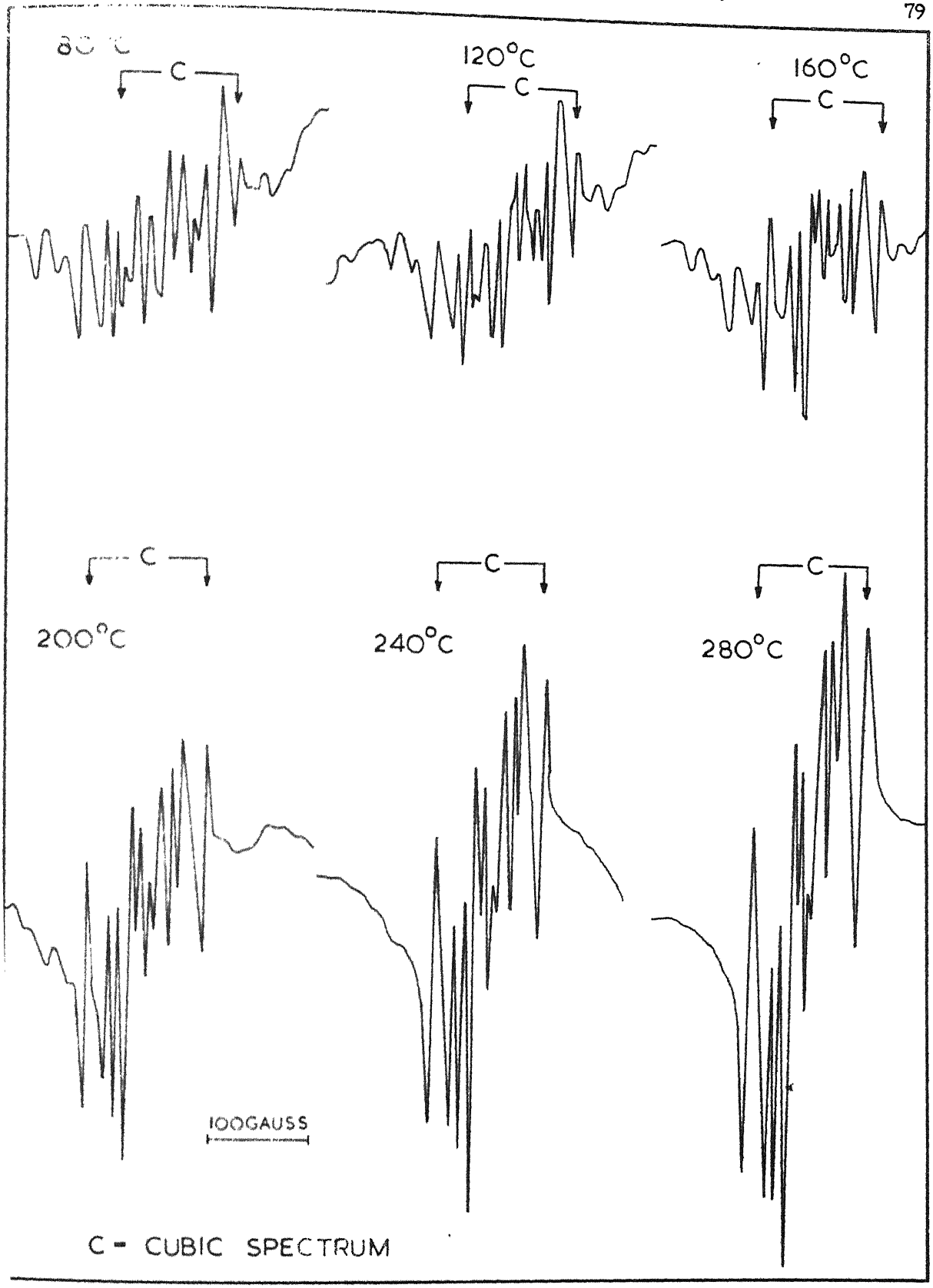

IG.6.9 TEMPERATURE VARIATION OF THE INTENSITY OF THE CUBIC SPECTRUM FOR H // <110>.

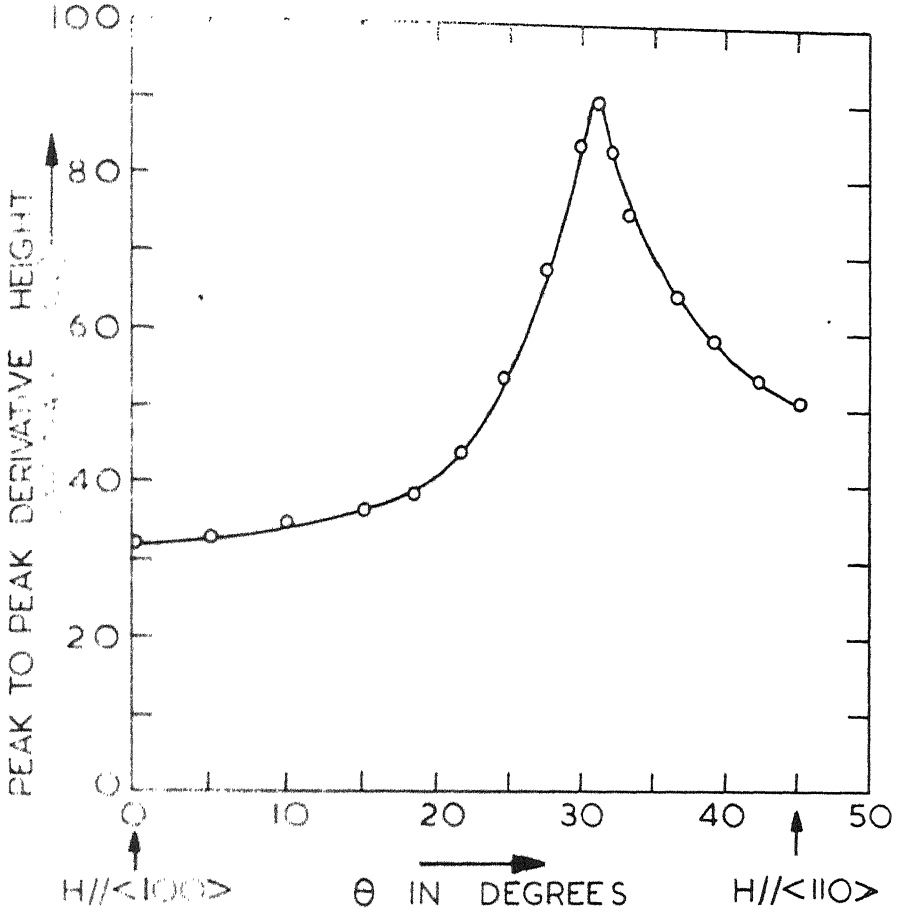

FIG. 6.10 ANGULAR VARIATION OF PEAK TO PEAK DERIVATIVE HEIGHT FOR THE CUBIC SPECTRUM OF Eu^{2+} — DOPED RbCl AT 300°C. θ REPRESENTS THE ORIENTATION OF H IN (001) PLANE.

CHAPTER VII

ELECTRON PARAMAGNETIC RESONANCE OF Mn^{2+}-DOPED RbCl AND OF 4RbCl. $MnCl_2$

Abstract

Mn^{2+} when doped in RbCl is found not to be associated with any vacancy or defect near it. The principal feature of the EPR spectrum for Mn^{2+} - doped RbCl is the occurrence of an exchange narrowed line with a g-value nearly equal to that of the electron. Some of the Mn^{2+} is also found to give a six line spectrum. The peak to peak (pp) derivative width and the g-value corresponding to the three concentrations of $MnCl_2$ in RbCl are reported. The formation of the complex Rb_4MnCl_6 from the stoichiometric ratio of RbCl and anhydrous $MnCl_2$ is envisaged. The pp derivative width is found to decrease as the concentration of Mn^{2+} in RbCl is increased. An attempt is made to understand as to why Mn^{2+} does not enter the substitutional sites, and further why Mn^{2+} ions prefer to accumulate together at nearby interstitial positions so as to give the exchange-narrowed line.

INTRODUCTION

The EPR of Eu^{2+} [1-5] and Mn^{2+} [6-9] has been studied in a number of alkali chloride hosts. The parameter b_2^0 for the spectrum III_1, which in the notations of Watkins[6] corresponds to the divalent impurity associated with a vacancy at the first neighbour cation position, has been determined for the two ions in many of the alkali chloride hosts. It is found to be positive for Eu^{2+} impurity and is negative for Mn^{2+}. The absolute value of b_2^0, however, decreases for both Eu^{2+} and Mn^{2+} as the host is changed in the series of alkali chlorides viz. for Mn^{2+} from LiCl to KCl and for Eu^{2+} from NaCl to RbCl. A formula which qualitatively explains the change of b_2^0 in the two cases was suggested in chapter VI.

The EPR of Mn^{2+} in RbCl has not been reported as yet. It would, therefore, be interesting to find the value of b_2^0 corresponding to the spectrum III_1 for Mn^{2+} in RbCl and then to compare the same with those of Mn^{2+} in other alkali chloride hosts. Therefore, an attempt to dope RbCl with Mn^{2+} was made. Several trials were made to dope RbCl with $MnCl_2$ so that Mn^{2+} in RbCl could get associated with a vacancy at a first neighbour cation position. But in the crystals grown from melt by the usual Stockbarger's method(described in chapter IV) no axial spectrum appeared. The crystals were then quenched at 600°C and further an attempt to introduce Mn^{2+} through diffusion was also undertaken, but all these attempts were of no avail.

In general the spectrum seemed to consist of one single line.

The proportional amount of $MnCl_2$ added to RbCl before the melting was varied with the hope that additional spectra might result, but every time only a single line spectrum appeared. Three different concentrations were tried. The peak to peak (pp) derivative width and the g-value of the single line are determined for each of these three concentrations. Some other features are also investigated. An explanation is sought for the nonoccurrence of first neighbour cation vacancy spectrum for Mn^{2+}-doped RbCl, and also for the occurrence of the exchange narrowed line even in lightly doped RbCl:Mn^{2+} crystals.

THE CRYSTAL GROWTH

The crystals were grown as described in chapter IV, by mixing RbCl and anhydrous $MnCl_2$ in a known ratio and then lowering the resulting mass through a temperature gradient. The crystals of two extreme concentrations designated as samples I and II were mainly investigated in the present work. For sample I, the amount of anhydrous $MnCl_2$ mixed with RbCl was ~.02% by weight of that of RbCl, while for the sample II the $MnCl_2$ and RbCl were mixed in the 1:4 ratio of their molecular weights. Sample I was nearly transparent with white turbidities. On the other hand the sample II was pink and polycrystalline. One more sample designated as III was prepared. The parent mixture for the sample III had ~ 1% of anhydrous $MnCl_2$ in it. The whole of the crystal grown from this mixture was not transparent. It seems that all of the Mn^{2+} present in the parent mixture could not enter the RbCl lattice. A part of the crystal was transparent while the portion which grew towards the end

of the growth process had some pink suspended mass in it.

THE EPR SPECTRA

The spectra of all the three samples I, II and III have the appearance of a usual exchange narrowed line. They are similar to that observed for Mn^{2+} - doped KCl particularly in the cloudy portion of it by Watkins[6]. The spectrum obtained for the sample I for H// ⟨1 0⟩ is as shown in figure 7.1. The spectra at other angles and of other two samples are similar in nature to that of figure 7.1, the only difference being in their g-values and the pp derivative widths.

The g-value and the pp derivative widths of the different spectra are determined and are given in table VII.1. For sample I the pp derivative width changed as the orientation of H in (001) plane was varied. It is maximum for H// ⟨100⟩ and continuously decreases as H is varied in (001) plane from a position//to ⟨100⟩ to that//to ⟨110⟩ . The spectrm due to sample II also showed a variation in its pp derivative width, with respect to the orientation of H. But as the sample II is polycrystalline, the variation of the pp derivative width of its spectrum was not studied, in detail. The pp derivative width for H// ⟨100⟩ and the g-value for the transparent portion of the sample III are also determined and are given in table VII.1. For the sample I the lowest portion of the crystal in the crystal growing crucible showed a weak cubic like spectrum (figure 7.4) as well. It has a g-value very nearly equal to that of the electron and has an A of magnitude 94.3 gauss. The spectrum of one more sample called IV, which was prepared by simply mixing RbCl and anhydrous $MnCl_2$ in the powder form and in the 4:1 ratio of their molecular weights, was also taken.

It was a broad line with pp derivative width of ~580 gauss and a g - value equal to that of the electron. The g-value and the pp derivative width for K_4MnCl_6 as reported by Swanson, Lawrie and Duffy[10] are also quoted in table VII.1 for the sake of comparison.

RESULTS AND DISCUSSIONS

The non - occurrence of axial spectrum:

No axial spectrum is observed in the present samples. The spectra for all the samples consist of a single strong exchange narrowed line. Only in sample I in which the concentration of Mn^{2+} is too less a very weak cubic spectrum is obtained. In LiCl, NaCl and KCl on the other hand Watkins[6] has reported the axial spectra. In KCl Watkins[6] also got the one line spectrum over and above the axial spectra. It appears that the intensity of the axial spectrum decreases as the difference between the radius of Mn^{2+} and that of the host cation increases, and is practically zero for the RbCl host.

The positions and the relative sizes of the anions and the cations for NaCl, KCl and RbCl are as shown in figure 7.2. When an Mn^{2+} substitutes at the host cation position a vacancy necessary for the charge compensation is created at the first neighbour cation position. This vacancy acts as an effective negative charge and, therefore, repels its neighbouring Cl^- ions. This is shown in figure 7.2 for the RbCl host. Now as the radius of Mn^{2+} is too small (.80 Å) it could easily drift towards the vacancy through the surrounding octahedron of Cl^-. In this process a new vacancy is created at the old position of the Mn^{2+}. The Mn^{2+} is pulled back and this process

should continue unless some of the neighbouring Rb^+ comes to the rescue and occupies the vacant position. Therefore, during the process of the growth of Mn^{2+} - doped RbCl crystals from the melt or from the solution, if some Mn^{2+} sits in the layer under formation, the necessary vacancy in the next layer would pull it out and practically no Mn^{2+} would remain in the grown lattice. For the KCl host the available space between the Cl^- of the octahedron (surrounding the K^+) is of the same order as the radius of Mn^{2+}; therefore, the probability for Mn^{2+} to drift is not unity and some of the Mn^{2+} ions remain at the substitutional positions so as to give the axial spectrum. For similar reason the drift of Mn^{2+} from the substitutional positions in LiCl and NaCl hosts is completely ruled out.

In those hosts where Mn^{2+} is able to drift through the surrounding octahedron of Cl^-, the best position of Mn^{2+} would evidently be the interstitial one. For charge compensation, it would either be associated with two cation vacancies or shall have two interstitial Cl^- near it. The probability for Mn^{2+} to be found without the vacancies or the interstitial Cl^- ions would be small and this, therefore, explains the very weak cubic-like six line spectrum (figure 7.4) observed in sample I.

As $MnCl_2$ molecule has a $D_{\infty h}$ symmetry[10], it would be quite reasonable to guess that an Mn^{2+} goes to an interstitial site and two Cl^- occupy the adjacent interstitial positions along the cubic axes of RbCl. The mechanism of charge compensation with the help of of two interstitial Cl^- ions is preferred because as described towards the end of this chapter it helps in explaining the observance of the

should continue unless some of the neighbouring Rb^+ comes to the rescue and occupies the vacant position. Therefore, during the process of the growth of Mn^{2+} - doped RbCl crystals from the melt or from the solution, if some Mn^{2+} sits in the layer under formation, the necessary vacancy in the next layer would pull it out and practically no Mn^{2+} would remain in the grown lattice. For the KCl host the available space between the Cl^- of the octahedron (surrounding the K^+) is of the same order as the radius of Mn^{2+}; therefore, the probability for Mn^{2+} to drift is not unity and some of the Mn^{2+} ions remain at the substitutional positions so as to give the axial spectrum. For similar reason the drift of Mn^{2+} from the substitutional positions in LiCl and NaCl hosts is completely ruled out.

In those hosts where Mn^{2+} is able to drift through the surrounding octahedron of Cl^-, the best position of Mn^{2+} would evidently be the interstitial one. For charge compensation, it would either be associated with two cation vacancies or shall have two interstitial Cl^- near it. The probability for Mn^{2+} to be found without the vacancies or the interstitial Cl^- ions would be small and this, therefore, explains the very weak cubic-like six line spectrum (figure 7.4) observed in sample I.

As $MnCl_2$ molecule has a $D_{\infty h}$ symmetry[10], it would be quite reasonable to guess that an Mn^{2+} goes to an interstitial site and two Cl^- occupy the adjacent interstitial positions along the cubic axes of RbCl. The mechanism of charge compensation with the help of of two interstitial Cl^- ions is preferred because as described towards the end of this chapter it helps in explaining the observance of the

exchange narrowed line even in lightly doped RbCl:Mn^{2+} crystals.

Narrowing of the spectrum - the exchange effect:

The pp derivative width is of the same order of magnitude for the three samples I, II & III. This indicates that the mechanism leading to the narrowing of the spectrum is almost the same for all these samples. In sample II, the parent mixture of which was made by mixing RbCl and anhydrous $MnCl_2$ in the 1:0.2603 ratio of their masses, the method of preparation thus being similar to that adopted by Swanson et al.[1] for K_4MnCl_6, the mechanism for the narrowing evidently seems to be the exchange of spins between the nearby Mn^{2+} ions[10]. A similar mechanism should, therefore, exist for the narrowing of the spectra in the samples I and III in which the concentration of Mn^{2+} is not that large. Because of the exchange the fourth moment of the line increases while the second moment remains unaffected[11]. Therefore, part of the absorption is shifted from the centre of the spectrum to its wings, thus giving the effect like the one observed.

The optical spectra:

The optical absorption spectrum taken with the help of a Cary - 14 recording spectrophotometer for the sample II shows absorption maxima almost near the same positions as obtained by Mehra and Venkateswarlu[12], and Mehra[13] for Mn^{2+}-doped NaCl and KCl. A detailed analysis has thereafter been carried out by Srivastava[14] of our laboratory. The spectra have further been investigated by him in detail at liquid nitrogen temperature and the enhanced intensity of the spectra at liquid N_2 temperature as compared to that at room

t mperature is explained to be due to the exchange of spins between the Mn^{2+} ions. The optical absorption spectra could not be observed for sample I and III, perhaps, because of the low concentration of Mn^{2+} in them. The resemblance of the optical absorption spectra for Mn^{2+} in NaCl, KCl and the sample II indicates that in sample II too Mn^{2+} has an octahedral coordination of the type $MnCl_6^{4-}$ as in NaCl and KCl.

Formation of Rb_4MnCl_6 and its EPR spectrum.

Swanson et al[10] had prepared K_4MnCl_6 by fusing together the stoichiometric quantities of KCl and anhydrous $MnCl_2$ under vacuum. The formation of K_4MnCl_6 had been confirmed by X-ray analysis. As the method of preparation of sample II in the present case coincides with that of Swanson et al[10] for K_4MnCl_6 and , further, as the pp derivative widths for K_4MnCl_6 and the sample II are of the same order (table VII.1), we expect the sample II to be the complex Rb_4MnCl_6. It may be remarked here that the sample IV in which the quantities of RbCl and anhydrous $MnCl_2$ are in the same ratio as in sample II, but which was not fused, gave in its EPR spectrum one single broad line of pp derivative width $\sim$ 580 gauss. The crystal structure of Rb_4MnCl_6 is not known, but it may be similar to that of K_4MnCl_6 quoted by Swanson et al[10]. The unit cell of K_4MnCl_6 is nearly cubic. The Mn^{2+} ions are located at (1/4, 1/4, 1/4) and (3/4,3/4,3/4) in the unit cell. Each Mn^{2+} ion is surrounded by an octahedral arrangement of chlorine ions. Potassium ions are located at the cube centre, at each of the corners of the cube, at the midpoint of each cube edge, and at the centre of each cube face. Nearest neighbour Mn^{2+} ions are separated by a distance of 7.4$\mathring{A}$ with the following linear arrangement.

Mn^{2+} ——— K^{+} ——— Mn^{2+}

←—3.7Å—→

←———7.4Å———→

Next nearest Mn^{2+} ions are separated by a distance of $a_o \sim 8.5$Å with the following linear arrangement

Mn^{2+} ——— Cl^{-} ——— Cl^{-} ——— Mn^{2+}

←—2.5Å—→←—3.5Å—→

←———8.5Å———→ „(10)*

The corresponding distances between the near neighbour Mn^{2+} ions for the case of Rb_4MnCl_6 could be expected to be slightly greater, but of the same order as those for K_4MnCl_6.

For K_4MnCl_6 Swanson et al[10] have suggested the superexchange via two Cl^{-} ions between the next nearest neighbour Mn^{2+} ions as the probable mechanism for the narrowing of the spectrum. The arrangement is linear and thus p-orbitals of the intervening Cl^{-} ions could predominantly be involved in the interaction. This mechanism involves two partial transfers of electrons, one from each Cl^{-} ion to the Mn^{2+} ion. The probability for superexchange through two Cl^{-} is thus very small. Swanson et al[10] considered the transfer through K^{+} ion a very unlikely process because the ionisation potential of K^{+} is too high, being equal to 31.8 volts. The superexchange through two Cl^{-} ions is , therefore, considered to be the main mechanism for the narrowing of the line. A mechanism of superexchange through two Cl^{-} ions might be responsible for the narrowing of the line in the case of sample II as well.

---

* The material under quotation marks " ...." regarding the structure of K_4MnCl_6 is quoted from reference (10).

The narrow line in lightly doped RbCl: Mn^{2+}

The exchange narrowed line is also observed in sample I i.e. RbCl doped with a mere 0.02% of $MnCl_2$. The pp derivative width in this case shows a systematic variation with respect to the orientation of H in a (001) plane. One can not, therefore, believe that the narrowing is merely because of Mn^{2+} going to and accumulating at the internal grain boundaries and the dislocation sites[15]. As remarked earlier Mn^{2+} prefers to occupy an interstitial position, when RbCl is doped with $MnCl_2$. To account for the charge compensation two Cl^- ions occupy those interstitial positions along ⟨001⟩ which are nearest to the Mn^{2+} ion. With the entry of another $MnCl_2$ into the lattice, the incoming Mn^{2+} would like to sit in a position which is closest to the interstitial Cl^- but is farthest from the already present Mn^{2+}. In effect, the linear arrangement $Cl^- - Mn^{2+} - Cl^-$ of interstitial ions would further extend to $Cl^- - Mn^{2+} - Cl^- - Mn^{2+}$, and for charge compensation to be accomplished two extra Cl^- ions would sit in nearby interstitial positions to this second Mn^{2+}, as shown in figure 7.3. It may be emphasized here that the radius of Mn^{2+} is small enough (.80Å) to allow its free motion in the lattice. In view of the above, the occupation of the closeby interstitial positions by Mn^{2+} even in a lightly doped RbCl crystal may be understood, and the resulting narrowing explained.

The process of Mn^{2+} ions getting grouped together could extend itself in all the planes and in all the cubic directions. Now, though the radius of Mn^{2+} is small, that of Cl^- (1.81Å) is much larger than the available space at the interstitial sites. The

Cl^- entering the interstitial positions would, therefore, cause the local distortions and, probably RbCl could at best be doped to the extent of the arrangement shown in figure 7.3. The resulting doped substance in that extreme case would be the solid solution $4RbCl.MnCl_2$ of $MnCl_2$ in RbCl*. As shown in figure 7.3 , in the case of RbCl doped with anhydrous $MnCl_2$ the super exchange takes place through a Cl^- between the nearest neighbour Mn^{2+} ions. The distance between such two Mn^{2+}, as determined from the crystal structure of RbCl, is 3.29Å. Further, it is not necessary that this process of accumulation of Mn^{2+} would take place around only a single interstitial point in the lattice. It could start at a number of interstitial sites. The sizes of ~~crumpled~~ toy the blocks of Mn^{2+} and Cl^- would evidently depend on the concentration of $MnCl_2$ in the RbCl lattice. As the concentration of $MnCl_2$ is increased, more number of Mn^{2+} would be participating in the process of exchange of spin with some particular Mn^{2+} and the line would, accordingly , be narrower. Thus one is able to explain why the pp derivative width is smaller for the sample III as compared to that for the sample I.

In the case of Rb_4MnCl_6 though the exchange occurs through two Cl^-, yet the distance of Mn^{2+} from the nearest Cl^- is ~2.5Å, (as for Rb_4MnCl_6 it is exactly equal to 2.5Å) a value much smaller than the corresponding distance in sample I; and, moreover, in Rb_4MnCl_6 the exchange takes place from all the six nearest neighbour Mn^{2+}, Therefore, the pp derivative width for Rb_4MnCl_6 could be expected to be smaller than that for the samples I and III and this is what has been observed (Table VII.1).

* When this solid solution $4RbCl.MnCl_2$ is made to grow in the form of a single crystal Rb_4MnCl_6 is expected to be formed.

Variation of the pp derivative width with the orientation of H:

No explanation could be afforded for the variation of pp derivative width as the orientation of H in a (001) plane was changed. The only remark which could be made is that this variation is not due solely to the cubic crystal field, because in that case we would have got the minimum width for H making an angle of 32° with the $\langle 100 \rangle$ axis in (001) plane. (This value of the angle for the minimum width (or max pp derivative height) is observed under the "cubic spectrum" sub-heading of chapter VI.) The width is minimum for H // $\langle 110 \rangle$.

Table VII.1

The pp derivative width and the g-value for the different Mn^{2+} - doped alkali chlorides and complexes. For sample I the variation of pp derivative width with θ, the oreintation of H with respect to ⟨100⟩ in a (001) plane is also shown.

Sample	θ	pp derivative width (in Gauss)	g
I	0^0	35.7	2.0011 ± .0003
	15^0	34.7	
	30^0	33.1	
	45^0	31.5	
II	—	~ 21	2.0024 ± .0003
III	H // ⟨100⟩	~ 27	2.0024 ± .0003
IV	—	~580	2.0023
$MnCl_2$[a] (Powder)	—	~ 25	2.0017

[a] T. A. Aranson et. al., J. Chem. Phys. 49, 4407 (1968)

Description of the samples:

I. RbCl single crystal containing about .02% of $MnCl_2$ (Anhydrous).

II. Substance obtained by fusing RbCl & $MnCl_2$ (Anhydrous) in the 4:1 ratio of their molecular weights.

III. Pink portion of the RbCl doped with ~1% of anhydrous $MnCl_2$.

IV. Obtained by simply mixing RbCl & $MnCl_2$ (Anhydrous) in the 4:1 ratio of their molecular weights.

REFERENCES

(1) R. Rohrig, Phys. Letters 16, 20 (1965).

(2) F. Porret and E. Lambert, Helv. Phys. Acta 40, 264(1967).

(3) S. D. Pandey, J. Chem. Phys. 47, 3094 (1967).

(4) P. G. Nair, K.V. Lingam and B. Venkataraman, J. Phys. Chem. Solids. 29, 2183 (1968).

(5) S. D. Pandey, Chem. Phys. Letters 3, in press(1969).

(6) G. D. Watkins, Phys. Rev. 113, 79 (1959).

(7) K.N. Shrivastava and P. Venkateswarlu, Proc. Indian Acad. Sci. 63, 284 (1966).

(8) K. Morigaki, M. Fujimoto, and J. Itoh, J. Phys. Soc. Japan 13, 1174 (1958).

(9) A. V. Jagannadham and P. Venkateswarlu, Proc. Indian Acad. Sci. 69, 67 (1969).

(10) T. W. Swanson, V. W Laurie and W. Duffy Jr., J. Chem. Phys. 49, 4407 (1968).

(11) J. S. van Wieringen, Disc. Faraday Soc. 19, 118 (1955).

(12) A. Mehra and P. Venkateswarlu, J. Chem. Phys. 45, 3381 (1966).

(13) A. Mehra, Phys. Stat. Sol. 29, 847 (1968).

(14) J. P. Srivastava: Absorption of Mn^{2+}(unpublished work).

(15) P. A. Forrester and E.E. Schneider, Proc. Phys. Soc . (London) B69, 833 (1956).

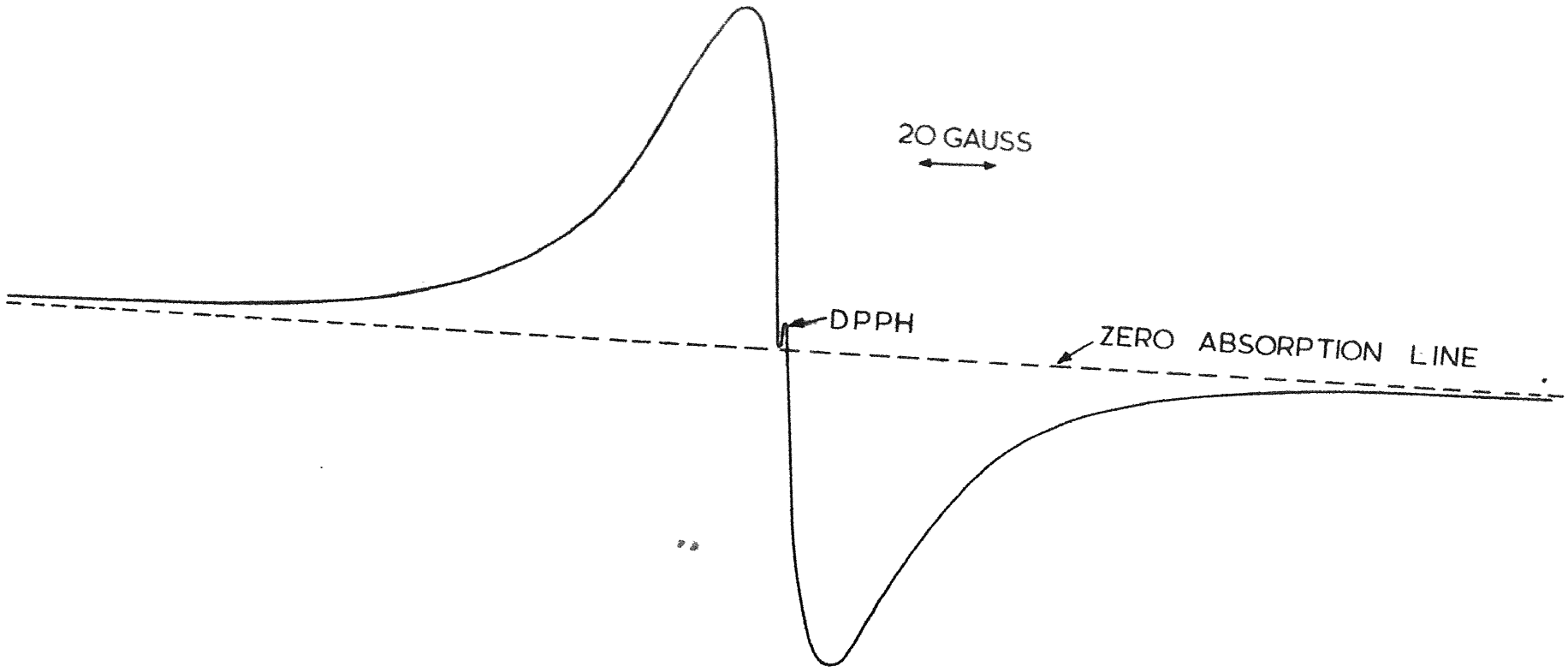

FIG. 7·1 THE EXCHANGED NARROWED LINE FOR H // <001> OF RbCl DOPED WITH ~0·02% OF $MnCl_2$

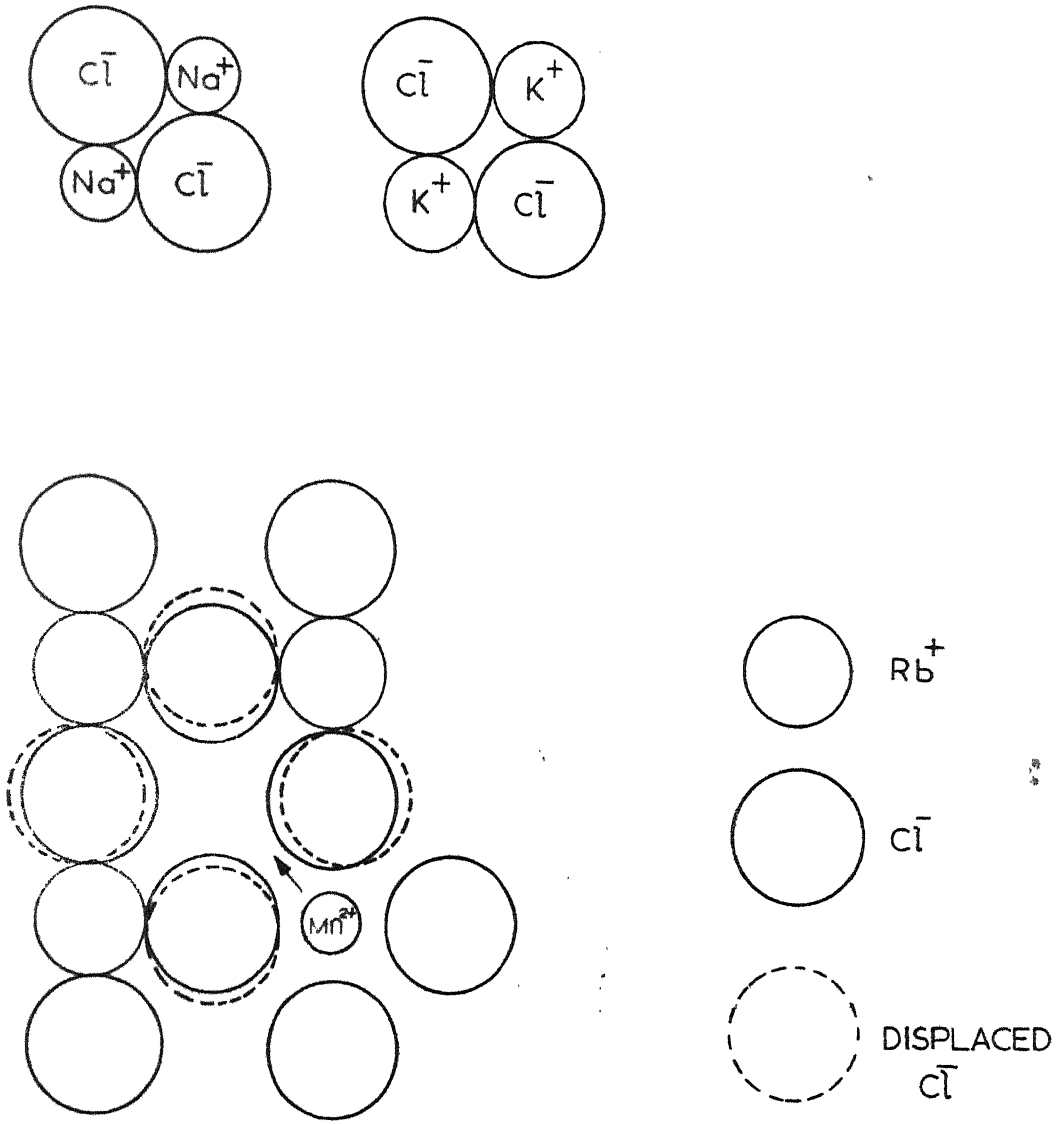

FIG·7·2 DIAGRAM SHOWING THE POSITIONS & THE RELATIVE SIZES OF THE ANIONS & THE CATIONS FOR NaCl, KCl & RbCl. IN THE CASE OF RbCl A POSITION OF THE NECESSARY VACANCY & THE LOCAL DISTORTIONS AROUND THAT, IF Mn^{2+} SUBSTITUTES FOR Rb^{+} ARE ALSO SHOWN.

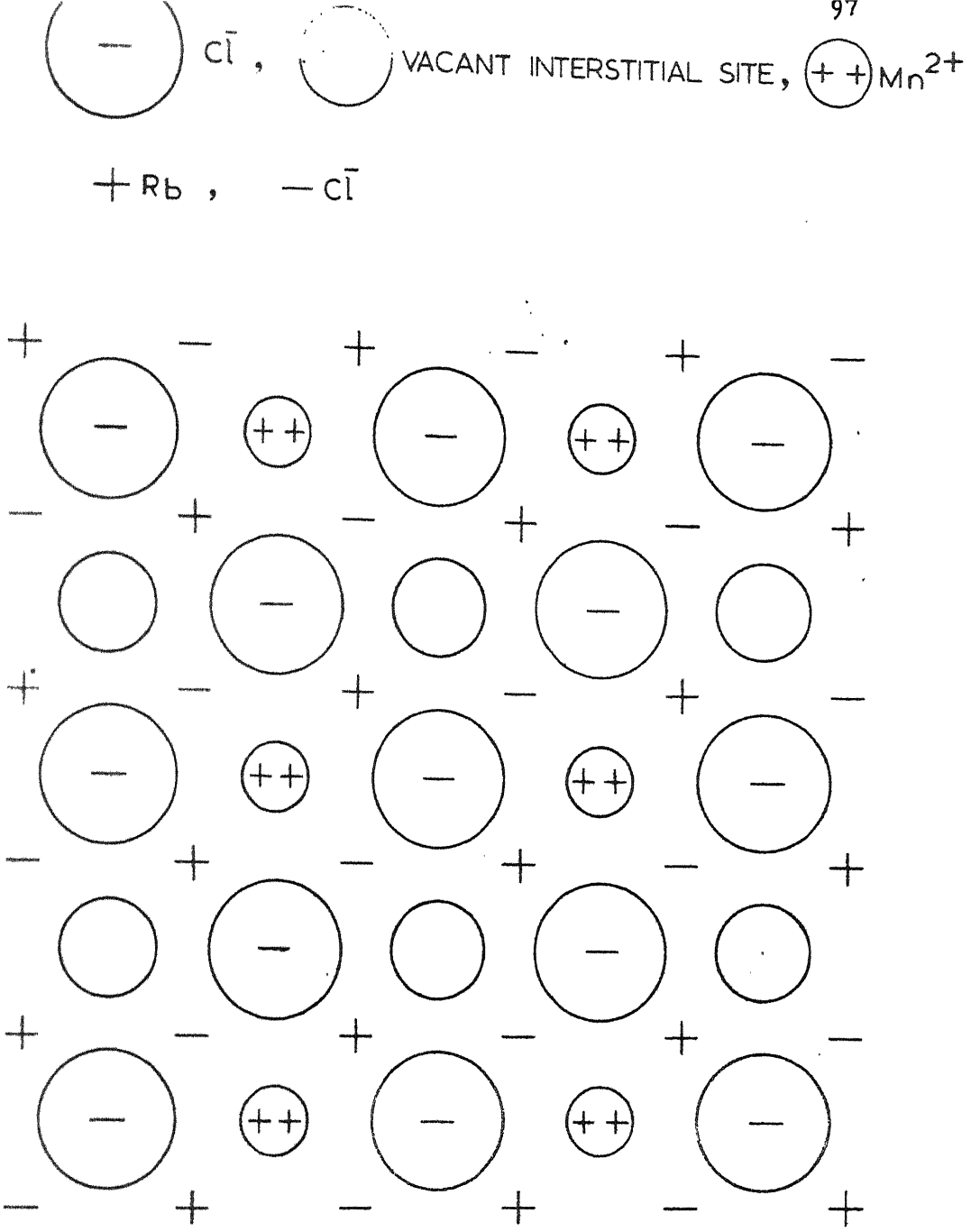

FIG.7·3 THE DIAGRAM SHOWING THE Rb^+ & Cl^- IN A (001) PLANE OF RbCl LATTICE. THE ASSOCIATED INTERSTITIAL SITES AS OCCUPIED BY Mn^{2+} & Cl^- IN A SOLID SOLUTION OF $MnCl_2$ IN RbCl ARE ALSO SHOWN. THE PLANE OF INTERSTITIAL IONS IS AT A DISTANCE OF $a_0/4$ FROM THAT OF Rb^+ & Cl^-.

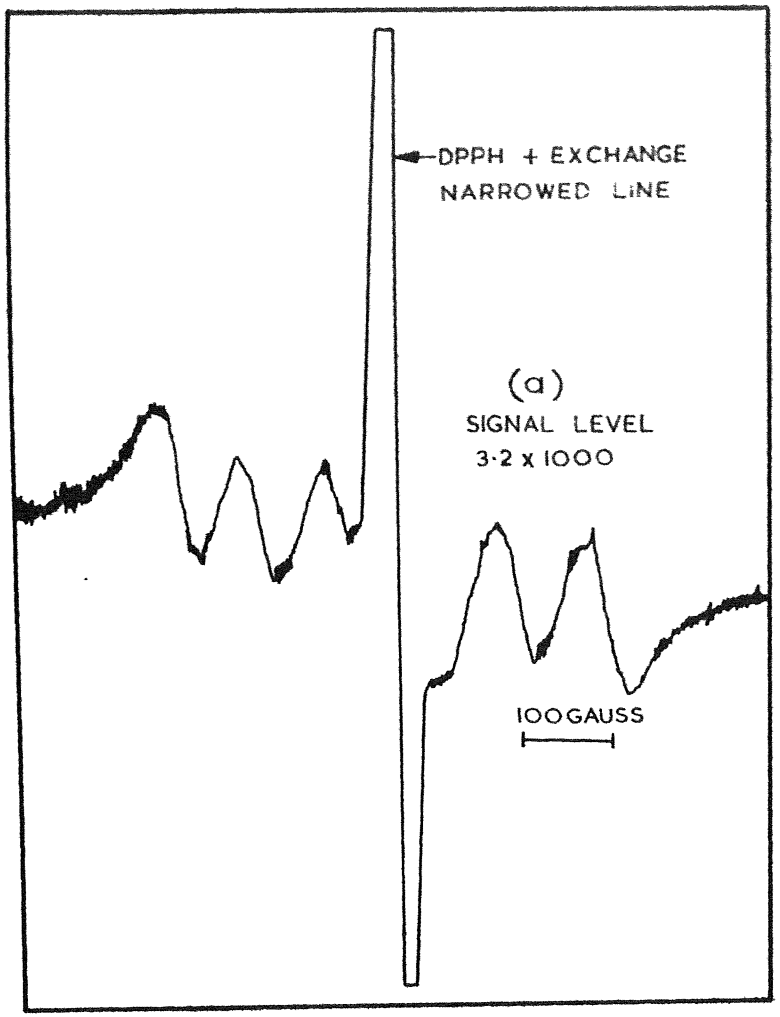

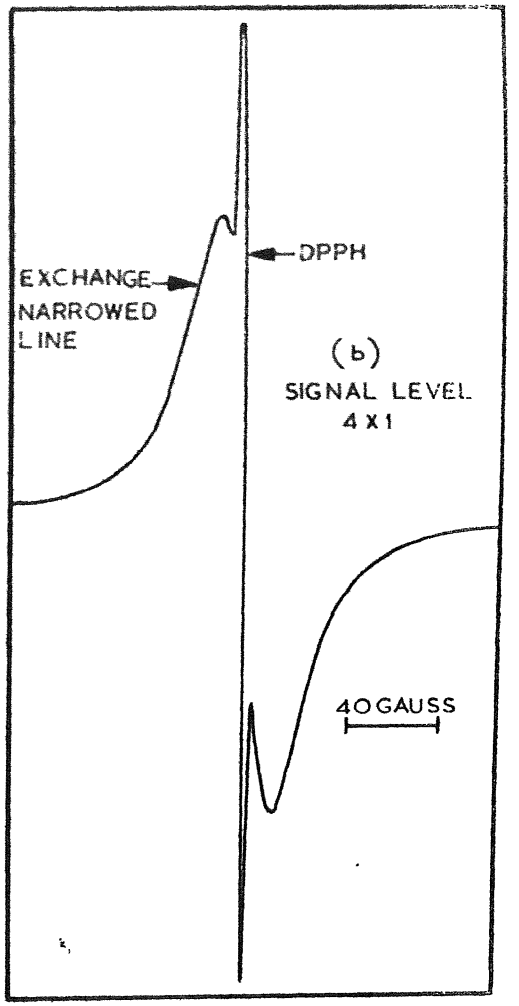

FIG.7.4 EPR SPECTRA OF RbCl DOPED WITH ~0.02% OF $MnCl_2$ WITH SIGNAL LEVEL SETTINGS AS INDICATED, OTHER SETTINGS ARE THE SAME. A SIX LINE CUBIC SPECTRUM IS SEEN FOR THE SETTING (a).

CHAPTER VIII

ELECTRON PARAMAGNETIC RESONANCE OF VO^{2+}-DOPED $(NH_4)_2SO_4$ CRYSTALS

Abstract

The spectra of VO^{2+} - doped $(NH_4)_2SO_4$ single crystals are reported. The V-O are found to occupy four types of sites in the lattice. The angular variation, of the positions of the hyperfine lines corresponding to the three sites I, II, and III, is studied. The lines of the site IV were observed for H//b but could not be followed for other orientations of H because of overlap with those of the other sets. The magnitudes of the principal values and the direction cosines with respect to the crystal axes of the principal axes of the g and A tensors, corresponding to the three sites, are determined. The corresponding orientations of V-O are also determined. In order to explain the experimentally determined orientations of V-O a classical model which treats the V-O as a line - charge is proposed.

The spectrum does not show any recognizable change when the temperature is swept through $-50^{\circ}C$, the ferroelectric transition temperature. The only change observed is in the hyperfine separation which continuously increases on cooling the crystal. The hyperfine separation at liquid Nitrogen temperature is $\sim 3\%$ more than that at room temperature.

The optical (near infrared) absorption spectrum is recorded at room temperature. The three absorption maxima observed at 12767, 16098 and 17177 cm^{-1} are related to the two strongly populated sites I and II of V-O in $(NH_4)_2SO_4$.

INTRODUCTION

Vanadyl ion complexes have been the subject of a number of recent studies. The electron paramagnetic resonance (EPR) of randomly oriented vanadyl ions has been studied by several investigators[1-8]. The study of the EPR of preferentially oriented vanadyl ions has mainly been done in GeO_2[9] and TiO_2[10] and in alums[11,12] and tutton salts[13]. In GeO_2 and TiO_2 the cation is surrounded by a regular octahedron of oxygens. The alums and the tutton salts possess almost regular octahedra of water molecules. These water octahedra surround the trivalent cations in the alums, whereas in the case of tutton salts the divalent cations are surrounded by water octahedra. On doping these above mentioned crystals with VO^{2+}, the cations surrounded by the octahedra of H_2O or oxygen get replaced by V^{4+} of VO^{2+}. The V^{4+} can thus have the necessary octahedral coordination as described in chapter III, and V-O, accordingly, prefers to point along one of the axes of the octahedron. It would, therefore, be interesting to find out the preferred orientations of V-O in those crystals which grow without the water of crystallization and in which the cations are not surrounded by a regular octahedral arrangement of oxygens (anions). It is found that $(NH_4)_2SO_4$ mixed with a little quantity of $VOSO_4.5H_2O$, when crystallized from solution, gives large single crystals with well developed faces and with a bluish-green colouration, the colour indicating the entry of VO^{2+} into the lattice. $(NH_4)_2SO_4$ crystals grow without the water of crystallization and, further, the $(NH_4)^+$ ions in them have many oxygens at nearby positions. Ammonium sulphate can, therefore, serve as an interesting host for finding the

preferred orientations of V-O. An EPR study of VO^{2+} - doped $(NH_4)_2SO_4$ is, therefore, undertaken, and the preferred orientations of V-O are determined. An optical absorption study of the above crystals is also taken up and the observed positions of the maxima are correlated to the different sites of V-O in the lattice.

CRYSTAL STRUCTURE OF $(NH_4)_2SO_4$

The crystal structure of ammonium sulphate has been determined by Ogg[14]. Recently Schlemper[15] has redetermined the structure by neutron diffraction. The room temperature space group[16] for ammonium sulphate is P_{nam}. The two fold screw rotation axes a, b, c are chosen such that the unit cell dimensions are 5.95, 10.56, and 7.73 Å respectively along these directions at 25°C. The crystal has one ordinary reflection plane bc, two glide reflection planes ab, ca, and centre of inversion. The projections of the unit cell of the lattice over the planes bc, ca and ab are shown in figure 8.1. In this figure the NH_4 sites are represented by circles. The S atom and two of the O atoms of SO_4 tetrahedron lie on the reflection plane bc, while the remaining two O atoms are equidistant from this plane. Similar is the case for NH_4 tetrahedra. There are two inequivalent sites for NH_4^+ ions in the unit cell and are designated as α and β The oxygen environment is different for these two types of NH_4^+ ions. The positions of the atoms in the unit cell at 25°C as given by Wycoff[16] are as quoted in table VIII.1. These positions are used to find the various angles in the text.

The first order ferroelectric transition temperature[17] is -50°C. In the ferroelectric phase, the crystal is polarized

along the a-axis and the centre of inversion and the bc plane of reflection are absent . Because of this reduction in symmetry each of the α and β ammonium ions gives the pairs of inequivalent ammonium ions α_1 , α_2 and β_1, β_2 . The low temperature space group is P_{na2_1}.

THE EPR SPECTRA

VO^{2+} doped in $(NH_4)_2 SO_4$ is found mainly to occupy four different types of sites, each giving its own characteristic eight line spectrum. Out of the four different spectra obtained three (denoted as I, II & III) have been analysed. The intensities of the hyperfine lines for the three spectra I, II, and III are approximately in the ratio 3: 3: 1. This ratio indicates the probability of V-O occupying the different sites. The spectra due to V-O at site IV were as strong as due to those at site III but could be observed only for H parallel to the crystal b-axis. For other orientations of H they overlapped with the lines of V-O at other sites. Angular variation of the positions of extreme hyperfine lines (m = -7/2 and m = 7/2) is plotted for the different orientations of H in the three basal planes, and is shown in figures 8.2, 8.3 and 8.4 for the planes ab, bc and ca respectively. (The continuous lines indicate the theoretically calculated angular variation whereas the circles indicate the experimental points). The extreme, (the first and the eighth) hyperfine lines of any hyperfine group are designated as (1,8). Those corresponding to the different sites I, II and III of V-O are, further, distinguished as $(1_I, 8_I)$, $(I_{II}, 8_{II})$ and $(1_{III}, 8_{III})$. The spectra obtained for H parallel to the crystal

a,b and c axes are shown in figures 8.5, 8.6 and 8.7 respectively.

g and A tensors:

For the sites I and II, as seen from figures 8.2, 8.3 and 8.1 , the eight line hyperfine group splits into two as H is moved in the basal planes , away from the crystal axes. If H is not in any of the basal planes, the splitting is into four. This indicates that there are four distinguishable but symmetry related sites for each type I and II of V-O positions. For the site III, the angular variation of the extreme hyperfine lines could not be followed in ab and bc planes. But the pretty small magnitude of separation $(l_{III} - s_{III})$ when H//b indicates that one of the principal axes of the $\hat{g}$ and A tensors, for this site of V-O , is very nearly parallel to the b-axis, the other two being in the crystal ca plane.

As described in chapter III, one could (for any site of V-O) find the values of g at different orientations θ of the magnetic field in the basal planes if H (m= - 7/2) and H(m = + 7/2) could be known at these angles. The extremum values of $g(\theta)$ in the three basal planes could then, give the elements of the g^2 tensor. However, these values could not be determined for all the basal planes as due to overlap it was not possible to find the values of H(m=-7/2) and H(m= +7/2) at some of the orientations of the magnetic field. The method described in chapter III for finding the elements of the $\hat{g}^2$ tensor could , therefore , not be adopted as such and the help of a least square fitting procedure was taken. The experimental g^2

values for the set of orientations of H in any basal plane are fitted to a formula

$$g^2 = \alpha + \beta \cos 2\theta + \gamma \sin 2\theta$$

and the best fit values of α, β and γ are determined. The values of α, β and γ thus determined, are processed in the manner described in chapter III to give the elements of the $\underset{\sim}{g}^2$ tensor. The elements of the $\underset{\sim}{g}^2$ tensor for the sites I and II of V-O in the lattice are given in tables VIII.2 and VIII.4 respectively. Further, as in chapter III, one could find the elements of $\underset{\sim}{g}.\underset{\sim}{A}.\underset{\sim}{A}.\underset{\sim}{g}$ tensor if the extremum values of the separation (H_1-H_8) of m = -7/2 and m = 7/2 hyperfine lines are known. But as (H_1-H_8) could not be determined for all orientations of the magnetic field for reasons mentioned already, a least squares method, similar to that as described for the determination of the $\underset{\sim}{g}^2$ tensor, was adopted and the best fit values of α, β and γ are processed to give the elements of $\underset{\sim}{g}.\underset{\sim}{A}.\underset{\sim}{A}.\underset{\sim}{g}$ tensor. The elements of the $\underset{\sim}{g}.\underset{\sim}{A}.\underset{\sim}{A}.\underset{\sim}{g}$ tensors for the sites I and II of V-O in the lattice are given in tables VIII.3 and VIII.5 respectively. With the help of $\underset{\sim}{g}.\underset{\sim}{g}$ and $\underset{\sim}{g}.\underset{\sim}{A}.\underset{\sim}{A}.\underset{\sim}{g}$ tensors, the elements of $\underset{\sim}{A}.\underset{\sim}{A}$ are determined. The matrices representing the $\underset{\sim}{g}.\underset{\sim}{g}$ and $\underset{\sim}{A}.\underset{\sim}{A}$ tensors on diagonalization give the principal values of $\underset{\sim}{g}^2$ and $\underset{\sim}{A}^2$ and thus of $\underset{\sim}{g}$ and $\underset{\sim}{A}$. The magnitude of the principal values of the $\underset{\sim}{g}$ and $\underset{\sim}{A}$ for the sites I and II are given in tables VIII.6 and VIII.8 respectively. The eigen vectors of $\underset{\sim}{g}.\underset{\sim}{g}$ and $\underset{\sim}{A}.\underset{\sim}{A}$ give the direction cosines relating the principal axes respectively of $\underset{\sim}{g}$ and $\underset{\sim}{A}$ to the crystal axes (a,b,c). These are given in tables VIII.7 and VIII.9 respectively for the sites I and II of VO^{2+} in $(NH_4)_2SO_4$. The principal values, and the

direction cosines with respect to the crystal axes (a,b,c) of the site III of V-O are determined directly by using the expression (3.10) of chapter III . The principal axes of $\underset{\sim}{g}$ & $\underset{\sim}{A}$ were assumed to coincide in pairs for this case. The parameters thus determined are given in tables VIII.10 and VIII.11.

The orientations of V-O in the lattice.

From the tables VIII.7 and VIII.9 for the direction cosines of the principal axes of the $\underset{\sim}{g}$ and $\underset{\sim}{A}$ tensors corresponding to the two sites I and II of V-O , we find that the z principal axes of $\underset{\sim}{g}$ and $\underset{\sim}{A}$ tensors i.e. those corresponding to the maximum principal value of $\underset{\sim}{A}$ and the minimum of $\underset{\sim}{g}$ include a very small angles of $\sim 3^{0}$ for the sites I and II of V-O. For the site III the principal axes of the $\underset{\sim}{g}$ and $\underset{\sim}{A}$ were already assumed to coincide in pairs. Now as the z principal axes of $\underset{\sim}{g}$ and $\underset{\sim}{A}$ are very nearly parallel for all the sites, a line which bisects the angle between them can be assumed to give the orientation of V-O in the lattice. Thus determined orientations, in terms of the angles Θ_{a}, Θ_{b} and Θ_{c}, of the three sites of V-O are given in table VIII.12. Here Θ_{a} is the angle between the b-axis and the projection of V-O on the bc plane, Θ_{b} is the angle between the c-axis and the projection of V-O in the ca plane, and Θ_{c} is the angle between the a-axis and the projection of V-O in the ab plane. The Θ_{a}, Θ_{b} and Θ_{c} for the other symmetry related positions for each type of site are connected to those given in table VIII.12 through the symmetry of the lattice.

Probable explanation of the observed orientations:

As V^{4+} of V-O invariably occurs in some sort of covalent coordination with the surrounding ligands, the present experiments,

wherein no superhyperfine structure is observed, indicate that in $(NH_4)_2SO_4$ the V^{4+} is surrounded by ligands with zero nuclear spin. V-O in $VO(H_2O)_5^{2+}$ occurs in coordination with five sp_σ hybrids of H_2O, and in $VOSO_4.5H_2O$ crystal[18] it has one oxygen of SO_4 and four sp_σ hybrids of H_2O to accomplish the coordination. Extending the arguments to the case of a lattice which has no H_2O molecules but has oxygens, V^{4+} of V-O could exclusively be bonded with six oxygens. This is what one expects for V-O in $(NH_4)_2SO_4$. Ammonium sulphate crystals, though grown from solution, do not possess the water of crystallization; and, further the available interstitial space in these crystals is not much. Therefore, it is difficult to imagine H_2O coordination for V^{4+} in $(NH_4)_2SO_4$ lattice. Nevertheless, the V^{4+} of V-O could go to an NH_4 site. The NH_4 sites in $(NH_4)_2SO_4$ are surrounded by the oxygens of SO_4 ligands. There are two types of NH_4 sites i.e. α and β in $(NH_4)_2SO_4$. They have different oxygen environments. The oxygen environment for β-NH_4 is more compact than that for α-NH_4. The V-O having an effective 2+ charge should, therefore, prefer to occupy a β-NH_4 positions. As shown in figure 8.8 the β-NH_4 has nine oxygens at its nearby positions. The positions of the oxygens are indicated by their projections on the plane bc. Out of the nine oxygens three are marked I, II and III, two are both at C and D and one each is at A and B. The two oxygens at C and the other two at D should serve as the four bonding oxygens of V-O. The fifth oxygen could be any one of the remaining five. In analogy with almost all the known complexes of V-O this fifth bonding oxygen should lie on the line which is perpendicular to the above mentioned rectangle. There is no oxygen at such a position, but there

are two of them at nearby positions, marked I and II in figure 8.8. Both of these (I & II) SO_1 - oxygens have almost equal probability of becoming the fifth bonding oxygen for V-O . Further, it is natural to assume that in the absence of any other constraint the V-O bond would remain parallel but opposite to the line joining the vanadium and the fifth bonding oxygen. The angles θ_a, θ_b and θ_c for the two orientations I and II of V-O are thus dependent on the crystal structure data of the lattice. The θ_a, θ_b and θ_c , for the two sites I and II of V-O , are calculated and are given in table VIII.13. These values of θ_a, θ_b and θ_c do not coincide with the experimental values as given in table VIII.12 . One, therefore, doubts the coordinates assigned to V^{4+} of V-O in the lattice. VO^{2+} is not an ammonium ion so as to have strong hydrogen bonding in the lattice and thus to occupy the same position in the lattice as held by β -NH_4 . The knowledge of the structure of the vanadyl complexes known till now, makes one to believe that V^{4+} of V-O would occupy a position which is symmetrical to all the four SO_4 - oxygens forming the rectangle . The centre of the rectangle is quite far from the β -NH_4 position. So V^{4+} could occupy a position which is nearest to N_o, the β-NH_4 (See fig.8.8), and is also symmetrical to the oxygen rectangle. As in figure 8.8, we imagine a line perpendicular to the plane of the oxygen rectangle and passing through its centre and drop a perpendicular over this line from the β -NH_4 position. The point so obtained, as shown by N in figure 8.8, would be the most favourable position for V^{4+} . If V^{4+} occupies this position and the V-O bond is antiparallel to the line joining the V^{4+} and the fifth oxygen, we have θ_a (I) = 61^o 18' and θ_a (II) = $10^o42'$. These values of θ_a

for the two sites are in close agreement with the experimental values given in table VIII.12. The agreement between the calculated and experimental values of Θ_a for the two sites thus improves if V^{4+} occupies the position N as compared to N_o.

Now , in order to explain the experimental values of Θ_b and Θ_c we must move the V-O away from the basal plane bc i.e. towards the crystal a-axis. As VO^{2+} has net 2+ charge, it could be moved by the electrostatic attraction of some extra negative charge in the lattice. When VO^{2+} enters a β-NH_4 position, a NH_4^+ vacancy is created to account for the charge compensation. This vacancy serves as an effective negative charge. Now, as the V-O is to be moved away from the basal plane bc, the plane of figure 8.8, the NH_4^+ vacancy should lie above or below this plane. Further, vacancy at α-NH_4 site would be favoured because its oxygen environment is less compact as compared to that of β-NH_4. The nearest and off the plane α-NH_4 position, with respect to the β-NH_4 at N_o , is the one shown in figure 8.8. Therefore if V^{4+} occupies the position N_o or N, the NH_4^+ vacancy at the above mentioned α-site would be favoured the most. The angles Θ_a, Θ_b and Θ_c for the two types I and II of V-O are now simultaneously explained by assuming that the V-O bond moves through a certain angle (determined by the pull of the vacancy and the effect of the other possible constraints) towards the α-NH_4 vacancy while keeping itself in a plane which is perpendicular to the plane of the figure 8.8. Restricting the motion of V-O in such a plane is justified because it would keep it away from the oxygens at the corners of the rectangle mentioned above.

The preferred orientation of V-O corresponding to the site III could be explained if the oxygen marked III (below the plane of the figure 8.8) serves as the fifth bonding oxygen for V^{4+}. In this case the V-O bond when acted upon by the attractive force of the α-NH_4 vacancy at F would be going out of the influence of the oxygens forming the rectangle, and so it (V-O) could freely move in the plane passing through the following three points, viz. the point N , the centre of the oxygen at III and the position of α-NH_4 at F., and may because of the effect of the constraints come to rest, when it (V-O bond) just reaches the ca plane in such a way that the angle between V-O and the c-axis at such a position of the bond is roughly equal to the experimental value of θ_b. As the line joining the V^{4+} and the fifth bonding oxygen (marked III in figure 8.8) is much off from the perpendicular to the plane of the oxygen rectangle, site III is not expected to be occupied with that great a probability as I and II. This is in conformity with the experimental results.

It is interesting to note that this classical model qualitatively explains the three experimentally observed preferred orientations of V-O in ammonium sulphate. This is more so because in a rigorous sense one has to consider the orbitals of V^{4+} and those of all the neighbouring oxygens and over and above the effect of the vacancy to find out the minimum energy positions of V-O in the lattice.

Low temperature (EPR) spectra:

There is no appreciable change in the spectra on cooling the crystal from room temperature to the liquid N_2 temperature.

The effect of the change in temperature is found on $|A_z|$ ($\equiv |A_2|$) for the site II of V-O in ammonium sulphate. $|A_z|$ (site II) is found to increase only by approximately 3% in going from room temperature to the liquid N_2 temperature. The above results for the temperature variation are explained in the following way.

On cooling the host crystal through the ferroelectric transition temperature two in-equivalent sites β_1 and β_2 each with different D and E are created from identical β-sites. There is no fine structure in the present case. The question of fine structure splitting is, therefore, out of context. One could still expect some difference in the values of A parameter for β_1 and β_2 sites, and thus a splitting on cooling the crystal through -50°C. The fact that there is no splitting of the spectra in the present case indicates that there is practically no dependence of A on D and E. These results are in conformity with those obtained by Chowdary and Venkateswarlu[19] for the above host but doped with Mn^{2+}. They have found that in crossing the ferroelectric transition temperature there is a negilgible change in the hyper - fine interaction parameter, where though D and E parameters change appreciably,.

OPTICAL SPECTRA

In the optical absorption spectrum taken with the help of a Cary - 14 spectrophotometer , we get three absorption maxima at 12767, 16098 and 17177 cm^{-1} respectively. The spectrum showing the variation of the optical density as a function of frequency (cm^{-1}) is as in figure 8.9(a).

The visible and near infrared spectrum of $VO(H_2O)_5^{2+}$ (20,21) consists of two broad maxima at approximately 16000 and 13000 cm^{-1}, corresponding respectively to the transitions $b_2 \rightarrow b_1^*$ and $b_2 \rightarrow e_\pi^*$ as expected for the tetragonally coordinated complexes of V-O . If the symmetry is less than tetragonal, as is expected from the nontetragonal character of $\underset{\sim}{g}$ and $\underset{\sim}{A}$ in the present sample, the e_π^* level should split into two orbital singlets and one should get two absorption maxima at $\sim 13000cm^{-1}$. But as is clear from figure 8.9(a) only one absorption maximum is found around this value i.e. at $12767cm^{-1}$. This indicates that the splitting of e_π^* due to the low symmetry additions over the main tetragonal symmetry of V-O is negligible and is atleast much less than the width of the line.

The origin of the two absorption maxima one at 16098 and the other at 17177 cm^{-1} is explained due to the presence of two types (I and II) of V-O complexes. This is shown in figure 8.9(b). The absorption maxima corresponding to the sites III and IV of V-O should be weak in intensity as was the case for their EPR spectra. It seems that the energy separation ΔE $(b_1^* \rightarrow b_2)$ is different for the two complexes I and II of V-O . For I it is $16098cm^{-1}$ whereas for the other it is 17177 cm^{-1} . But as there is only one absorption maximum near $13000cm^{-1}$ i.e. at $12767cm^{-1}$, we are led to believe that the energy separation $\Delta E(e_\pi^* \rightarrow b_2)$ does not change appreciably at least within the width of the lines, in going from site I to site II.

CORRELATION BETWEEN OPTICAL AND EPR DATA

Taking into consideration the experimental fact that the e_π^* level is not split in the present complexes, the expressions (3.3),

(3.1) and (3.5) of chapter III for the principal values of the $\underset{\sim}{g}$ tensor reduce respectively to

$$g_z = g_{\parallel} = 2.0023\left[1 - 4\lambda\gamma_z^2/\Delta E(b_2 \rightarrow b_1^*)\right]$$

$$g_x = 2.0023\left[1 - \lambda\gamma_x^2/\Delta E(b_2 \rightarrow e_{\pi}^*)\right]$$

and $$g_y = 2.0023\left[1 - \lambda\gamma_y^2/\Delta E/(b_2 \rightarrow e_{\pi}^*)\right]$$

Here λ is the spin-orbit interaction parameter and γ_x, γ_y and γ_z are the principal values of the covalency parameter.

The above expressions for g_x, g_y and g_z suggest that g_x and g_y should be approximately equal and should be much different from g_z. This is what one observes for the present complexes. The small difference in the values of g_x and g_y is, perhaps, indicative of the nonaxial character in the covalency and shows that γ_x is quite different from γ_y.

Table VIII.1

The positions of the various atoms in the unit cell for $(NH_4)_2SO_4$ at 25°C. (x,y and z represent the coordinates in units of a,b and c respectively along the corresponding axes.)

Atom	x	y	z
$NH_1(\alpha)$	+0.417	+0.685	+0.250
$NH_1(\beta)$	-0.311	+0.000	+0.250
S	+0.417	+0.250	+0.250
O(1)	+0.417	+0.056	+0.250
O(2)	+0.549	+0.315	+0.250
O(3)	+0.351	+0.315	+0.045

Table VIII.2

Elements of g.g for the site I of VO^{2+} doped in $(NH_4)_2SO_4$ at 25°C, where a,b and c are the crystallographic axes. The signs of the off - diagonal elements in tables VIII.2 and VIII.3 apply to the same one of the symmetry related spectra.

g.g	a	b	c
a	3.9034	-0.0065	-0.0233
b	-0.0065	3.8925	-0.0758
c	-0.0233	-0.0758	+3.7615

Table VIII.3

Elements of $\underset{\sim}{g}.\underset{\sim}{A}.\underset{\sim}{A}.\underset{\sim}{g}$ (in units of $10^4 Mc^2$) for the site I of VO^{2+} doped in $(NH_4)_2SO_4$, at 25^oC, where a,b and c are the crystallographic axes. The signs of the off-diagonal elements in tables VIII.2 and VIII.3 apply to the same one of the symmetry related spectra.

$\underset{\sim}{g}.\underset{\sim}{A}.\underset{\sim}{A}.\underset{\sim}{g}$	a	b	c
a	19.49	7.00	12.37
b	7.00	33.10	32.96
c	12.37	32.96	91.80

Table VIII.4

Elements of $\underset{\sim}{g}.\underset{\sim}{g}$ for the site II of VO^{2+} doped in $(NH_4)_2SO_4$, at 25^oC, where a,b and c are the crystallographic axes. The signs of the off-diagonal elements in tables VIII.4 and VIII.5 apply to the same one of the symmetry related spectra.

$\underset{\sim}{g}.\underset{\sim}{g}$	a	b	c
a	3.9007	-0.0577	-0.0088
b	-0.0577	3.7658	-0.0312
c	-0.0088	-0.0312	3.9127

Table VIII.5

Elements of g.A.A.g (in units of $10^4 Mc^2$) for the site II of VO^{2+} doped in $(NH_4)_2SO_4$, at 25°C, where a,b and c are the crystallographic axes. The signs of the off-diagonal elements in tables VIII.4 and VIII.5 apply to the same one of the symmetry related spectra.

g.A.A.g	a	b	c
a	24.88	25.14	6.30
b	25.14	96.40	15.86
c	6.30	15.86	21.05

Table VIII.6

Magnitude of the principal values of g and of A (in units of $10^{-4} cm^{-1}$) for the site I of VO^{2+} in $(NH_4)_2SO_4$, at 25°C.

$\lvert g'_1 \rvert$ = 1.976	$\lvert A_1 \rvert$ = 68.2
$\lvert g'_2 \rvert$ = 1.982	$\lvert A_2 \rvert$ = 73.7
$\lvert g'_3 \rvert$ = 1.930	$\lvert A_3 \rvert$ = 180.2

Table VIII.7

Direction cosines relating the crystal axes (a,b,c) to the principal axes $(1',2',3')$ of $\tilde{g}$ and to the principal axes (1,2,3) of $\tilde{A}$ for the site I of VO^{2+} in $(NH_4)_2SO_4$, at 25°C. In each row the relative sign for the direction cosines is for the symmetry related spectrum with parameters given in tables VIII.2 and VIII.3.

For $\tilde{g}$	a	b	c
$1'$	0.976	-0.212	-0.046
$2'$	0.172	0.887	-0.428
$3'$	0.132	0.410	0.902
For $\tilde{A}$	**a**	**b**	**c**
1	0,813	-0.570	0.117
2	0.561	0.714	-0.419
3	0.156	0.406	0.900

Table VIII.8

Magnitude of the principal values of g and of $\tilde{A}$ (in units of $10^{-4}cm^{-1}$) for the site II of VO^{2+} in $(NH_4)_2SO_4$, at 25°C .

$\lvert g_1' \rvert$	= 1.981	$\lvert A_1 \rvert$	= 67.4
$\lvert g_2' \rvert$	= 1.934	$\lvert A_2 \rvert$	= 178.9
$\lvert g_3' \rvert$	= 1.979	$\lvert A_3 \rvert$	= 72.5

Table VIII.9

Direction cosines relating the crystal axes (a,b,c) to the principal axes (1′,2′,3′) of $\tilde{g}$ and to the principal axes (1,2,3) of $\tilde{A}$ for the site II of VO^{2+} in $(NH_4)_2SO_4$, at 25°C. In each row the relative sign for the direction cosines is for the symmetry related spectrum with parameters given in tables VIII.4 and VIII.5

For $\tilde{g}$	a	b	c
1′	0.797	-0.384	0.466
2′	0.338	0.923	0.182
3′	-0.500	0.012	0.866

For $\tilde{A}$	a	b	c
1	0.807	-0.141	-0.574
2	0.300	0.934	0.192
3	0.509	-0.327	0.796

Table VIII.10

Magnitude of the principal axes of $\tilde{g}$ and of $\tilde{A}$ (in units of $10^{-1}cm^{-1}$) for the site III of VO^{2+} in $(NH_4)_2SO_4$, at 25°C .

$\lvert g_1' \rvert$	= 1.984	$\lvert A_1 \rvert$	= 69.3
$\lvert g_2' \rvert$	= 1.978	$\lvert A_2 \rvert$	= 70.5
$\lvert g_3' \rvert$	= 1.928	$\lvert A_3 \rvert$	= 180.2

Table VIII.11

Direction cosines relating the crystal axes (a,b,c) to the principal axes (1′,2′,3′) of $\underset{\sim}{g}$ and to the principal axes (1,2,3) of $\underset{\sim}{A}$ for the site III of VO^{2+} in $(NH_4)_2SO_4$, at 25°C. In each row the relative sign for the direction cosines is for one of the symmetry related spectra. The principal axes of $\underset{\sim}{g}$ and $\underset{\sim}{A}$ tensors are assumed to coincide.

For $\underset{\sim}{g}$ or $\underset{\sim}{A}$	a	b	c
1′ or 1	0.000	1.000	0.000
2′ or 2	-0.647	0.000	0.763
3′ or 3	0.763	0.000	0.647

Table VIII.12

The orientations of V-O for its three sites I, II and III in $(NH_4)_2SO_4$ at 25°C. Here Θ_a is the angle between the projection of V-O on the bc plane and the b-axis, Θ_b is the angle between the projection of V-O on the ca plane and the c-axis, and Θ_c is the angle between the projection of V-O on the ab plane and the a-axis.

Site ⟶	I	II	III
Θ_a	66°	11°	--
Θ_b	9°	60°	40°
Θ_c	72°	71°	--

Table VIII.13

The theoretical values of Θ_a, Θ_b and Θ_c for the sites I* and II of V-O . It is assumed that there is no vacancy near it.

Site →		I	II
Θ_a (in bc plane from b)	=	60^o	8^o
Θ_b (in ca plane from c)	=	0^o	0^o
Θ_c (in ab plane from a)	=	90^o	90^o

* Assumption of a NH_4^+-vacancy brings the theoretical values of Θ_a, Θ_b and Θ_c nearer to the experimental ones.

REFERENCES

(1) B. M. Kozyrev, Disc. Faraday Soc. 19, 135 (1955).

(2) R. H. Sands, Phys. Rev. 99, 1222 (1955).

(3) D.E. O'Reilly, J. Chem. Phys. 29, 1188 (1958).

(4) R. J. Faber and M.T. Rogers, J. Am. Chem. Soc. 81, 1849 (1959).

(5) C.M. Roberts, W.S. Koski and W. Caughry, J. Chem. Phys. 31, 591 (1961).

(6) A. J. Saracens, D. T. Fanale and N.D. Cogreshall, Anal. Chem. 33, 500 (1961).

(7) M. D. Sastry and P. Venkateswarlu, ~~J. Chem. Phys. 49, 1714 (1968).~~ Mol. Phys. 13, 161 (1967).

(8) K.V.S. Rao, M.D. Sastry and P. Venkateswarlu, J. Chem. Phys. 49, 1714 (1968).

(9) H. J. Gerritsen and H.R. Lewis, Phys. Rev. 119, 1010 (1960).

(10) I. Siegel, Phys. Rev. 134, A 193 (1964).

(11) A. Manoogian and J.A. Mackinon, Canad.J. Phys. 45, 2769 (1967).

(12) K.V.S. Rao , M.D. Sastry and P. Venkateswarlu, J. Chem. Phys. 49, 4984 (1968).

(13) R. H. Borcherts and C. Kikuchi, J. Chem. Phys. 40, 2270 (1964).

(14) A. Ogg, Phil. Mag. 5, 354 (1928).

(15) E. O. Schlemper and W.C. Hamilton, J. Chem. Phys. 44, 4498 (1966).

(16) R.W.G. Wycoff, Crystal Structure (Inter/Science Publishers, Inc. Vol.2, Chaper 8).

(17) B.T.Matthias and J.P.Remeika, Phys.Rev. 103, 262 (1956).

(18) M.B. Palma - Vittorelli et al, Nuovo Cimento 3, 718 (1956).

(19) B.V.R.Chowdari and P. Venkateswarlu, Proc. Indian Aca. Sci. 67, 130 (1968).

(20) S.C. Furman and C.S. Garner, J. Am. Chem. Soc. 72, 1785 (1950).

(21) C. J. Ballhausen and H.B. Gray 1, 111 (1962).

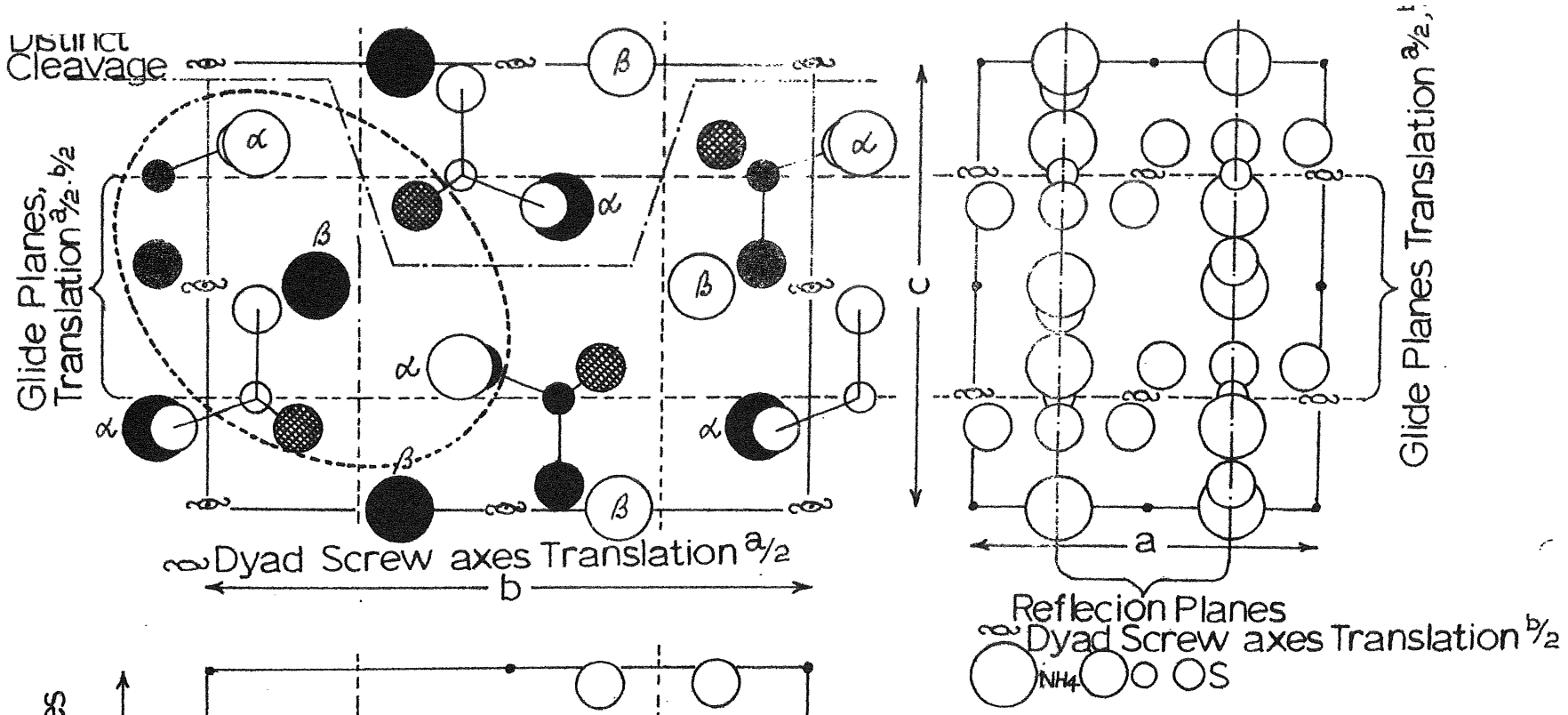

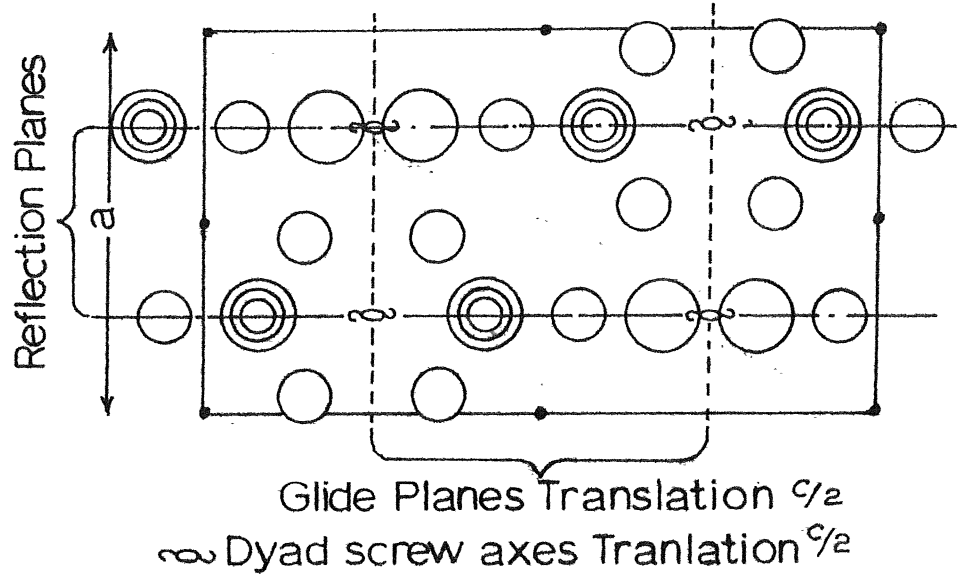

PROJECTIONS OF AMMONIUM SULPHATE CRYSTAL

Fig. 8.1

Note : A portion of this figure is bounded by dotted line and its enlargemer

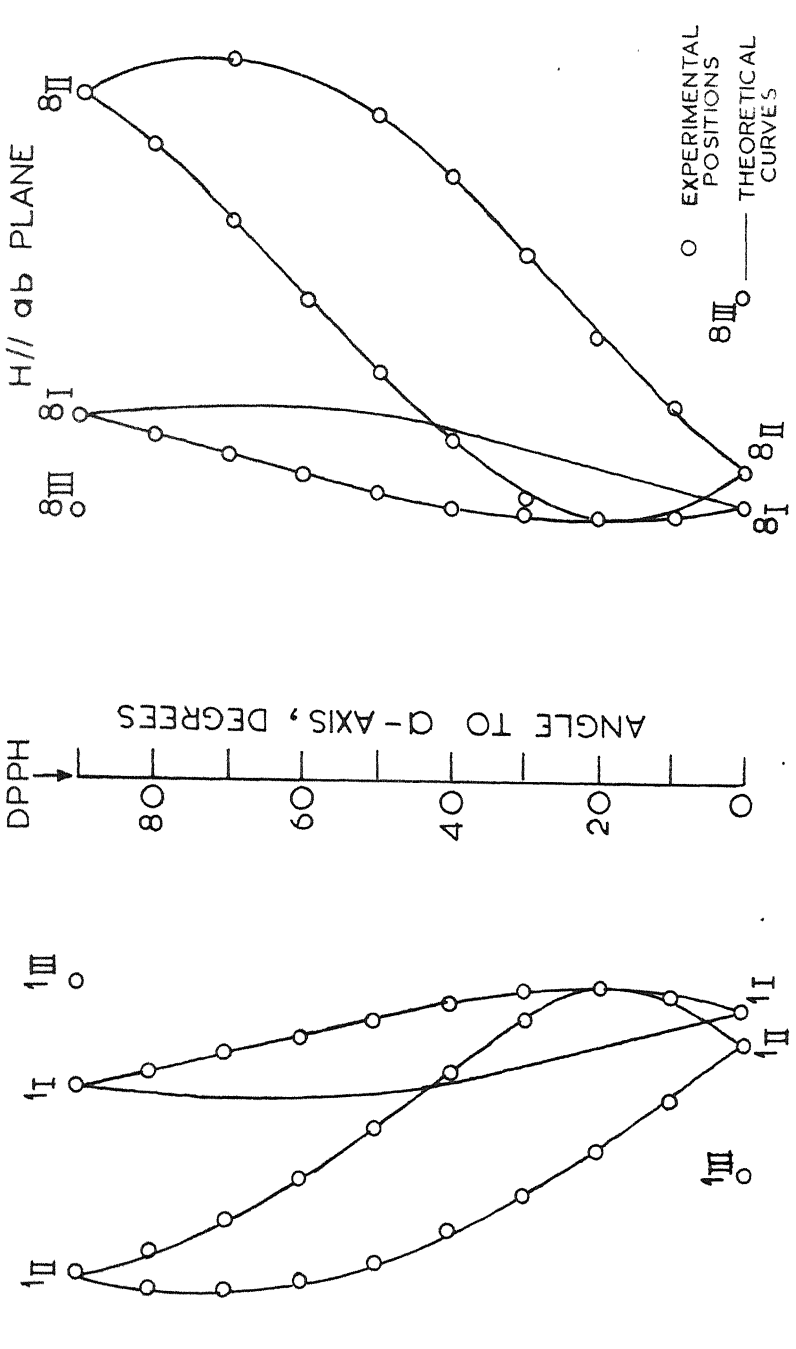

FIG.8·2 A PLOT OF THE POSITIONS OF EXTREME HYPERFINE LINES FOR THE SITES I, II & III OF VO^{2+} IN $(NH_4)_2 SO_4$. THE FIELD ORIENTATIONS ARE PARALLEL TO THE CRYSTALLOGRAPHIC ab PLANE.

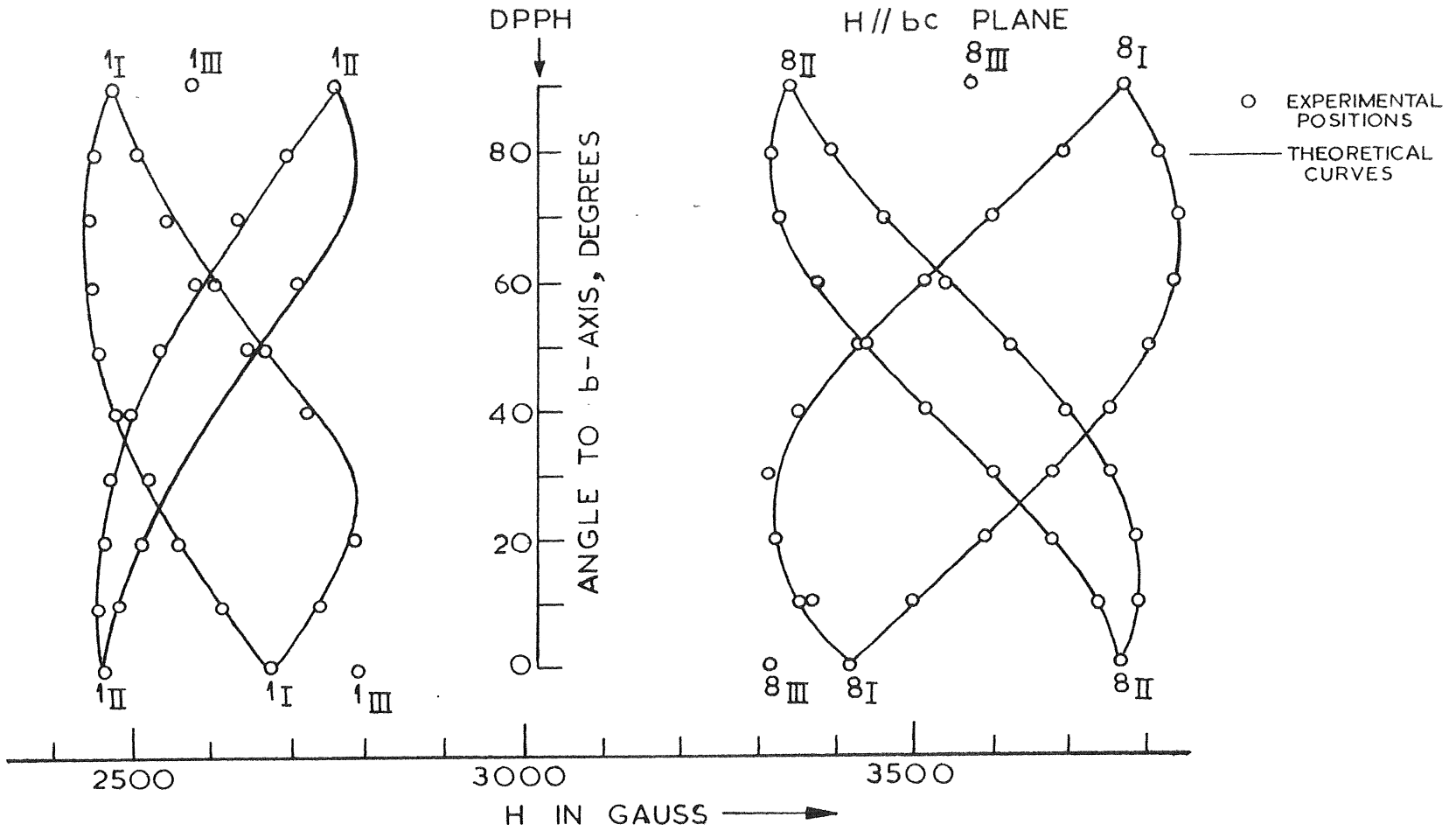

FIG·8·3 A PLOT OF THE POSITIONS OF EXTREME HYPERFINE LINES FOR THE SITES I, II & III OF VO^{2+} IN $(NH_4)_2SO_4$ · THE FIELD ORIENTATIONS ARE PARALLEL TO THE CRYSTALLOGRAPHIC bc PLANE.

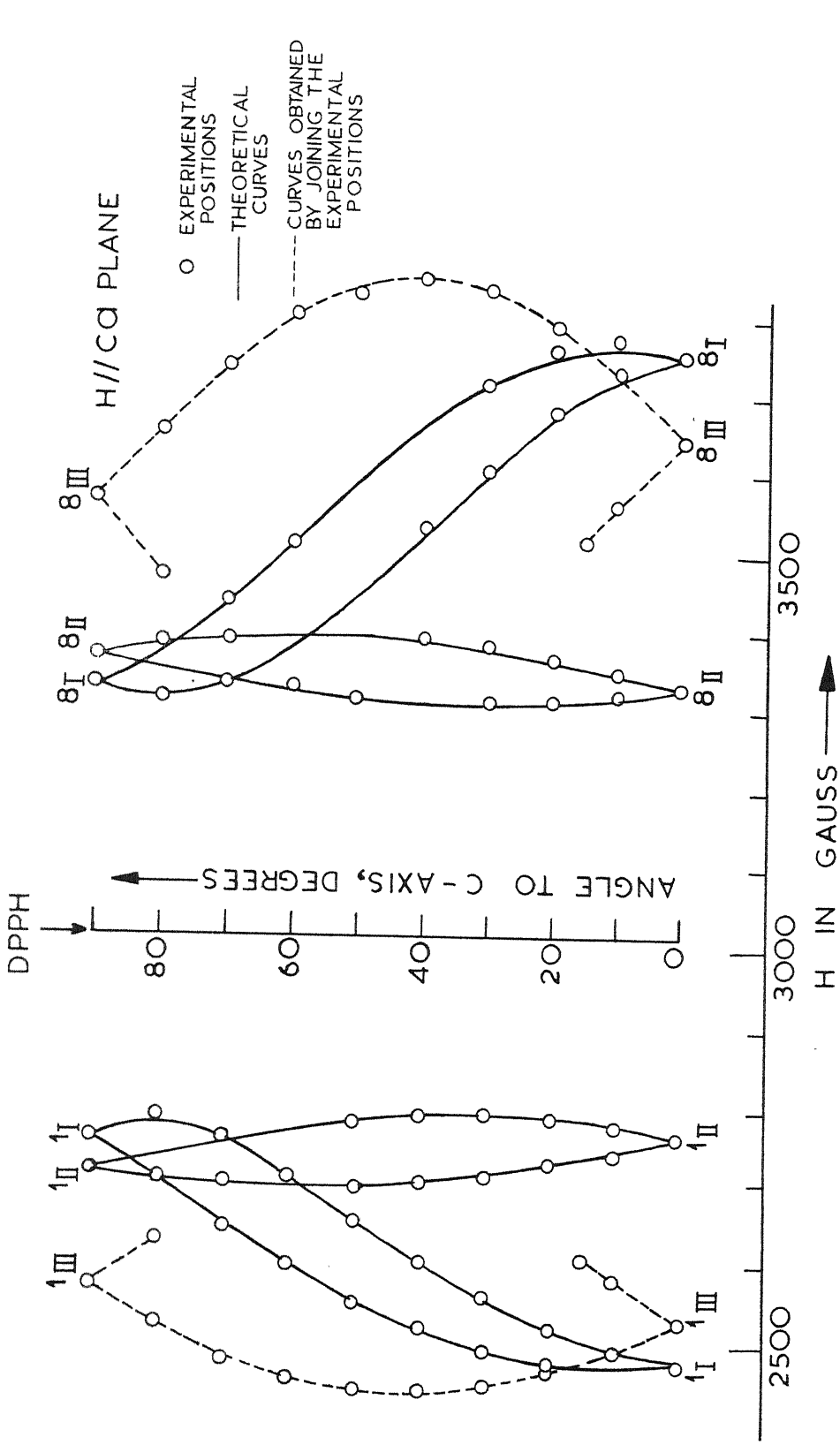

FIG. 8.4 A PLOT OF THE POSITIONS OF EXTREME HYPERFINE LINES FOR THE SITES I, II & III OF VO^{2+} IN $(NH_4)_2SO_4$. THE FIELD ORIENTATIONS ARE PARALLEL TO THE CRYSTALLOGRAPHIC CA PLANE.

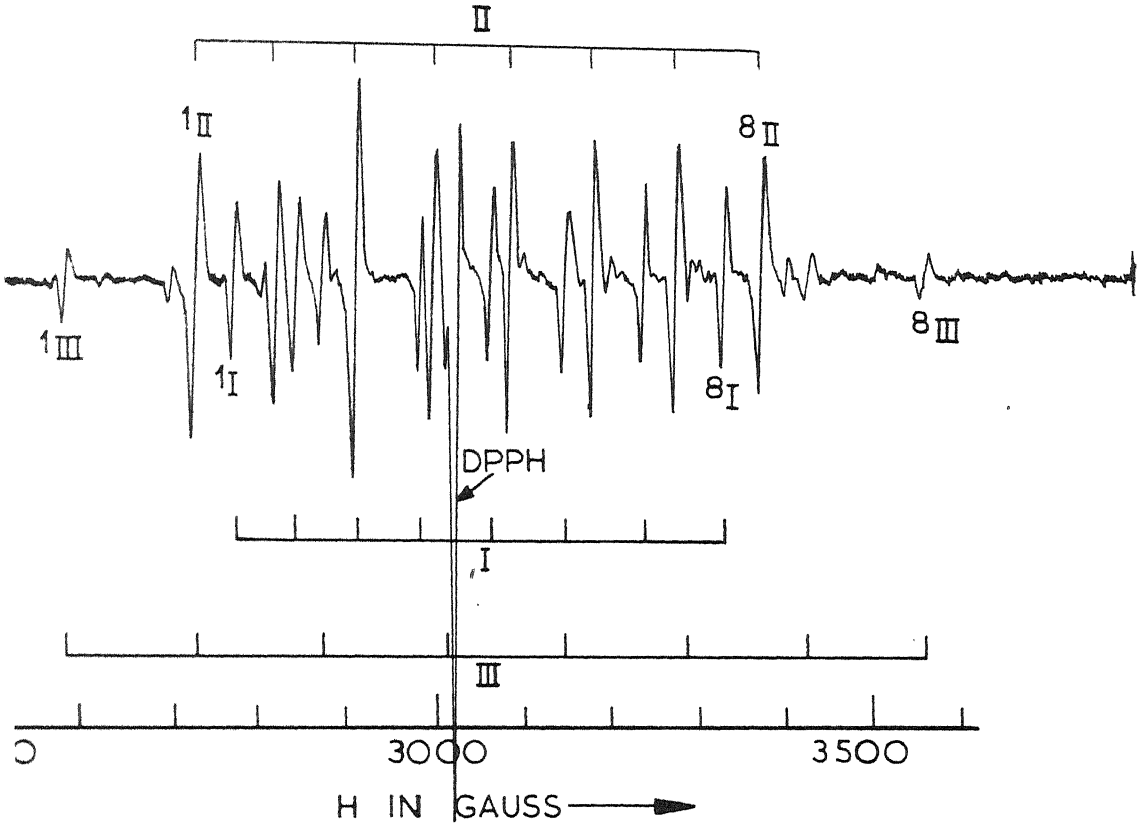

5 EPR SPECTRUM OF VO^{2+} DOPED $(NH_4)_2 SO_4$ AT 25 °C FOR H// CRYSTAL a-AXIS. THE EIGHT HYPERFINE LINES CORRESPONDING TO THE DIFFERENT ORIENTATION I, II & III OF VO^{2+} ARE GROUPED TOGETHER AND MARKED ACCORDINGLY.

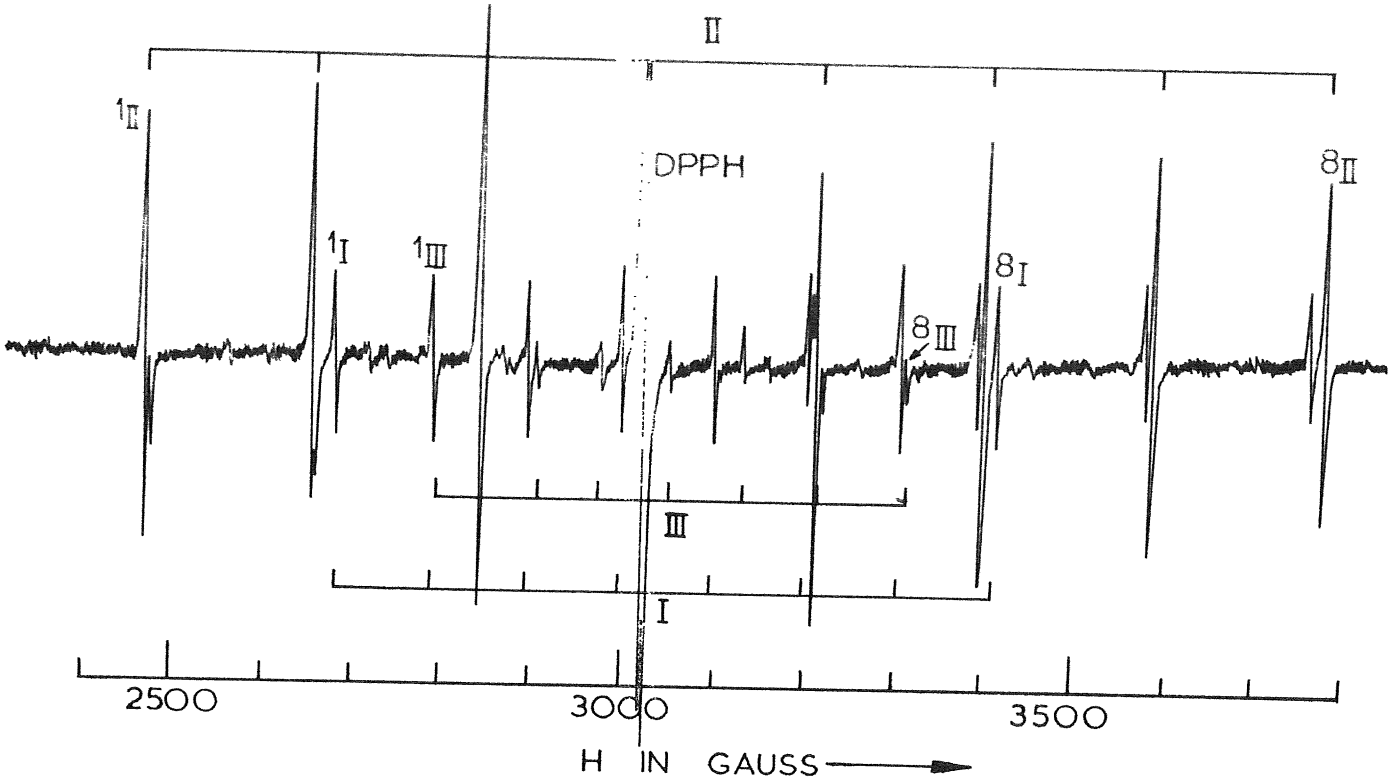

FIG.8·6 EPR SPECTRUM OF VO^{2+} DOPED $(NH_4)_2 SO_4$ AT 25 °C FOR H// CRYSTAL b- AXIS. THE EIGHT HYPERFINE LINES CORRESPONDING TO THE DIFFERENT ORIENTATIONS I, II & III OF VO^{2+} ARE GROUPED TOGETHER AND MARKED ACCORDINGLY.

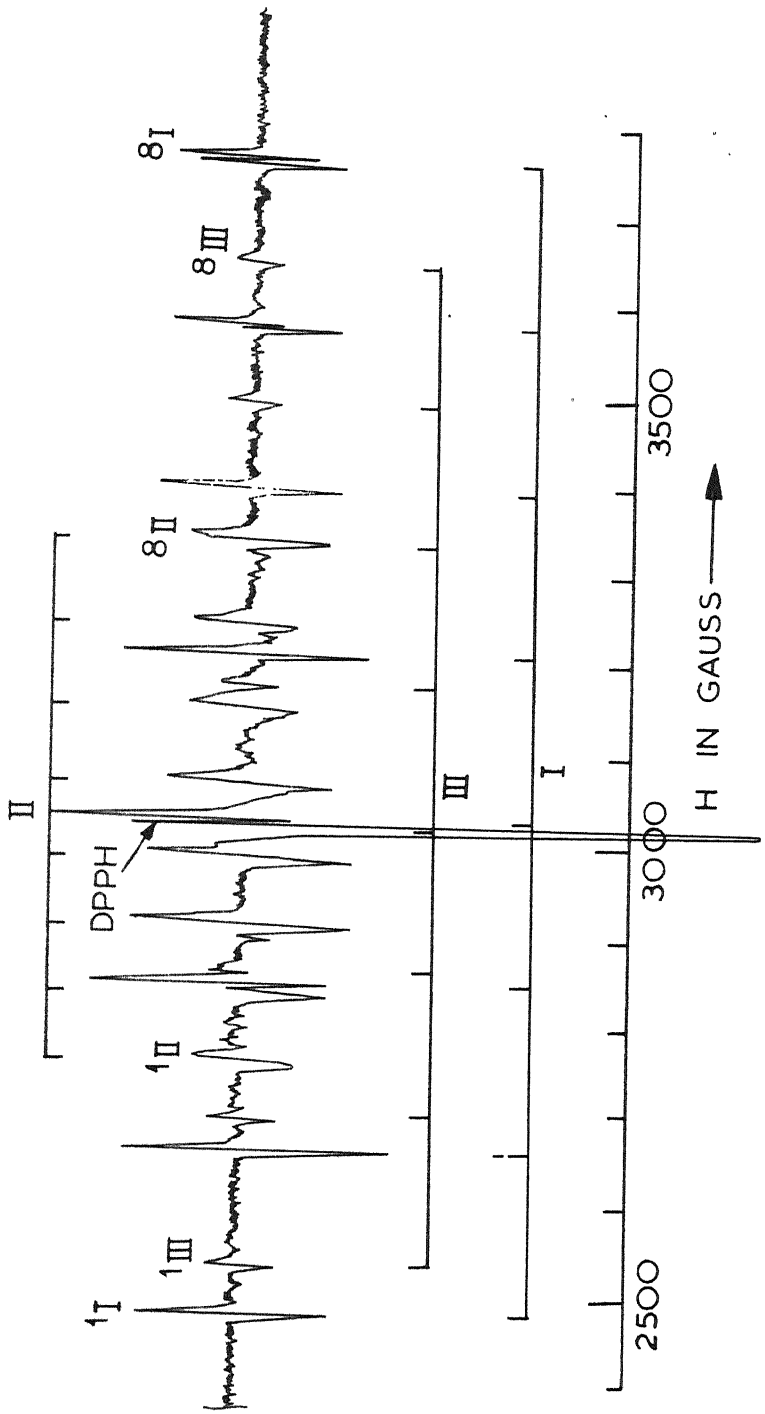

FIG. 8.7 EPR SPECTRUM OF VO^{2+} DOPED $(NH_4)_2 SO_4$ AT 25 °C FOR H// CRYSTAL C-AXIS. THE EIGHT HYPERFINE LINES CORRESPONDING TO THE DIFFERENT ORIENTATIONS I, II & III OF VO^{2+} ARE GROUPED TOGETHER AND MARKED ACCORDINGLY.

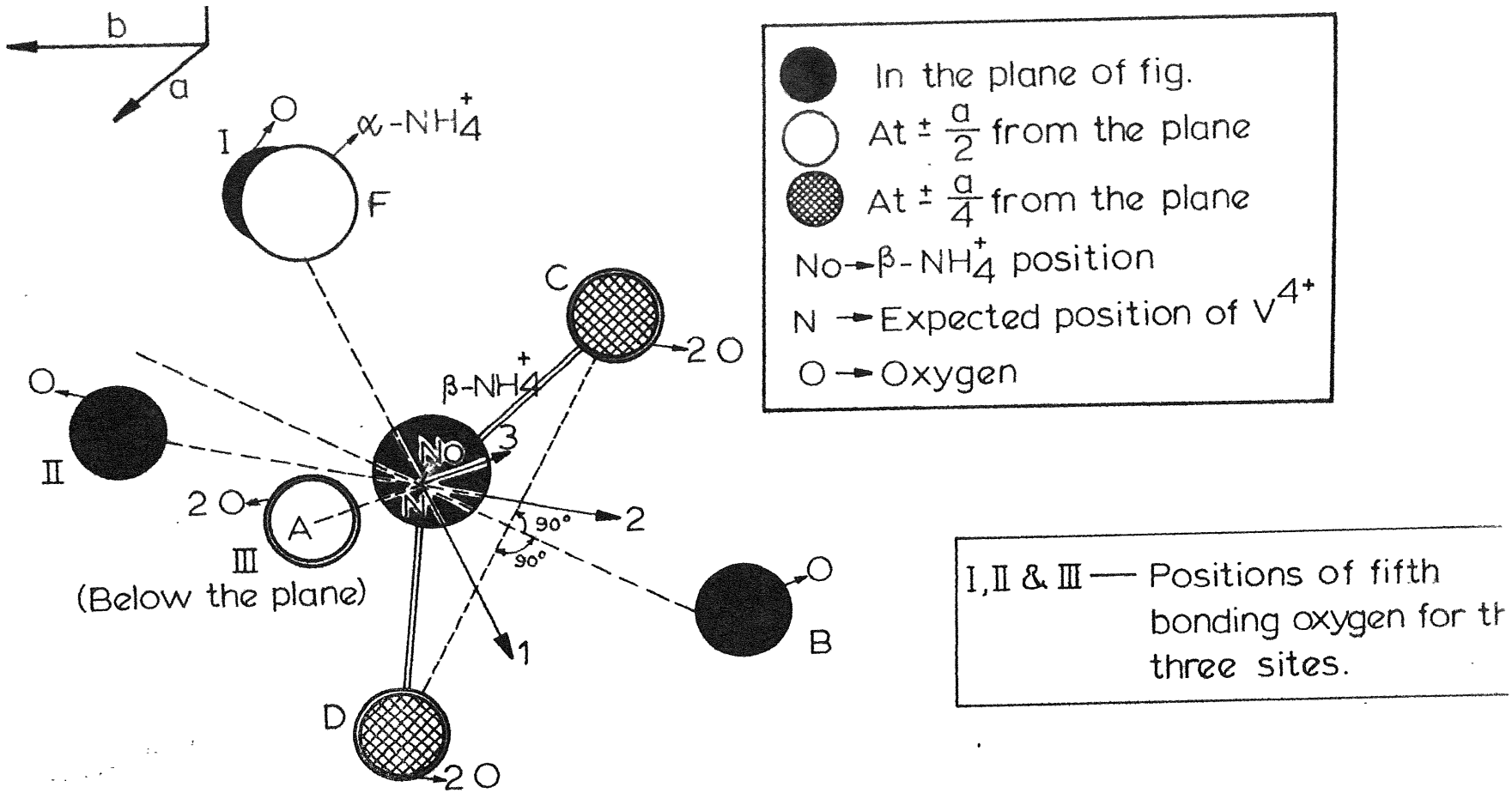

Fig.8.8- Diagram showing a β-NH_4^+ site, its oxygen environment and the nearest off the plane α-NH_4^+ site. The arrows 1, 2 and 3 represent the probable positions of V-O in the absence of vacancy for the three sites I, II & III. (The effect of vacancy, not shown here, is to pull V-O towards it) This figure is the enlargement of a portion of fig. 8.1, bounded by a dotted line.

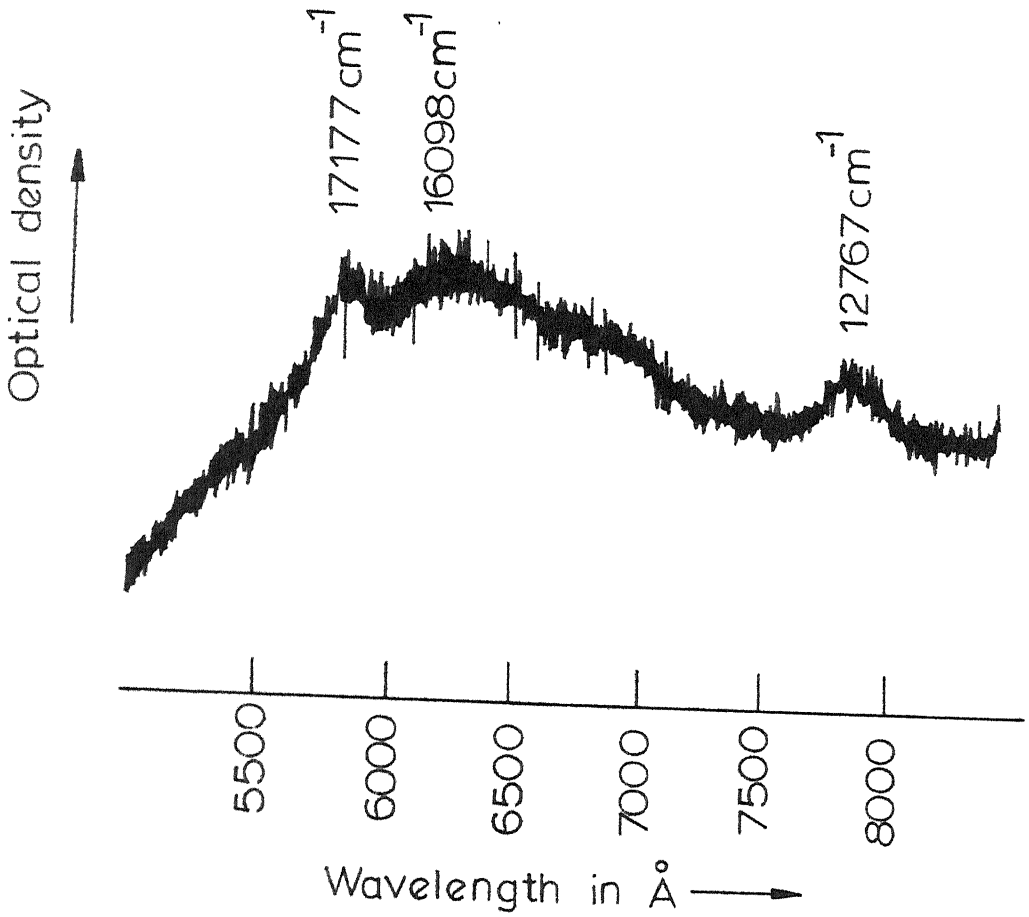

Fig. 8.9(a) - Absorption spectrum of Vo^{2+} - doped $(NH_4)_2SO_4$ from 12000 to 19000 cm^{-1}.

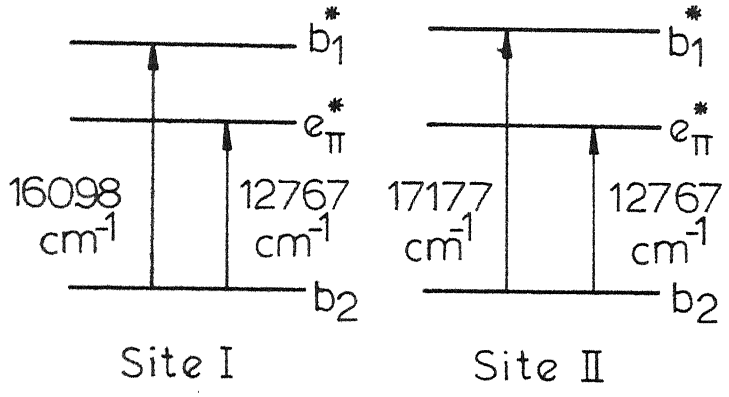

Fig. 8.9(b) - Significant energy levels for the two sites I & II of V-O.

Biographical Note

Shankar Datt Pandey was born at Lucknow (U.P.) on 28th of August 1941. He passed the High School and Intermediate Examinations of U.P. Board from A.B.V. Inter College, Kanpur in 1955 and 1957 respectively. He graduated in 1959 from the D.A.V. College, Kanpur Campus of Agra University, thereafter continued his studies in the same College and received his M.Sc.(Physics) degree in 1961. In all the above four examinations he was placed in the category of first divisioners and had a top rank in the Board or University concerned.

Soon after his M.Sc., he joined Indian Institute of Technology, Kanpur as a research assistant. He started his research career with Professor Putcha Venkateswarlu in 1962. He passed (cpi = 9.57) the pre-Ph.D. examination of IIT Kanpur in 1964. Until the end of 1964, he was involved in a research problem entitled "Infra red studies of para-substituted fluoro benzenes". When facilities for Electron Paramagnetic Resonance studies were provided (at IIT Kanpur), he changed his field of interest to such studies. At present he is a senior research assistant in IIT Kanpur.

This thesis was typed by Shri A.A. Khan and the tracings for the figures were made by Shri Bajpai and Shri D.S. Panesar.